OPTIMIZATION AND LEARNING-ENABLED INTEGRATED CLOUD AND EDGE SOLUTIONS FOR CONTROL AND DEPLOYMENT OF FLEET EV CHARGING

by

Abhijith Ravi

A dissertation submitted to the faculty of
The University of North Carolina at Charlotte
in partial fulfillment of the requirements
for the degree of Doctor of Philosophy in
Electrical Engineering

Charlotte

2024

Approved by:

Dr. Linquan Bai

Dr. Valentina Cecchi

Dr. Badrul Chowdhury

Dr. Tao Hong

Prof. Evan Houston

ABSTRACT

ABHIJITH RAVI. Optimization and Learning-Enabled Integrated Cloud and Edge Solutions for Control and Deployment of Fleet EV Charging. (Under the direction of DR. LINQUAN BAI)

Transportation electrification is one of the core policies actively driven by countries around the world. The strategic integration of electric vehicles (EVs) holds the key to a reliable and resilient future for the power grid. To address the challenges of integrating EVs into distribution grid operation, this dissertation presents a comprehensive framework with advanced optimization and machine learning techniques for the control and deployment of fleet EV (FEV) charging. This dissertation addresses the challenges of integrating FEVs into distribution grid operations through cloud-based and edge-based approaches. Cloud-based solutions provide centralized optimization methods deployed on platforms operated by utilities or distribution system operators, while edge-based solutions enable decentralized control at the grid edge, where advanced methods such as federated reinforcement learning can be applied.

In Chapter 2, this dissertation develops a two-stage stochastic optimization model designed for the strategic placement of FEV charging stations (FEVCSs) to enhance the resilience of distribution networks. By focusing on high-impact, low-probability (HILP) events (such as hurricanes), this centralized optimization model that could be deployed on a cloud platform of a utility system accounts for uncertainties in both the power grid and transportation networks, ensuring operational efficiency and grid reliability during outages.

In Chapter 3, the focus shifts to a cloud-based approach for aggregating EV charging and other distributed energy resources for market participation. A bilevel stochastic optimization framework is developed to model the FEVCS, as part of a Distributed Energy Resource Aggregator (DERA) of providing energy and ancillary services in the ISO day-ahead market. This model demonstrates the potential of FEVCSs to pro-

vide ancillary services and capacity reserves, accounting for their impact on locational marginal prices (LMPs).

Chapter 4 introduces a novel cloud-edge collaboration framework based on federated reinforcement learning to enable decentralized control of FEVCSs in the distribution system. The proposed Federated Learning-Enhanced Conflict-Aware Multi-Agent Reinforcement Learning (FLE-CA-MARL) framework allows individual FEVs, modeled as agents, to coordinate their actions locally at the edge of the grid, contributing to voltage regulation and grid stability. This hybrid approach, which combines cloud-level coordination with edge-based decision-making, effectively addresses the computational complexity, latency, and data privacy challenges inherent in large-scale EV charging management.

The work in this dissertation enables grid-optimized intelligent deployment and management of FEV charging by developing a suite of cloud-based optimization models and edge-based distributed control using federated reinforcement learning. The simulation results on different IEEE test cases demonstrate the effectiveness of this work in enabling FEVs to improve grid resilience, voltage stability, and market participation. This work offers a scalable and adaptive solution for the future deployment of FEVCS in modern smart grids.

ACKNOWLEDGEMENTS

At the end of this fulfilling journey towards my Ph.D., I would like to express my heartfelt gratitude to my Ph.D. advisors, Dr. Linquan Bai and Dr. Valentina Cecchi, for their continuous guidance, encouragement, and trust throughout this process. Their expertise and insightful feedback have been invaluable in shaping my research.

I would also like to extend my deep appreciation to my Ph.D. committee members, Dr. Badrul Chowdhury, Dr. Tao Hong, and Prof. Evan Houston, for their thoughtful suggestions and critical insights, which greatly contributed to the development of this work.

A special thanks to friends and alumni Oluwatimilehin Adeosun, Naveen Kodanda Pani, Anuprabha Ravindran, Roozbeh Karandeh, Tumi Lawanson, Sujay kaloti, and Vivek Pulikkal for their valuable help and advice along the way. Their shared experiences and guidance were instrumental during my Ph.D. journey.

I am also deeply grateful to my dear friend Andrew Amuna, who passed away, but whose unwavering support helped me through one of the hardest times in my life after the loss of my father. His empathy and kindness will always be remembered.

I would like to express my heartfelt gratitude to Nithya Sri Srinivasan, whose kind response at a critical time, when my decision to come to UNC Charlotte was in the balance, helped me move forward. Her support, especially when I struggled to receive responses from others, made a significant impact.

Finally, I am sincerely grateful for the opportunities and resources provided by the William States Lee College of Engineering, the Department of Electrical and Computer Engineering (ECE), Energy Production and Infrastructure Center (EPIC), the Systems Engineering and Engineering Management (SEEM) department, and the Graduate School at UNC Charlotte, whose support has been essential over the past few years.

DEDICATION

To my curious son, Shiva Manden - your laughter and presence are my greatest joys.

To my loving wife, Aswathi Manden - your unwavering support has been my strength.

To my caring mother, Ajitha Kumari - though distance separates us, your love has always been with me.

To my proud father, Ravi Iyyatil - your memory and guidance light my path, even in your absence.

To all my family and friends who have held the best for me in their hearts - your belief in me has meant the world.

This journey is for all of you.

TABLE OF CONTENTS

LIST OF TABLES

LIST OF FIGURES

LIST OF ABBREVIATIONS

ADMS Advanced Distribution Management System

ADN Active Distribution Network

DER Distributed Energy Resource

DERA Distributed Energy Resource Aggregator

DRL Deep Reinforcement Learning

ECE Electrical and Computer Engineering

EV Electric Vehicle

FDRL Federated Deep Reinforcement Learning

FEV Fleet Electric Vehicle

FEVCS Fleet Electric Vehicle Charging Station

FL Federated Learning

ISO Independent System Operator

LMP Locational Marginal Pricing

LSE Load Serving Entity

MG Microgrid

PM Price Maker

POMDP Partially Observable Markov Decision Process

PT Price Taker

PV Photovoltaic

RL Reinforcement Learning

SOC State of Charge

SOCP Second Order Cone Programming

TD3 Twin Delayed Deep Deterministic Policy Gradient

V2G Vehicle-to-Grid

VVO Volt/VAR Optimization

CHAPTER 1: INTRODUCTION AND OVERVIEW

The electrification of transportation represents one of the most transformative technological shifts in the modern energy landscape. Fleet electric vehicles (FEVs), particularly medium- and heavy-duty vehicles (MH-DVs), are integral to this transformation, offering significant potential to enhance grid resilience and market participation. This dissertation explores the optimal integration of Fleet Electric Vehicle Charging Stations (FEVCS) into power distribution networks, focusing on the challenges of managing grid resilience, strategic market participation, and overall voltage stability.

The ongoing decarbonization, digitalization, and decentralization of the power grid are fundamentally reshaping how energy is generated, distributed, and consumed [1]. In the United States, vehicles powered by fossil fuels are responsible for 27% of total greenhouse gas (GHG) emissions, promoting a nationwide shift toward the electrification of the transportation sector to reduce emissions and achieve a sustainable transportation system. MH-DVs alone account for 23% of the GHG emissions from ground transportation, making them a critical target for electrification. These vehicles are crucial for applications such as public transportation, logistics, and freight delivery services that require high energy but offer limited flexibility in operation.

The strategic deployment and intelligent control of FEVCSs can play a crucial role in enhancing power grid resilience and market participation [2]. Each MH-DV fleet can have the potential to be a source or a sink of energy in the grid through vehicle-to-grid (V2G) capabilities. Consequently, medium and heavy-duty FEVs have the capacity to inject or draw power in the range of MWs, which makes them highly energy-dense. Realizing this, several utilities have already included FEVs as a key component of their grid modernization and decarbonization strategies [3].

However, the rapid adoption of FEVs in the transportation sector can pose significant challenges to the power grid. The uncontrolled and uncoordinated charging of numerous FEVs can lead to increased peak demand, voltage deviations, and power quality issues in the distribution grid [4]. This highlights the critical need for strategic planning and intelligent control of fleet EV charging stations to ensure grid reliability, stability, and resilience. This has sparked the interest of academia and industry in solving the challenges associated with the increased adoption of EVs. As a result, optimal techno-economic integration of EV charging infrastructure into the existing power systems is a key research area.

This dissertation explores optimal strategies for integrating FEVs into the grid, highlighting the potential benefits, challenges, and innovative solutions necessary for a successful transition. The aim of this chapter is to lay the groundwork for the comprehensive approach presented in subsequent chapters, which address the optimal deployment and control of FEVCS in the power grid.

The structure of this chapter of the dissertation is as follows: Section 1.1 presents the background of FEVCS, introducing the components of FEVCS, the behavior of FEVCS, and the difference between an FEVCS and a Transportable Energy Storage System (TESS) from a power grid researcher's perspective. Section 1.3 connects FEVCS to different grid functionalities explored in this dissertation. Additionally, Section 1.2 shares the challenges and motivations associated with FEVCS integration into the grid. Section 1.4 presents the contributions of the work along with the outline of the rest of the dissertation.

1.1 Background

Grid modernization presents a dynamic and multifaceted challenge for planners and operators, driven by rapid innovation in power generation, the growing proliferation of DERs, and the ongoing electrification of transportation. The integration of new technologies such as FEVCS into this evolving grid requires careful planning to main-

tain grid stability, reliability, and resilience [5]. Independent system operators (ISOs) or the regulated utility that powers consumers in a region, are required to estimate the growth of the load and the readiness of the existing infrastructure. As a result, load forecasting of the feeder loads is a critical step for any entity involved in controlling the generation, transmission, and distribution of electrical energy. Other variable resources, such as solar and wind, have been extensively explored, but the electrification of transportation poses new challenges that need to be addressed. High-capacity fast chargers, ranging from 50 kW to 350 kW, are being deployed to rapidly charge heavy-duty vehicles, which can exacerbate peak load issues in the distribution system [6]. Chargers of larger capacities are also being explored for FEVs to reduce charging times. Such charging rates have significant impacts on the existing distribution grid, causing voltage deviations, overloading of transformers and feeders, harmonics, and power quality issues [7].

In this dissertation, the term "FEV" refers specifically to medium- or heavy-duty trucks. These vehicles, with their large battery capacities and relatively regular charging schedules, can be considered DERs capable of providing various grid services, such as peak load shaving, frequency control, energy mobility, and voltage support. Figure 1.1 illustrates a futuristic smart warehouse equipped with an FEVCS capable of supporting 20 vehicles. The integration of FEVCS is not only critical in achieving the zero-emission goals, but also in improving the overall stability of the power grid. The different components of an FEVCS are presented in the following subsection.

1.1.1 Key Components of the FEVCSs

1.1.1.1 Battery System

The battery is the heart of an EV truck, determining its energy storage capacity and operational range. In research, battery storage is commonly represented by the state of charge (SOC). While the chemical composition of the battery is outside the scope of this dissertation, the charging and discharging behavior represented by changes in

Figure 1.1: A futuristic smart warehouse [8]

SOC plays a critical role in FEVCS performance and grid interaction. With current technology, the battery life of an EV truck reduces with the increase in the number of cycles of charging and discharging that it goes through.

1.1.1.2 Powertrain and Propulsion System

The powertrain converts the electrical energy of the battery into mechanical energy to propel the vehicle. The powertrain, which includes the motor and the drivetrain, is a key factor that determines the efficiency and energy consumption of the EV truck.

1.1.1.3 Control Systems

Control systems in FEVs regulate energy flow between the battery, the powertrain, and the external connections of the grid, determining how the vehicle interacts with the grid, including decisions on the direction of the transmission of power and the management of the power quadrant. The charging control system is crucial for determining the vehicle's real-time interaction with the grid, including the choice of charging or discharging, and hence is within the scope of this dissertation.

1.1.1.4 Inverter Placement

The inverter converts DC power from the battery to AC power for grid interaction and vice versa. Although the inverter can be located within the vehicle or in the charging infrastructure, most vehicles use an on-board charger to offer flexibility for the customer to choose the charging station they can charge from. Hence, for all the works in this dissertation, it is assumed that the inverter is placed in the vehicle. In the case where the inverter is in the charging station, the benefits to the grid are enhanced.

1.1.1.5 Charging Infrastructure

FEVs typically use level-2 chargers or DC fast chargers for regular charging. The choice of charging infrastructure for an EV is usually made by the fleet operator. The duty cycle of the services that the FEVs provide and the battery storage of the vehicle are two key factors that influence the choice of the charging infrastructure. In the works of this dissertation, DC fast charger is assumed to be the choice of the charging infrastructure. Bidirectional chargers enable vehicle-to-grid (V2G) services, allowing the vehicle to inject or draw power during its interaction with the power grid. This capability is essential in capturing the full potential of an FEV from the grid's perspective. In addition, the number of chargers in a charging infrastructure is dependent on the size of the fleet. Most FEVCS systems are governed by a fleet charging management system that optimizes charging schedules to limit peak load impacts on the grid while simultaneously charging multiple vehicles. Although an aggregated FEVCS is modeled in this dissertation, the fleet-level charging management system is not within the scope of this dissertation.

1.1.1.6 Differentiating FEVCS from Transportable Energy Storage Systems

In power systems research, FEVCS and Transportable Energy Storage Systems (TESS) serve distinct roles, each with its set of operational characteristics and impli-

cations for grid management.

FEVCSs are primarily loads, serving the transportation demand of the customers with fleet vehicles. The FEVCSs are not simply stationary infrastructures for charging FEVs; they integrate a dynamic component through the mobility of the vehicles. The mobility of FEVs introduces significant flexibility and complexity to power system models. As vehicles connect and disconnect from the FEVCS, the SOC varies based on their occupancy and usage patterns. The charging strategy adopted by the FEVCS is dependent on the requirement to charge the battery to full charge by the time of departure. Most fleet vehicles that use depot charging have patterns that can be identified. Moreover, the mobility of the vehicles within the FEVCS can easily be utilized by the grid using other charging stations on the power grid. Additionally, the policy-driven approach to increasing the EV infrastructure and fleet electrification incentivizes researchers, utilities, and the FEV customers to maximize the return from FEVCS.

TESS, in contrast, are designed as relocatable energy storage units, often transported via tracks or other mobile platforms to locations where additional grid support is required. Unlike FEVCS, TESS lacks integrated vehicle mobility and is typically deployed in a fixed location until moved for strategic purposes. Their movement is primarily intended for planned energy redistribution rather than dynamic, real-time interaction with the grid. As a result, modeling TESS is less challenging compared to FEVCS. Moreover, TESS requires high capital investment from the utility's perspective. TESS is an interesting option for applications like strategic energy storage, planned grid support, and emergency power supply.

1.1.2 Operational Modes of EV Charger Operation

This dissertation assumes that vehicles can operate in V2G mode with the ability to support the grid for voltage regulation. The interaction between EV chargers and the power grid can be represented through the four PQ quadrants shown in the Figure 1.2.

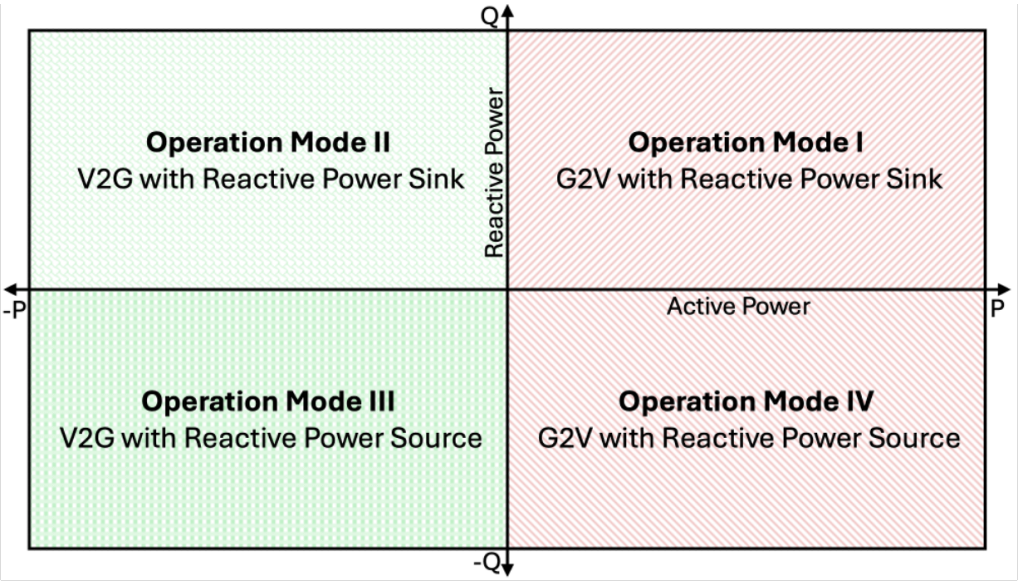

Figure 1.2: Quadrants of EV charger operation

Operation mode 1 lies in quadrant 1 with the EV charging while absorbing reactive power from the grid. However, in most cases in real life, the quadrant 1 operation happens with minimal reactive power absorption from the grid. Operation mode 2 lies in quadrant 2 with the EV charger in the V2G mode, while absorbing reactive power from the grid. This is a highly probable mode of operation since injecting active power can increase the voltage at the charger's node, which can then be regulated by absorbing reactive power from the grid. Operation mode 3 enables the charger to inject active power into the grid while injecting reactive power to elevate the voltage of the grid. This provides energy and voltage support to the power grid. Operation mode 4 provides reactive power support to boost the voltage of the grid while the EV is being charged. Quadrant 4 may also be one of the most common quadrants EVs will operate in once they are allowed to provide reactive power support to the grid. The following subsection presents different strategies that fleet operators may use to interact with the power grid.

1.1.3 Management Strategies of FEVCS

The primary goal of all fleet operators is to provide transportation for customer-specific applications. Hence, the flexibility of fleet operators in utilizing the FEVs for grid services is highly dependent on the duty cycle of the vehicles. With the long hours of idle time that conventional fleet vehicles have, providing grid services is a good secondary goal that most fleet operators can integrate. This option of a secondary goal is less attractive due to the possible loss in battery life with the existing battery storage technology. On the other hand, as researchers, it is our responsibility to pursue all approaches to optimize the integration of any emerging technology on the power grid. This is also because technological bottlenecks can be overcome in time. As a result, one domain where several researchers have tried different assumptions is the modeling of FEVCS's behavior on the power grid. This dissertation employs three different options for fleet management in the assumptions formed for the models implemented. The assumed fleet management strategies are explained in the subsections below.

1.1.3.1 Aggregated Under a Third Party

FEVCSs can be aggregated under a third-party operator who manages their interaction with the grid. FEVCSs on their own may have large energy storage and power injection capability, but aggregated under third-party service providers, they have a high chance of being an important market player in deregulated electricity markets. This strategy enables coordinated and large-scale provision of grid services, enhancing the probability of maximizing their returns from the grid. Hence, the strategic bidding model in this dissertation assumes FEVCSs that are aggregated under a DERA or DSO.

1.1.3.2 Controlled by the Fleet Operator

Some FEVCSs may opt to interact independently with the utility serving power. This is highly probable in situations where the FEVCS is powered by a vertically integrated utility. In such scenarios, the incentive for aggregation is reduced to a great extent. Hence, fleet operators can choose to provide services to the utility based on local requirements. This could be relevant for services like voltage support in distribution networks. The distributed VVO framework proposed in this dissertation assumes that FEVCSs will be controlled by their own fleet operator.

1.1.3.3 Hybrid Approaches

Some FEVCSs may employ strategies to use part of the fleet under third-party services while fleet operators control the rest of the fleet. Other hybrid approaches can be proposed through conditional agreements with the third party or utility. The application discussed in Chapter 2 of this dissertation that highly suits this strategy is the FEVs' role in enhancing grid resilience during HILP events. Not all fleet operators can afford to lose all their FEVs post-disaster, even if it is for the restoration of grid service. Thus, a hybrid grid-support strategy may be suitable for numerous fleet owners.

Given the unique capabilities of FEVCS, such as high power demand, energy density, and the ability to operate in V2G mode, their integration poses several operational challenges for the power grid. These challenges stem from the complex interactions between FEVCS and the distribution network, which must be managed to avoid compromising grid reliability and stability. The following section discusses the key challenges of FEVCS integration and how these issues can be addressed through strategic planning and control mechanisms.

1.2 Challenges of FEVCS Integration on the Power Grid

The rapid electrification of fleets introduces substantial challenges for grid operators, particularly in managing the increased demand for high-capacity charging and its impact on grid infrastructure. The Table.1.1 shows the average battery capacity of a single FEV [9]. For a transit bus with an average battery storage of 345 kWh, a fleet of 20 vehicles can hold up to 6.9 MWh energy. Similarly, for a medium-duty step van with an average battery capacity of 163 kWh, a fleet of 50 such vehicles will store up to 8.15 MWh. Moreover, the charger ratings for heavy-duty chargers range from 250 kW to over 1 MW per vehicle[9]. The high-power chargers are more essential for the long-haul vehicles, which require ultra-fast mid-shift charging to replenish their batteries in 30 minutes. The International Organization for Standardization (ISO) is developing the ultra-fast charger CharIN Megawatt Charging System (MCS) with a potential maximum power of 4.5 MW in Europe and the United States. The evidence suggests that these chargers can potentially act as loads with high-power and short duration at some locations on the grid. Hence, these large battery capacities and high-power chargers pose a significant challenge to the distribution network if multiple FEVCS loads charge simultaneously during any time of the day. The author's master's thesis explores the impact of light-duty EVs and MH-DEVs on the distribution network and the system-level load [10]. Even with FEVs modeled as load, the demand variation FEVCS introduces into the distribution level and the transmission level is significant. Furthermore, the V2G technology has enabled EVs to be loads or generators based on the customer's decision to absorb or inject power into the grid. This further complicates the uncertainty involved in hosting these massive loads from a DSO perspective. Hence, unmanaged, unchecked, and unplanned integration and operation of FEVCS can be dangerous to the operation and planning of the power grid [11]. Thus, it is essential to strategically plan the integration of FEVCS into the power grid from a grid planner's standpoint.

Table 1.1: Average battery capacity in medium- and heavy-duty vehicle models

Vehicle Category	**Average Battery Capacity (kWh)**				**Change 2019-2022**
	2019	**2020**	**2021**	**2022**	
Transit bus	264	322	225	345	31%
School bus	155	141	207	137	-12%
Shuttle bus	104	119	120	150	45%
Coach	316	347	233	266	-16%
Cargo van	69	90	57	60	-13%
Medium-duty step van	–	134	155	163	22%*
Medium-duty truck	124	139	99	92	-26%
Heavy-duty truck	293	232	372	311	6%
Yard tractor	150	184	160	197	31%

Additionally, the energy storage of MH-DEV fleets holds giant potential to be a DER that can offer regular services or post-disaster services to the power grid. When compared to other loads on the distribution feeders, these loads are highly dense in energy and power. Thus, the FEVCS's ability to influence the grid parameters would be much better than smaller loads on the same network. Moreover, according to NREL's fleet DNA project, most trucks operate less than 5 hours a day [12]. As a result, based on the duty cycle, a fleet operator can utilize FEVs for providing ancillary services like peak shifting, demand response, reserves, frequency regulation, and voltage regulation to the DSO or ISO.

Figure 1.3 shows the possible locations of different FEVCSs based on a real distribution feeder in the North Carolina state of the U.S[10]. The physical locations of several fleets may not be highly flexibly, the point of interconnection (POI) of these FEVCSs have the flexibility to be connected to either a different subnetwork or a different distribution feeder under the same or different substation transformer. Identifying the strategic POI for FEVCS is crucial for enhancing grid resilience. Proper POI selection enables FEVCS to provide critical services such as peak load shaving and voltage support while minimizing disruptions to local distribution networks.. Furthermore,

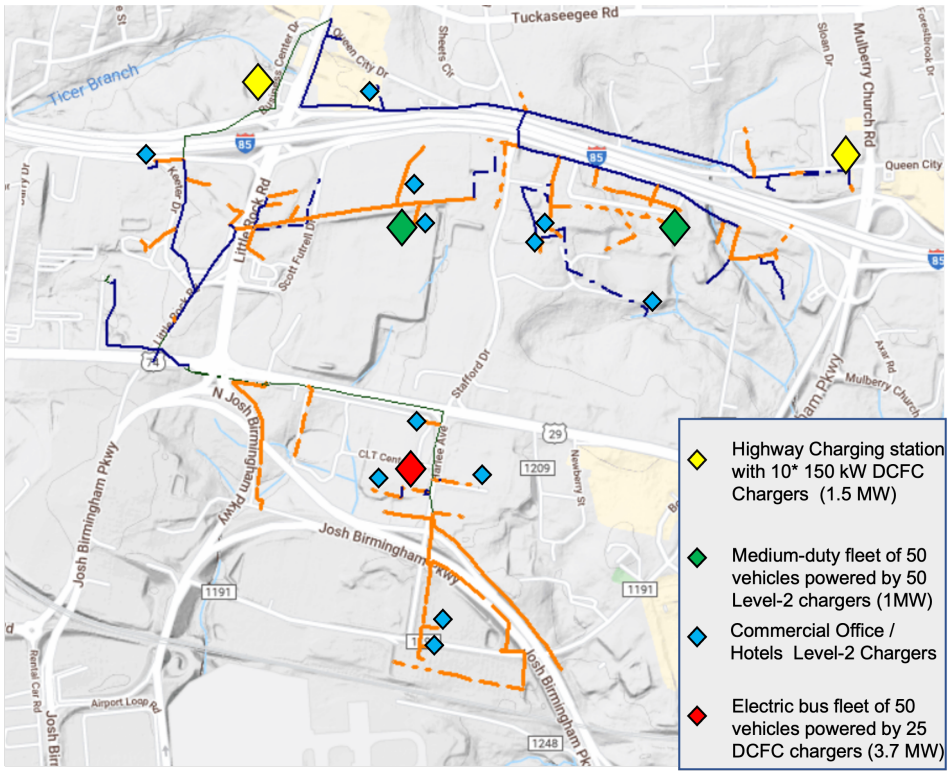

Figure 1.3: Possible EV loads on a real distribution feeder

one of the bottlenecks in extensively using FEVCSs for the everyday operation of the grid is degradation of battery life of the FEVs[13]. However, the ongoing research and development in battery technologies are rapidly overcoming those bottlenecks. The integration of ML and big data analytics into the optimization of battery further accelerates this progress [14]. Therefore, it is also essential to research, identify and define the role and potential of the FEVCS as a service provider on the grid. This nature of the FEVCS motivates the holistic approach devised in this dissertation. The following section will introduce several key grid functions and the roles of FEVCSs in the power grid.

1.3 Motivations and Vision: Integrating FEVCS into Key Grid Functions

As FEVCS integration expands, these systems will play a key role not only in infrastructure planning but also in energy markets and real-time grid operations. Each of these areas requires tailored solutions that address the unique technical and

economic challenges posed by FEVCS. This dissertation explores these challenges through three primary approaches: cloud-based solutions for resilience planning and market participation, and a cloud-edge collaboration framework for adaptive, real-time control of Volt-VAR Optimization (VVO) in distribution networks.

The following sections outline how cloud-based and cloud-edge collaboration approaches are suited for addressing different aspects of FEVCS integration, as discussed in Chapters 2, 3, and 4.

1.3.1 Infrastructure Planning and Resilience

The first key area of FEVCS integration is infrastructure planning, with a focus on enhancing grid resilience through optimal siting of charging stations. Grid resilience can be viewed from two complementary perspectives: planning resilience and operational resilience. While *planning resilience* focuses on planning measures that can enhance the resilience of the power grid, *operational resilience* is about pre- and post-diaster measures to enhance the resilience of the grid. In the pursuit of enhancing the grid resilience, both planning and operational perspective have to be considered while modeling the problem of strategically siting the FEVCS within the distribution network.

Chapter 2 of the dissertation addresses the planning resilience perspective by developing a cloud-based solution for the optimal siting of FEVCS. This approach leverages a two-stage stochastic optimization model to account for uncertainties in the distribution network, enabling utilities to strategically place FEVCS in locations that enhance overall grid resilience. By carefully selecting sites for FEVCS, this model ensures that charging stations not only serve transportation needs but also provide backup power during emergencies, helping the grid recover from outages.

1.3.2 FEVCS in Energy Markets

In addition to infrastructure planning, FEVCS can play a significant role in energy markets, particularly through their participation as part of a price-maker Distributed Energy Resource Aggregator (DERA). DERAs aggregate DERs, including FEVCS, to participate in the ISO energy and reserve markets. By aggregating multiple DERs, a DERA can strategically bid in the day-ahead market, influencing market prices and offering essential grid services such as reserve power and voltage support.

The FEVCS is a DER with high power density, energy density, and mobility. Such an FEVCS alone or as part of a DER aggregator, can act as a source of energy, reserve, or both in the ISO markets. For strategic bidding in Chapter 3, this dissertation assumes that a DERA can monitor and control all the resources that it owns or has signed a contract for to be part of the aggregated DERs. Hence, the challenge of strategic bidding for a DERA in the day-ahead energy and reserve market must be addressed by a cloud-based solution at the DERA or DSO level to ensure that none of the distribution-level constraints are violated during the strategic bidding process.

While the primary focus of Chapter 3 is on market participation, this cloud-based approach also indirectly enhances grid resilience. By encouraging more DERAs to participate in the energy and reserve markets, the solution strengthens the gridâs generation and reserve portfolios, making it more resilient to fluctuations in supply and demand. As more DERAs, including FEVCS, engage in market operations, the grid benefits from increased flexibility and resource diversity, improving its ability to respond to unexpected events.

1.3.3 Cloud-Edge Collaboration for Real-Time Control

The final key area of FEVCS integration is real-time grid edge control, where the focus shifts from long-term planning and market participation to the dynamic operation of the distribution network. FEVCS can introduce significant challenges to

grid stability, particularly in managing voltage profiles and reactive power flow. To address these challenges, Chapter 4 presents a cloud-edge collaboration-based solution for unified, adaptive Volt-VAR Optimization (VVO) using FEVCS.

Cloud-edge collaboration leverages the strengths of both centralized cloud-based control and decentralized edge-based decision-making. While the cloud provides a high-level overview and coordination of the grid, edge devices, such as FEVCS, make localized decisions based on real-time data, enabling faster response times and reducing communication latency.

In Chapter 4, the proposed cloud-edge framework uses Federated Reinforcement Learning (FRL) to enable decentralized control of FEVCS, allowing them to operate in real-time as part of the grid's VVO system. This system ensures that FEVCS not only charge efficiently but also provide reactive power support, which is crucial for maintaining voltage stability in distribution networks. By dynamically adjusting charging schedules and reactive power injection, FEVCS can mitigate the impact of their own charging on the grid while actively contributing to voltage regulation.

The adaptive control framework presented in Chapter 4 significantly enhances operational resilience by enabling the grid to respond to real-time fluctuations in demand and supply. The use of FL ensures that the system is scalable, capable of integrating large numbers of FEVCS without overwhelming centralized control systems. This decentralized, real-time approach strengthens the grid's ability to withstand and recover from operational disturbances, further contributing to overall resilience.

1.3.4 Comprehensive Approach to FEVCS Integration

By integrating cloud-based solutions for infrastructure planning and market participation with a cloud-edge collaboration framework for real-time control, this dissertation provides a holistic approach to FEVCS integration into the power grid. Each chapter focuses on a specific aspect of FEVCS deployment, offering tailored solutions that align with the technical and economic challenges posed by these systems.

Chapter 2 presents a cloud-based solution for optimizing FEVCS placement to enhance grid resilience, particularly during HILP events. Chapter 3 introduces a cloud-based solution for strategic bidding in energy markets, allowing FEVCS to participate in the day-ahead market as part of a price-maker DERA, indirectly strengthening grid resilience by expanding resource portfolios. Chapter 4 proposes a cloud-edge collaboration-based solution for adaptive VVO using FEVCS, enhancing operational resilience through real-time control and reactive power support.

This dissertation adopts a comprehensive approach to integrate FEVCS into the power grid. The proposed solutions consider technical, economic, and strategic aspects to optimize FEVCS placement and operation, while addressing grid reliability, resilience, and market interactions. The following section outlines the key contributions of this work, detailing the methods and findings presented in the subsequent chapter

1.4 Contributions and Dissertation Outline

The contributions of this dissertation are structured across several chapters, each focusing on different aspects of the research problem.

The first set of contributions is presented in **Chapter 2**, which investigates the optimal placement of Fleet Electric Vehicle Charging Stations (FEVCS) within power distribution networks. The results of this study were published in the special issue *"Towards a Sustainable Future: The Role of Electric Vehicles and Smart Grids in the Energy Transition"* of the journal *Applied Sciences* under the title *Optimal Siting of EV Fleet Charging Station Considering EV Mobility and Microgrid Formation for Enhanced Grid Resilience* [15]. The specific contributions of this chapter include:

1. Addressing a novel research problem by exploring the optimal placement of FEVCS within a power distribution network, the research aims to enhance grid resilience, considering both the power distribution and the transportation network.

2. Developing a two-stage stochastic optimization approach with an MISOCP model for the optimal siting of FEVCSs, considering EV mobility and the impact of extreme weather events. The first stage involves selecting the most favorable location for FEVCSs, while the second stage minimizes the weighted sum of the Value of Lost Load (VoLL) under potential fault scenarios, integrating transportation network considerations into the grid restoration scheme.

3. Evaluating the influence of renewable-supported BESS on the optimal placement of FEVCS and demonstrating the potential of BESS to improve the flexibility of the grid.

In **Chapter 3**, the focus shifts to the strategic participation of DERs in wholesale markets and the role of an FEVCS within a DERA. The findings of this chapter were initially published in the conference *2021 IEEE Power & Energy Society General Meeting (PESGM)* with the title *Modeling the Strategic Behavior of an Active Distribution Network in the ISO Markets*, and then extended to a journal published in *IEEE Transactions on Smart Grid* with the title *Stochastic Strategic Participation of Active Distribution Networks With High-Penetration DERs in Wholesale Electricity Markets* [16]. The contributions in this chapter are as follows:

1. Proposing a stochastic bilevel optimization approach to model and analyze the strategic participation of an active distribution network (ADN) with high penetration of DERs in wholesale markets. The capability of DERs in providing both energy and ancillary services is modeled.

2. Accounting for the availability, flexibility, and uncertainties of DERs in both transmission and distribution systems and market operations. DERs contribute to local voltage regulation in ADN operation while strategically participating in the wholesale market.

3. Analyzing the interactions between ADN and DER operation and the ISO energy and ancillary service markets. The model simulations present the impact of a network-constrained strategic ADN's influence on LMPs and reserve prices in the ISO market.

4. Developing an FEVCS model that represents the V2G and reactive power support capability of aggregated EVs' interaction with the ISO network.

Chapter 4 focused on proposing an AI-based distributed control framework for VVO in FEVCSs. Contributions from this chapter have been submitted to *IEEE Transactions on Smart Grid*, with the paper titled *A Federated Learning-Enhanced Conflict-Aware Multi-Agent Reinforcement Learning Framework for Decentralized Volt-VAR Control in Distribution Networks with Fleet EV Charging Stations*.

The contributions of Chapter 4 are as follows :

1. Introducing a Federated Learning-Enhanced Conflict-Aware Multi-Agent Reinforcement Learning (FLE-CA-MARL) control framework specifically designed for FEV-level collaborative learning within a DN. By enabling decentralized decision-making among FEV agents, the framework ensures that both local voltage regulation and global voltage control are optimized, demonstrating scalability and adaptability across diverse network configurations.

2. Utilizing a novel conflict-aware MARL (CA-MARL) environment is utilized, to model the coordinated reactive-power support of multiple active FEV agents connected within an FEVCS. This mechanism effectively penalizes conflicting, and incorrect actions associated with the reactive power injections, ensuring that the agents collectively contribute to the optimal control of charging in the FEVCS while maintaining local voltage stability, avoiding convergence to suboptimal policies.

3. Incorporating a Partially Observable Markov Decision Process (POMDP) model for an FEV agent, enabling decentralized optimization with limited grid state information, a crucial advancement in managing real-world uncertainty and improving grid stability, as agents make decisions with incomplete knowledge of the overall grid state.

4. Testing the framework across scenarios involving both localized (single FEVCS) and distributed (multiple FEVCSs) agent configurations. These tests validate the framework's effectiveness in coordinating agent actions, ensuring robust voltage regulation and grid stability across varying conditions and load profiles.

Finally, the conclusions derived from the results and analysis of the aforementioned works are compiled in Chapter 5.

In this chapter, the critical role that the FEVCSs can play in enhancing power grid resilience and facilitating market integration has been presented. The increasing transportation electrification and the unique capabilities of FEVCS as a DER offer promising solutions to the challenges faced by the modern power grids. However, the widespread deployment introduces complexities related to optimal siting, grid interactions and handling uncertainties from extreme weather events.

Given the potential of FEVCS, a key challenge remains: how can they be strategically deployed to maximize their benefits to the grid in improving resilience during HILP events? To address this question, the following chapter presents a detailed approach for the optimal deployment of FEVCS on the distribution grid. A two-stage stochastic optimization model that incorporates both the mobility of FEVs and the uncertainties in grid conditions, enabling the FEVCS to enhance grid-service restoration, thus increasing the resilience. This model builds upon the foundation set in Chapter 1 and begins by outlining the strategic deployment of FEVCS in power distribution networks.

CHAPTER 2: STRATEGIC DEPLOYMENT OF FEVCS: A RESILIENCE-ORIENTED APPROACH

2.1 Literature Review & Contributions

In power systems, resilience refers to the ability to recover quickly from disasters, or, more broadly, to anticipate high-impact, low-probability, extraordinary events, recover quickly from these disruptive events, and improve its operations and structure for similar events in the future[27]. This paper focuses on post-disturbance degraded state and restorative state of a high-impact low probability (HILP) event.[28] presents an in-depth literature review of resilience enhancement strategies through EVs. The authors emphasized the need to include EVs in public policies on disaster management. According to [29], coordinated transformation of electricity and transportation systems could enhance the resilience and environmental performance of energy systems. Although battery degradation and warranty issues are the most important integration challenges, creating a market for ancillary services in vertically integrated utility is essential. With the increasing frequency of HILP events, novel ancillary services to support grid restoration while utilizing distributed generators (DGs) and EVs need to be in place to achieve a highly resilient power grid.

The literature on enhancing grid resilience through various operational and planning measures reveals a diversity of approaches, as summarized in Table 2.1. A significant portion of the existing work focuses on strategies like line hardening and DG placement to fortify the grid against HILP events. Operational measures such as network reconfiguration and dynamic microgrid formation are commonly adopted to ensure rapid recovery during disruptions. However, relatively fewer studies have incorporated the mobility and strategic placement of FEVCS within the distribu-

Table 2.1: Comparison between proposed model and different research works on resilience enhancements in distribution networks

	Resilience Enhancement measures							**Optimization Model**	**Resilience Stage**	
	Planning measures			**Operational measures**						
	Line Hardening	**DG**	**Fleet EVCS**	**Network reconfiguration**	**Dynamic Microgrid formation**	**Transportation Network**	**EV Fleet Scheduling**		**Planning**	**Operation**
[17]	×	×	×	×	×	×	×	Stochastic	×	✓
[18]	×	×	×	×	×	×	×	Robust	×	✓
[19]	×	×	×	✓	✓	✓	×	Deterministic	×	✓
[20]	×	×	×	×	×	✓	✓	Stochastic	×	✓
[21]	✓	×	×	×	×	×	×	Stochastic	✓	×
[22]	×	✓	×	×	×	×	×	Stochastic	✓	×
[23]	✓	×	×	×	×	×	×	Stochastic	✓	×
[24]	✓	✓	×	✓	✓	×	×	Stochastic	✓	×
[25]	✓	✓	×	✓	✓	×	×	Stochastic & Risk-based	✓	✓
[26]	×	✓	×	✓	✓	✓	×	Risk-based	✓	×
*	✓	×	✓	✓	✓	✓	✓	Stochastic	✓	×

tion network-a gap this research aims to address. The proposed model stands out by integrating the transportation network into the grid resilience framework, providing a comprehensive approach to mitigating risks associated with both electrical and transportation infrastructure.

Chapter 2 of this dissertation focuses on finding the optimal location of FEVCS to enhance the resilience of the power grid. Building on the comprehensive analysis of existing resilience enhancement strategies, this dissertation makes several key contributions to the field. The following are the contributions of this paper:

1. This study addresses a novel research problem by exploring the optimal placement of FEVCS within a power distribution network. The research aims to enhance grid resilience, considering both the power distribution and the transportation network, a perspective that has been largely unexplored in the existing literature.

2. A two-stage stochastic optimization approach with a mixed integer second order cone programming (MISOCP) model is developed for optimal siting of FEVCSs considering EV mobility and the impact of extreme weather events. The first stage deals with the selection of the most favorable location for FEVCSs, while the second stage minimizes the weighted sum of the VoLL under potential fault scenarios, integrating transportation network considerations into the grid restoration scheme.

3. The study evaluates the influence of renewable-supported BESS on the optimal placement of FEVCS and demonstrates the potential of BESS to improve the flexibility of the grid.

2.2 Problem Statement

The total storage capacity of a fleet of 20 medium or heavy-duty electric vehicles can reach 4-8 MWh. Since most trucks operate less than 5 hours a day [12],such a

fleet can dedicate part of its fleet to provide ancillary services to the grid to enhance the reliability and resilience of the power grid. HILP events such as hurricanes can lead to the failure of distribution network infrastructure, causing power outages in the network. Grid operators now have new options to resolve unplanned outages

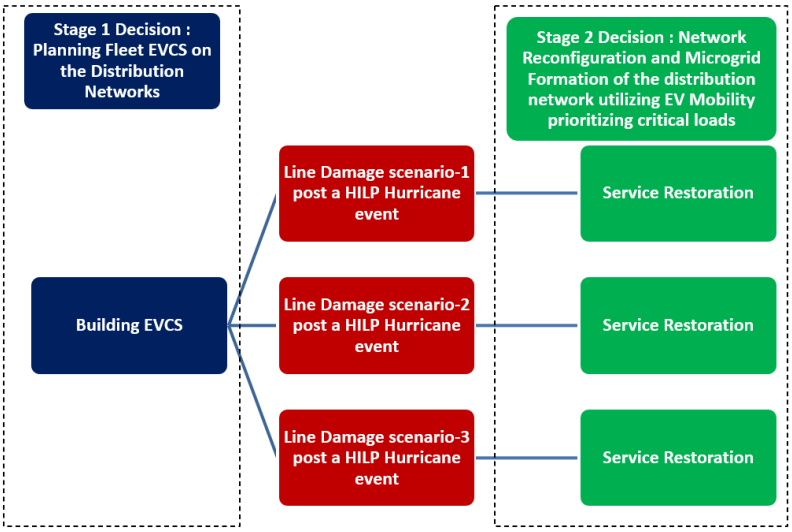

Figure 2.1: Two-stage stochastic optimization model

due to the proliferation of distributed resources on the grid. The utilities monitor significant weather events so that the maintenance team can respond to potential faults in the distribution network. After a weather event has passed, several faults may occur in a power distribution network. These faults can create multiple healthy and faulty sections in the network. A smart grid can use DERs in the network to form microgrids and power the healthy sections of the network. EV fleet storage can be utilized to form and operate islanded networks, minimizing the impact of customer outages. MEVs and HEV fleets can opt to support the grid during HILP events. FEVCSs in strategic locations can enhance the resilience of the power distribution network. The time required by the vehicles to charge and move energy from one node to another should be considered. In this paper, the problem of strategically placing FEVCSs to enhance the resilience of the distribution network is modeled as a two-stage stochastic optimization model. Figure 2.1 presents the proposed two-stage

stochastic optimization model.

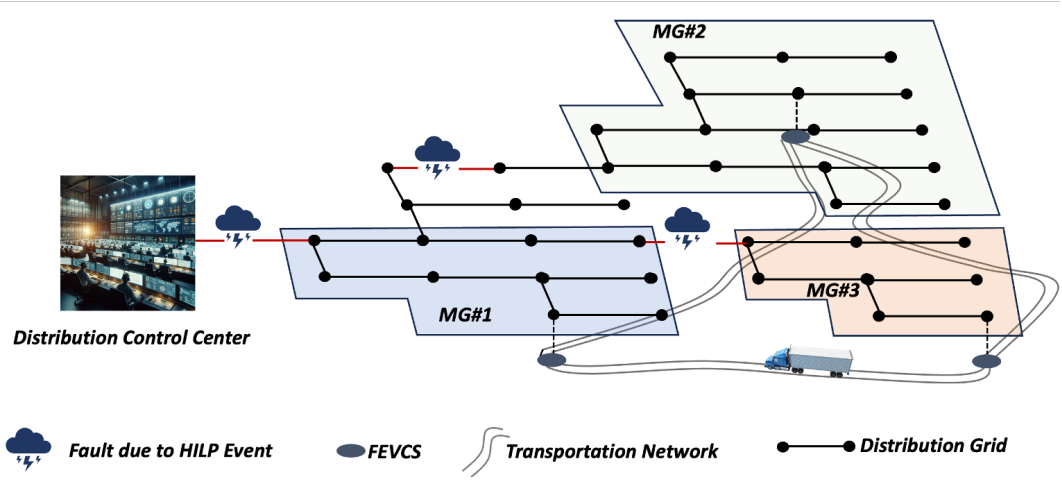

Figure 2.2: Service restoration using DERs

A 3-node transportation network and a 39-node distribution network for the second stage model are represented in Figure 2.2. The figure presents a scenario with faults on three branches. The protection scheme on the distribution network is assumed to isolate faults using reclosers and circuit breakers. With the fault repairs in progress, the next step is to energize the maximum number of nodes. Microgrids can be formed by employing DERs like renewable generators, energy storage, and fleet vehicles. In this problem, fleet vehicles' mobility can be considered using a transportation network. The fleet vehicles can act as BESSs or can move energy from one microgrid to another during grid-service restoration by microgrid formation. In the scenario shown in Figure 2.2, three microgrids are used to power most nodes of the distribution network. There is some flexibility in the node that can be used to power an energy consumer in the real world. The problem addressed in this paper is to find the optimal location to connect FEVCS customers to the grid. Building FEVCSs at strategic locations can improve grid resilience while progressing towards the goal of reducing GHG emissions.

2.2.1 Rationale for Model Selection

Among the various optimization techniques considered in the existing literature, robust optimization models are designed to ensure resilience under the most adverse conditions by focusing on worst-case scenarios. However, this approach often leads to overly conservative decisions, which may not be economically viable. Deterministic models, while offering computational efficiency, fail to account for the inherent uncertainties in power systems, particularly those arising from extreme weather events, making them less suitable for scenarios that require adaptability.

Risk-based models, on the other hand, offer a balanced approach by incorporating risk metrics into the decision-making process. However, these models can be complex to implement and require precise risk quantification, which can be challenging in the dynamic and interconnected environment of grid operations, especially when the exact distribution of risks is difficult to determine.

In contrast, the two-stage stochastic optimization model employed in this research offers a more practical and effective framework for managing uncertainty. This model leverages stochastic scenarios of distribution line failures to simulate the probabilistic nature of such events, thereby capturing a wide range of possible outcomes. The first stage of this model involves making pre-disruption investment decisions, such as the optimal placement of FEVCSs, based on these scenarios. The second stage then adapts these decisions after the actual event occurs, optimizing the response to minimize the cost of load shedding and other disruptions.

By using scenario reduction techniques, this model maintains computational efficiency while retaining the integrity of the risk representation, ensuring that the most critical scenarios are considered without overwhelming computational resources. This combination of scenario-based planning and adaptive decision-making makes the two-stage stochastic model particularly well-suited for addressing the dual challenges of grid and transportation network resilience, providing a balanced and robust solution

in the face of uncertainty.

2.3 Modeling

In this chapter, a stochastic model is presented as a solution to a planning problem aimed at enhancing the resilience of a distribution network. The first stage models the investment decision with options of hardening and placement of FEVCS as methods to improve resilience. In the second stage, a joint grid restoration scheme with network reconfiguration and microgrid formation is modeled in the presence of DGs and fleet vehicles. Investing decisions in the first stage are based on the expected cost of load shedding, weighted by the probability distribution of line damage scenarios for the second stage.

2.3.1 First Stage: Distribution System Planning

The distribution planning model minimizes the investment cost required for the upgrade of the infrastructure. The options for investments to enhance the resilience provided are hardening represented by R_b and installation of FEVCS represented by E_e. In the third term, N_H represents the number of HILP events in a year times the weighted sum based on probability of the objective function of all fault scenarios in the second stage. Eq(2.2) defines the budget limit in investment of infrastructure. (2.3) indicates each EVCS can only be assigned to one bus.

$$min \sum_{b} C_b^R \times R_b + \sum_{e} C_e^E \times E_e + N_H \times \sum_{s} \pi_s \times \rho(s) \tag{2.1}$$

$$\sum_{b} C_b^R \times R_b + \sum_{e} C_e^E \times E_e \leq B \tag{2.2}$$

$$\sum_{e} E_e \leq 1, \ \forall i \tag{2.3}$$

2.3.2 Second Stage : Joint Restoration Scheme

In the event of a natural disaster that affects the grid, there may be line damages in the distribution network and also a failure in supply from the transmission substation. Microgrids play a vital role in grid restoration during this crisis. The grid restoration scheme considered in the model utilizes microgrid formation that uses available DGs and fleet vehicles. The objective function of the joint restoration scheme is to minimize the expected cost of load shedding, Eq. (2.4).

$$\rho(s) = min \sum_{s} \sum_{t} \sum_{i} (VoLL_i \times s^d_{i,t,s}) + \sum_{s} \sum_{t} \sum_{j} (l_{j,t,s} \times r_l) \tag{2.4}$$

$\rho(s)$ represents the objective function, which is a function of scenario s. The objective function minimizes the sum of value of load lost (VoLL) times the load shedding and I^2r losses. $VoLL_i$ represents the VoLL at node i and $p^d_{i,t}$ represents the load at node i. The constraints for the joint restoration scheme are network reconfiguration and microgrid formation constraints, DG constraints, time-space network (TSN) constraints, and fleet vehicle constraints.

2.3.2.1 Network reconfiguration and Radiality constraints

Network reconfiguration constraints define the switching action that segregated the nodes, ensuring the radiality of the microgrids. The binary variable $A_{i,m,s}$ will be 1 if the i-th node belongs to the microgrid $m \in S_M$ in the scenario $s \in S_S$. Here, S_M represents the set of all microgrids and S_S the set of all scenarios considered in the second stage.

$$Ar_{i,s} = \sum_{m=1}^{S_M} A_{i,m,s} \leq 1, \ \forall i, m, s \tag{2.5}$$

The node i can be connected to microgrid m in scenario s if the m-th member of $S_{I_{DG}}$ is selected as the root bus.

$$A_{i,m,s} \leq A_{j,m,s},\ j \in S_{I_{DG}} \forall i, m, s \tag{2.6}$$

The binary variable $O_{l,s}$ is set to zero if two nodes of a distribution line do not belong to the same microgrid. i' represents the index for the terminal bus of line l Eq.(2.7) is linearized utilizing linear methods to eq.(2.9)-(2.11).

$$O_{l,s} \leq A_{i,m,s} \times A_{i',m,s},\ \forall i, i', m, s \tag{2.7}$$

$$O_{l,s} = \sum_{m \in S_M} O_{l,m,s},\ \forall l, s \tag{2.8}$$

$$O_{l,m,s} \leq \sum_{i} A_{i,m,s},\ i \in S_{IB},\ \forall l, m, s \tag{2.9}$$

$$O_{l,m,s} \leq \sum_{i'} A_{i',m,s},\ i' \in S_{TB},\ \forall l, m, s \tag{2.10}$$

$$O_{l,m,s} \geq \sum_{i} A_{i,m,s} + \sum_{i'} A_{i',m,s} - 1, i \in S_{IB}, i' \in S_{TB}\ \forall l, m, s \tag{2.11}$$

Constraints below represents the status of a line and a bus considering damaged lines during scenario generation utilizing the binary variable $F_{l,s}$ and hardening in the first stage controlled by the binary variable R_l. Eq. (2.12) controls the effect of hardening on line damage. Eqs. (2.13) and (2.14) ensure that the health status of

the line and bus generated during the line damage scenario is applied to the model.

$$O_{l,s} \leq 1 - (1 - F_{l,s}) \times (1 - R_l),\ \forall l, s \tag{2.12}$$

$$A_{i,m,s} = A_{i',m,s},\ i \in S_{IB}, i' \in S_{TB} \forall l', LH_{l,s} \neq 0, l, s \tag{2.13}$$

$$A_{i,m,s} \leq BH_{i,s},\ \forall i, m, s \tag{2.14}$$

The radiality of each distribution network is ensured utilizing a necessary and sufficient condition from [30]. The necessary condition requires the number of buses minus the number of branches to be equal to one, which is ensured using constraints (2.15)-(2.17).The sufficient condition is to ensure connectivity of each microgrid which is included in the model employing constraints(2.18)-(2.21).$\kappa_{m,s}$ is a binary variable which is 1 if microgrid m is selected.$\beta_{i,i',l,m,s}$ represents the fictional flow on line l with nodes $i\&i'$.$\beta^{(2)}_{i',m,s}$ represents fictional supply of master DG m .

$$\sum_i A_{i,m,s} \leq M \times \kappa_{m,s},\ \forall l, s \tag{2.15}$$

$$\kappa_{m,s} \leq M \times \sum_i A_{i,m,s},\ \forall l, s \tag{2.16}$$

$$\sum_l O_{l,m,s} = \sum_i A_{i,m,s} - \kappa_{m,s},\ \forall l, s \tag{2.17}$$

$$\sum_{i \in S_{TB}} \sum_l \beta^{(1)}_{i,i',l,m,s} - \sum_{i \in S_{IB}} \sum_l \beta^{(1)}_{i,i',l,m,s} = A_{i',m,s}\ , i' \neq S_{I_{DG}} \forall m, s \tag{2.18}$$

$$\sum_{i\in S_{TB}}\sum_{l}\beta^{(1)}_{i,i',l,m,s}-\sum_{i\in S_{IB}}\sum_{l}\beta^{(1)}_{i,i',l,m,s}=-\beta^{(2)}_{i',m,s}\,,i'=S_{I_{DG}}\forall m,s \tag{2.19}$$

$$-O_{l,m,s}\times M\leq\beta^{(1)}_{i,i',l,m,s}\leq O_{l,m,s}\times M,\ i\in S_{TB},i'\in S_{IB}\forall l,m,s \tag{2.20}$$

$$A_{i',m,s}\leq\beta^{(2)}_{i',m,s}\leq M\times A_{i',m,s},i'\in S_{I_{DG}}\forall m,s \tag{2.21}$$

2.3.2.2 DG constraints

DGs are utilized by microgrids as the primary source of energy during restoration to reduce the load shedding.Constraints (2.22)-(2.24) models the active, reactive and apparent power of limits of DGs.

$$0\leq P^{DG}_{g,t}\leq P^{DG,max}_{g} \tag{2.22}$$

$$Q^{DG,min}_{g}\leq Q^{DG}_{g,t}\leq Q^{DG,max}_{g} \tag{2.23}$$

$$\left\|P^{DG}_{g,t}\ \ Q^{DG}_{g,t}\right\|\leq S^{DG,max}_{g} \tag{2.24}$$

2.3.2.3 Time-space network constraints

TSN model is utilized to represent the movement of fleet vehicles along the grid during a disaster.The binary variable $G_{f,ee',t}$ is 1 if the vehicle f is on an arc from FEVCS e to e' during time t. The constraint (2.25) models movement during a period of time. Eq. (2.26) models the relationship between the state of a vehicle and the

progression of time. Eq. (2.27) defines the initial position of the vehicles.

$$G_{f,ee',t} = 1,\ \forall f \in S_F, t \in T \tag{2.25}$$

$$\sum_{(m,e')\in K_m^-} G_{f,ee',t} = \sum_{(m,e')\in K_m^+} G_{f,ee',t+1},\ \forall f \in S_F, e \in S_{EVCS} \cup S_V, t \in T \tag{2.26}$$

$$\sum_{(m,e')\in K_m^+} G_{f,ee',1} = G_{f,e}^0,\ \forall f \in S_F, e \in S_{EVCS} \cup S_V \tag{2.27}$$

2.3.2.4 Operational constraints of fleet vehicles

If $E_{e,s}$ is a binary variable which represents the choice to build an FEVCS at the candidate location node e, $\gamma_{e,s}$ is the binary variable that represents an active node during microgrid formation with an FEVCS installed at the node e. Eq.(2.28) is linearized using eq(2.29)-(2.31).

$$\gamma_{e,s} = Ar_{e,s} \times E_{e,s},\ \forall e, s \tag{2.28}$$

$$\gamma_{e,s} \leq Ar_{e,s},\ \forall e, s \tag{2.29}$$

$$\gamma_{e,s} \leq E_{e,s},\ \forall e, s \tag{2.30}$$

$$\gamma_{e,s} \geq E_{e,s} + A_{e,s} - 1,\ \forall e, s \tag{2.31}$$

Similarly, $\alpha_{f,e,t,s}$ connects the active EVCS node to the fleet vehicle's movement along the grid. $G_{f,ee,t,s}$ represents the active arc ee of the fleet vehicle f at a time t in the scenario, s which means that the vehicle is connected to node e of the time-space network. The constraint (2.32) is linearized using equations (2.33)-(2.35).

$$\alpha_{f,e,t,s} = \gamma_{e,s} \times G_{f,ee,t,s},\ \forall f, s \tag{2.32}$$

$$\alpha_{f,e,t,s} \leq \gamma_{e,s},\ \forall f, s \tag{2.33}$$

$$\alpha_{f,e,t,s} \leq G_{f,ee,t,s},\ \forall f, s \tag{2.34}$$

$$\alpha_{f,e,t,s} \geq G_{f,ee,t,s} + \gamma_{e,s} - 1,\ \forall f, s \tag{2.35}$$

The charging and discharging of fleet vehicles are represented by the constraints (2.36)-(2.47).Constraints (2.36) and (2.37) restrict the charging and discharging of fleet vehicles to happen only at an active node with FEVCS when the vehicle is on the arc $e - e$. Constraints (2.38)-(2.40) control the charge mode of the vehicle to be charging or discharging over a period of time. The constraint (2.41) defines a single variable that represents the power transfer of the fleet vehicle. The constraint (2.42) represents the apparent power limit of the fleet vehicles.

$$0 \leq P^{FV,ch}_{f,e,t,s} \leq \alpha_{f,e,i,s} \times P^{EVCS,max}_{e},\ \forall f, t, s \tag{2.36}$$

$$0 \leq P^{FV,dch}_{f,e,t,s} \leq \alpha_{f,e,i,s} \times P^{EVCS,max}_{e},\ \forall f, t, s \tag{2.37}$$

$$0 \leq P_{f,e,t,s}^{FV,ch} \leq Y_{f,t,s}^{ch} \times P_{e}^{EVCS,max},\ \forall f,t,s \tag{2.38}$$

$$0 \leq P_{f,e,t,s}^{FV,dch} \leq Y_{f,t,s}^{dch} \times P_{e}^{EVCS,max},\ \forall f,t,s \tag{2.39}$$

$$Y_{f,t,s}^{dch} + Y_{f,t,s}^{ch} \leq \alpha_{f,e,i,s},\ \forall f,t,s \tag{2.40}$$

$$P_{f,e,t,s}^{FV} = \frac{P_{f,e,t,s}^{FV,dch}}{\eta^{dch}} - \eta^{dch} P_{f,e,t,s}^{FV,ch},\ \forall f,t,s \tag{2.41}$$

$$\left\| P_{f,e,t,s}^{FV}\ \ Q_{f,e,t,s}^{FV,dch} \right\| \leq \alpha_{f,e,i,s} \times S_{f}^{EVCS,max} \tag{2.42}$$

The constraints related to the SOC of the fleet vehicles modeled in (2.43)- (2.47). Constraint (2.43) defines the relationship of the initial SOC of the EV with the SOC of hour 2 which is activated by $\alpha_{f,e,t,s}$. The constraint (2.44) defines the relationship of the SOC of the EV when t is not equal to 1. The relationship between the SOC of the EV when the EV is not connected to an FEVCS is shown in (2.45) and (2.46). The upper and lower limit of the SOC of EV is defined in constraint (2.47).

$$-M \times (1 - \alpha_{f,e,t,s}) \leq SOC_{Initial}^{FV} - SOC_{f,t,s}^{FV} - \frac{\Delta T}{Batt_{f}^{FV,cap}} \times P_{f,e,t+1,s}^{FV} \leq$$

$$M \times (1 - \alpha_{f,e,t,s}),\ \forall f, t = 1, s \tag{2.43}$$

$$-M \times (1 - \alpha_{f,e,t,s}) \leq SOC^{FV}_{f,t-1,s} - SOC^{FV}_{f,t,s} - \frac{\Delta T}{Batt^{FV,cap}_{f}} \times P^{FV}_{f,e,t+1,s} \leq M \times (1 - \alpha_{f,e,t,s}),\ \forall f, t \neq 1, s \tag{2.44}$$

$$-M \times \sum_{e} \alpha_{f,e,t,s} \leq SOC^{FV}_{Initial} - SOC^{FV}_{f,t,s} - \frac{\Delta T}{Batt^{FV,cap}_{f}} \times P^{FV}_{f,e,t+1,s} \leq M \times \sum_{e} \alpha_{f,e,t,s},\ \forall f, t = 1, s \tag{2.45}$$

$$-M \times \sum_{e} \alpha_{f,e,t,s} \leq SOC^{FV}_{f,t-1,s} - SOC^{FV}_{f,t,s} - \frac{\Delta T}{Batt^{FV,cap}_{f}} \times P^{FV}_{f,e,t+1,s} \leq M \times \sum_{e} \alpha_{f,e,t,s},\ \forall f, t \neq 1, s \tag{2.46}$$

$$SOC^{min}_{f} \leq SOC_{f,t+1,s} \leq SOC^{max}_{f},\ \forall f, t, s \tag{2.47}$$

2.3.2.5 Power flow constraints

Nodal active power balance is modeled using constraint (2.48). Since in the equation (2.48) $p^{FV}_{f,e,t,s}$ is the product of $P^{FV}_{f,e,t,s}$ and $\alpha_{f,e,t,s}$,we use the constraints (2.49)-(2.51) to linearize the equation. The constraint (2.52) and (2.53) defines decision variables for switchable loads. The constraint (2.54) defines a decision variable to represent the load shedding at each node in each scenario.

$$\sum_{i \in N1(j)} (p_{ij,t} - l_{ij,t} r_{ij}) - \sum_{k \in N2(j)} p_{jk,t} + \sum_{m \in S_M} \left[\sum_{g \in S_G} P^{DG}_{g,t} + \sum_{f \in S_{FV}} p^{FV}_{f,e,t,s} - p^{d}_{j,t} \right] = 0 \tag{2.48}$$

$$p^{FV}_{f,e,t,s} \leq P^{EVCS,max}_{e},\ \forall f,t,s \tag{2.49}$$

$$p^{FV}_{f,e,t,s} \leq P^{FV}_{f,e,t,s},\ \forall f,t,s \tag{2.50}$$

$$p^{FV}_{f,e,t,s} \geq P^{FV}_{f,e,t,s} - P^{EVCS,max}_{e},\ \forall f,t,s \tag{2.51}$$

$$p^{d}_{j,t} = Ar_{j,s} \times P^{d}_{j,t},\ \forall j,t,s \tag{2.52}$$

$$q^{d}_{j,t} = Ar_{j,s} \times Q^{d}_{j,t},\ \forall j,t,s \tag{2.53}$$

$$s^{d}_{j,t} = P^{d}_{j,t} - p^{d}_{j,t},\ \forall j,t,s \tag{2.54}$$

Similarly, nodal reactive power balance is modeled using the constraint (2.55) which is linearized by (2.56)-(2.58) to linearize the equation.

$$\sum_{i \in N1(j)} (q_{ij,t} - l_{ij,t}x_{ij}) - \sum_{k \in N2(j)} q_{jk,t} + \sum_{m \in S_M} \left[\sum_{g \in S_G} Q^{DG}_{g,t} + \sum_{f \in S_{FV}} q^{FV}_{f,e,t,s} - q^{d}_{j,t} \right] = 0 \tag{2.55}$$

$$q^{FV}_{f,e,t,s} \leq Q^{EVCS,max}_{e},\ \forall f,t,s \tag{2.56}$$

$$q^{FV}_{f,e,t,s} \leq Q^{FV,dch}_{f,e,t,s},\ \forall f,t,s \tag{2.57}$$

$$q^{FV}_{f,e,t,s} \geq Q^{FV,dch}_{f,e,t,s} - Q^{EVCS,max}_{e},\ \forall f,t,s \tag{2.58}$$

The upper and lower limits for nodal voltages of active nodes are modeled using (2.59). The voltages of the master DGs are set using the constraint (2.60). The nodal voltage drop constraints bounded by the Big-M method are modeled using the (2.61).The relation between power flow, current, and voltage is defined using (2.62). The constraint (2.63) is used to model the limits of branch current flow in the distribution network. Constraints (2.64) and (2.65) model the active and reactive power flow through the closed branches of the distribution network.

$$A_{i,m,s} \times (V_{(i,min)})^2 \leq u_{i,t} \leq A_{i,m,s} \times (V_{(i,max)})^2,\ \forall i,t,s \tag{2.59}$$

$$u_{i,t} = A_{i,m,s} \times (V^{DG,set}_{m})^2,\ \forall i \in S_{I_{DG}}, \forall i,t,s \tag{2.60}$$

$$-M \times (1 - O_{l,s}) \leq u_{i,t,s} - u_{j,t,s} - 2(r_{ij}p_{ij,t} + x_{ij}q_{ij,t}) + ((r_{ij})^2 + (x_{ij})^2)l_{ij,t} \leq M \times (1 - O_{l,s}),\ \forall l,t,s \tag{2.61}$$

$$\|2p_{ij,t}\ \ 2q_{ij,t}\ \ (l_{ij,t} - u_{i,t})\| \leq (l_{ij,t} + u_{i,t}) \tag{2.62}$$

$$0 \leq l_{l,t,s} \leq O_{l,s} \times (I^{Max})^2, \ \forall l, t, s \tag{2.63}$$

$$-O_{l,s} \times (p_{ij}^{Max}) \leq p_{ij,t,s} \leq O_{l,s} \times (p_{ij}^{Max}), \ \forall i, t, s \tag{2.64}$$

$$-O_{l,s} \times (q_{ij}^{Max}) \leq q_{ij,t,s} \leq O_{l,s} \times (q_{ij}^{Max}), \ \forall i, t, s \tag{2.65}$$

Model of BESS used in [31] was used to represent the behavior of BESS during grid service restoration.

2.3.3 Scenario Generation & Reduction

It is clear from Figure 2.1 that distribution network's line damage scenarios post an HILP event links the first stage to the second stage of the model. Since hurricanes are addressed in the problem, wind speed data from [32] was utilized to feed into a custom PDF sampler and reconstructor from [33]. This custom-pdf reconstructor was utilized to generate wind speeds to generate hurricane wind speeds. Fragility functions from [24] were employed to generate 100 line damage scenarios. [34] was used to reduce the 100 scenarios to 3 scenarios.

2.4 Numerical Results

2.4.1 Feeder & Case Description

The model was tested on a modified IEEE-33 node distribution network and a 4-node transportation network. The feeder has residential load connected to nodes 1-22, commercial load from nodes 22-33, and a hospital load at node 30. Figure 2.4 shows the load profiles utilized for the different load types. The loads and VoLL for

all the nodes in the case are shown in Figure 2.5. The 33-node network is divided into 4 zones shown as Z1, Z2, Z3, and Z4 in Figure 2.3.The distributed generation available in the network includes three solar farms and a conventional gas generator of 1 MW each at nodes 18, 22, 25, and 33, respectively. A candidate node was selected from each zone as a potential FEVCS location. nodes 18,22, 25, and 33 were selected as the search window for the optimal location of the FEVCS. The fault is assumed to be active for 8 hours. During a fault, it is assumed that the upstream substation does not provide power to the network. The FEVCS is assumed to have more than three charging ports available to support grid restoration. Only three representative EVs are considered in all cases. A representative EV can be considered as several FEVs with the same routing behavior. This assumption is to incorporate the variation of usable EV storage with minimum computational load. The size of the chargers can be varied to incorporate the increase or decrease in usable EV storage. The considered FEVCS is made up of 125 kW capacity chargers. Vehicles are considered to have usable storage of 300 kWh each. Six fleet vehicles are considered available for grid restoration. To reduce the computational load, two fleet vehicles are considered to follow the same behavior. Thus, the representative EV considered for the base cases has a storage of 600 kWh and a charger rating of 250 kW. Cases 0,1, and 2 are cases with zero, one, and two FEVCS on the distribution network, respectively.The above cases do not have any BESS in the network. Cases 3, 4, and 5 are cases with zero, one, and two FEVCS with solar farms supported by BESS.

2.4.2 Simulation Results & Analysis

Results from scenario-2 of the three scenarios considered in the second stage are presented in this section. The faults in scenario 2 are on branches 16-17, 17-18, 21-22, 6-26, 9-15, and 22-12. The model's response to these faults for Case-0 is shown in Figure 2.6. The conventional generator is only capable of supporting loads on nodes 18 and 26-33.

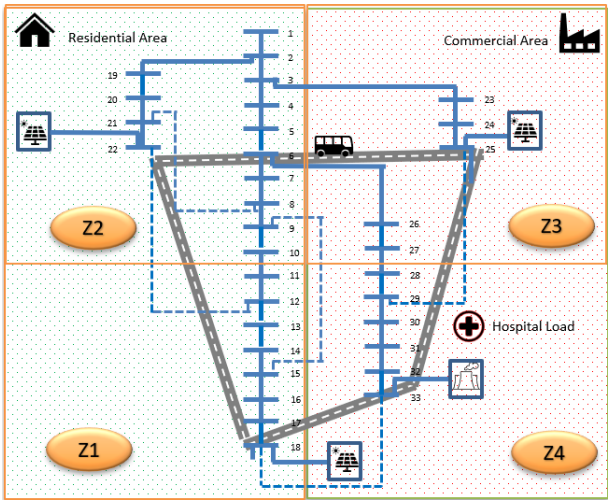

Figure 2.3: 4-node transportation and 33- distribution network of the test case

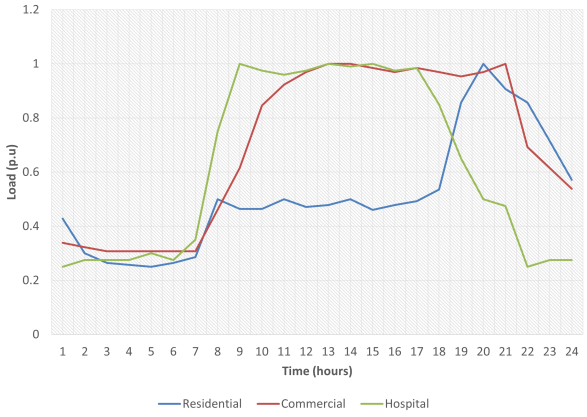

Figure 2.4: Load profiles for different load types

2.4.2.1 Case-1: Optimal location of the FEVCS

The optimal location of the first FEVCS for the presented network is node 25. As shown in Figure 2.7a, nodes 18 and 25-33 are active during the fault. Since there are no other EVCSs in this case, node 25 was selected as the FEVCS can act as energy storage to power node 25. Node 25 was added to the active grid because the VoLL of the nodes in Zones Z3 and Z4 is higher. Figure 2.7b shows the generation, load and V2G during the fault. The SOC of the fleet vehicles and the power of V2G is shown in Figure 2.7c. In the next subsection, the model solves the problem of second-best location for FEVCS of the network in the presence of a FEVCS at node 25.

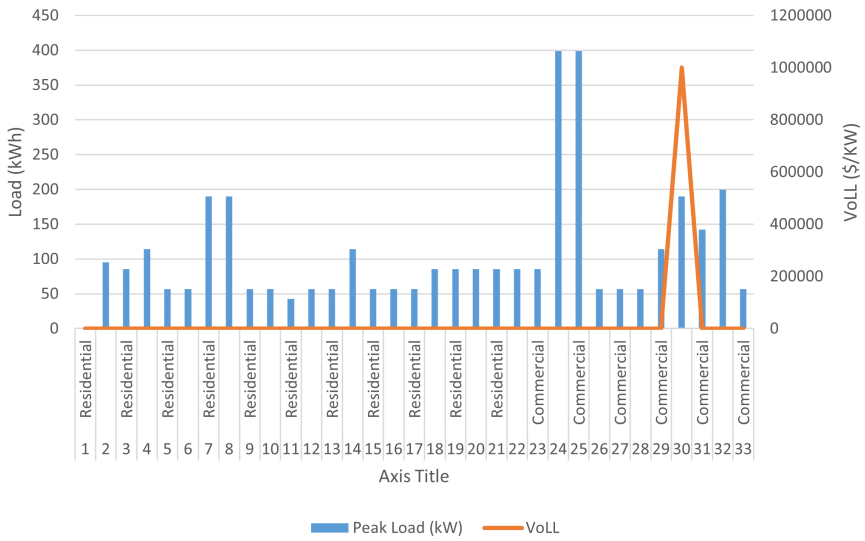

Figure 2.5: Load and VoLL for different nodes

2.4.2.2 Case 2: Second-best locations for FEVCS

The second-best location of the FEVCS is estimated to be at node 22. In this case, FEVCSs at nodes 22 and 25 act as energy storage for the grid. Compared to case-1, one more node is active in the network, reducing the VoLL of case-1. The mobility of the fleet vehicles is presented in the Table 2.2. The Fleet vehicle EV#1 is not used for restoration during the hours 14:00â16:00, the vehicle is located at node 3 of the transportation network which overlaps with the distribution network at node 25. From Figure 2.8b, it is clear that EV#1 is used from hour 18:00 to 21:00 during which the storage of EV#1 reduces to the minimum value. The mobility of the vehicles is utilized by the model for vehicles EV#2 and EV#3. The demand to keep up Microgrid-3 controlled by the DG at node 25 is higher than the demand in Microgrid-2 controlled by node 22. Therefore, the model uses EV#3 at node 25 for hours 16:00 and 17:00 and then sends EV#3 to node 22 since the available storage cannot provide sufficient energy to node 25. Then EV#2 with higher storage is utilized to energize node 25 to provide sufficient energy to manage the supply demand balance of the presented configurations.

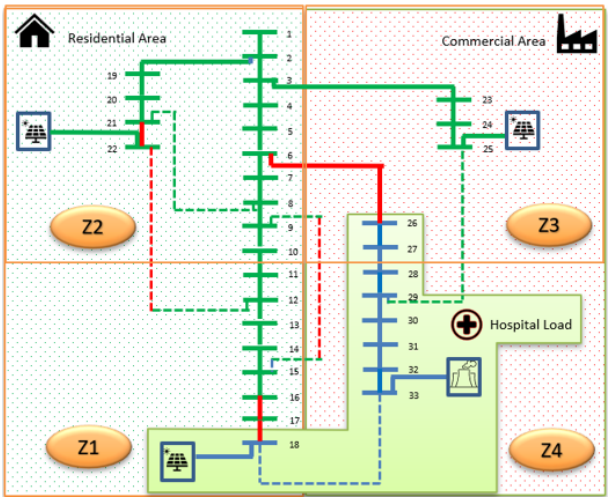

Figure 2.6: Grid service restoration in fault Scenario-2 Case-0

Table 2.2: Mobility of fleet vehicles in the transportation network-Case 2

Time	**15:00**	**16:00**	**17:00**	**18:00**	**19:00**	**20:00**	**21:00**
EV#1	2-3	3-2	2-3	*3-3*	*3-3*	*3-3*	*3-3*
EV#2	1-1	1-2	**2-2**	**2-2**	2-3	**3-3**	**3-3**
EV#3	4-3	**3-3**	**3-3**	3-2	**2-2**	**2-2**	**2-2**

2.4.2.3 Impact of BESS on the FEVCS Location

BESS of 1 MW capacity and 2.5 MWh storage was added to all solar farms in Cases 0, 1 and 2 to obtain Cases 3, 4, and 5. The network configuration of the restored grid is presented in Figure 2.9. The active nodes in the restored distribution network have increased from Case-2. In Case 4, the model solved the optimal location of FEVCS in the presence of renewables backed by BESS. The optimal location of the FEVCS is node 25 in the distribution network. It is clear from Figure 2.10a that when compared to Case-3, Case-4 adds node 24 and sheds node 26. node 24 has a higher VoLL compared to node 26 due to the commercial load capacity on node 26. Compared to Case 2, EV#1 and EV#2 charge when there is surplus energy during some hours to support the grid during other hours. As shown in Figure 2.10b, EV#1

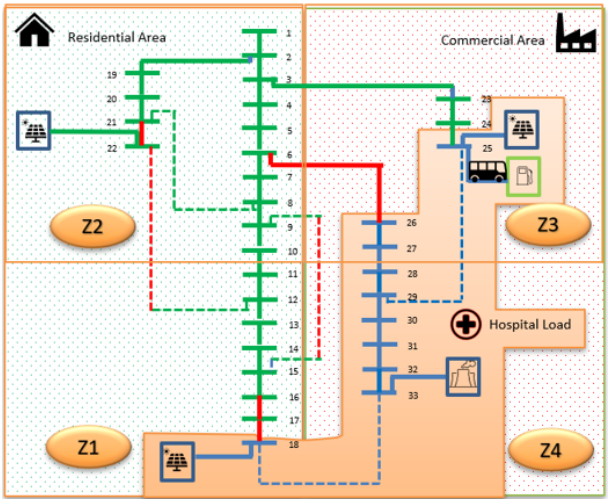

(a) Grid service restoration

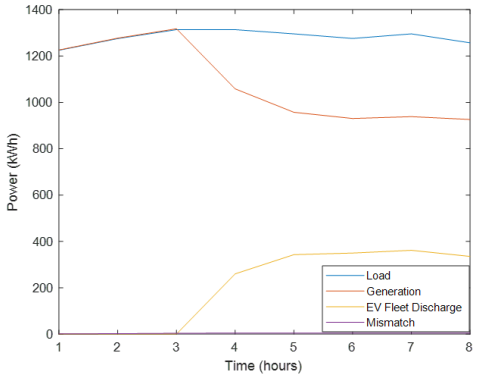

(b) Generation-load balance in Microgrid 3 with optimal EVCS

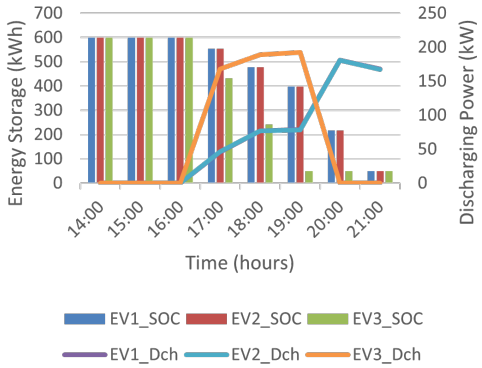

(c) Variation of SOC & charging power of FEVs

Figure 2.7: Results for fault Scenario-2 Case-1

discharges during hour 17:00, charges during hour 18:00, and discharges during hours 19:00â21:00. Adding BESS for the solar farm at node 25 has provided the network with this flexibility compared to Case 2.

The model solved the problem in case 5 for the best two locations for FEVCS on the presented network in the presence of renewables backed by BESS, with a MIP GAP of 0.13%. The best two locations for the FEVCSs are node 25 and node 22. In comparison to Case-4, Case-5 powers a lower number of nodes because the model prioritizes loads with higher VoLL in Case-5. Both microgrids have one FEVCS each. The configuration after service restoration of the distribution network in Case 5 is

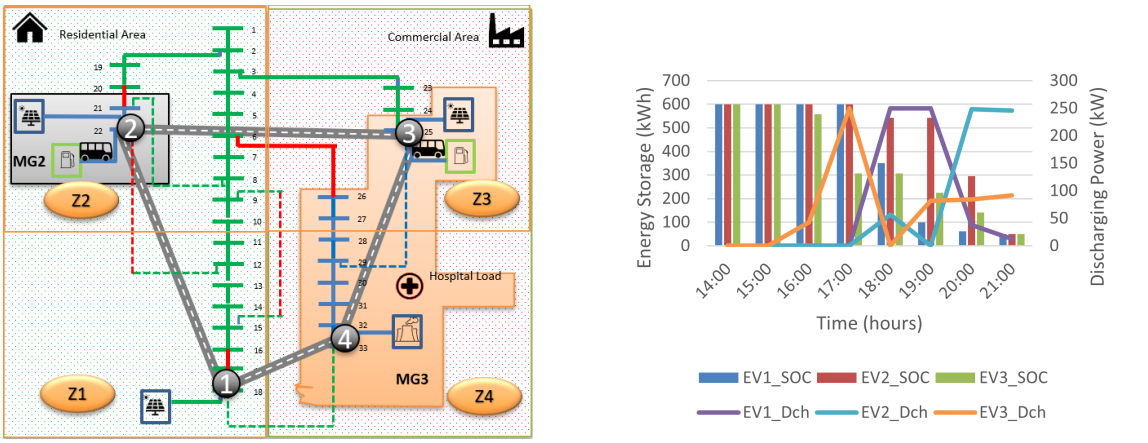

(a) Grid service restoration

(b) Variation of SOC & charging power of FEVs

Figure 2.8: Results from fault Scenario-2 Case-2

shown in Figure 2.11. Table 2.3 shows the mobility and variation of SOC of the EVs. EV#1 is called to node 3 at 16:00. At 17:00 hour, EV#1 is in the Arc 3-3 of the TSN, indicating that EV #1 is connected to node 3 of the transportation network, which is node 25 of the power distribution network. EV#1 discharges at the hours 17:00 and 18:00 supporting MG#3. At hour 19:00, EV#1 is called to node 2 to support MG#2 in hours 20:00 and 21:00. EV#2 is called to node 25 at 15:00. EV#2 discharges at node 25 to support MG#3 and is called to node 22 to charge from MG#2 at hour 18:00. EV#2 goes back to node 25 during hour 19:00 and supports Microgrid MG#3 in hours 20:00 and 21:00. EV#2 transports energy from the MG#2 to MG#3 to power more critical loads on MG#2. Similarly, EV#3 is called to node 22 in hour 14:00. EV#3 supports MG#2 during hour 15:00, recharges during hour 16:00 and supports MG#3 during hours 18:00-20:00. Figure 2.12 shows the variation of the objective function for all cases. Adding BESS to the mix has increased the impact of FEVCS in improving the objective function.

2.4.3 SOCP Relaxation Gap & Simulation Setup

The accuracy of SOCP relaxation was tested to compare the power flow obtained from conic relaxation with the original non-convex model by evaluating the relaxation

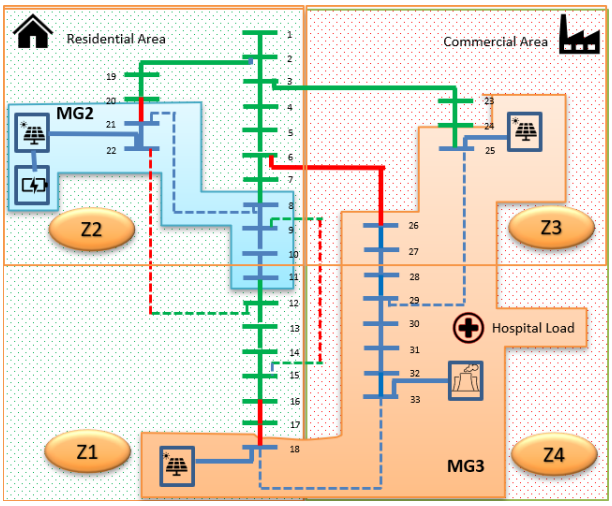

Figure 2.9: Grid service restoration in fault Scenario-2 Case-3

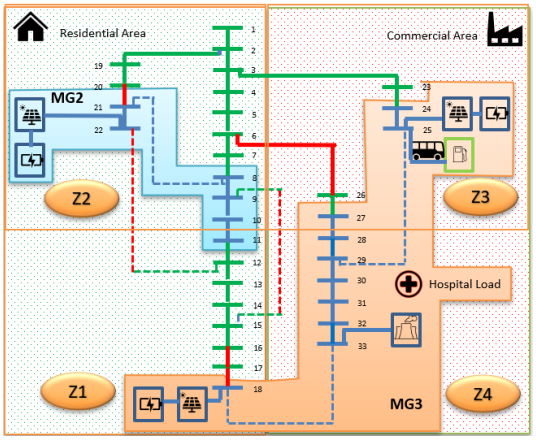

(a) Grid service restoration

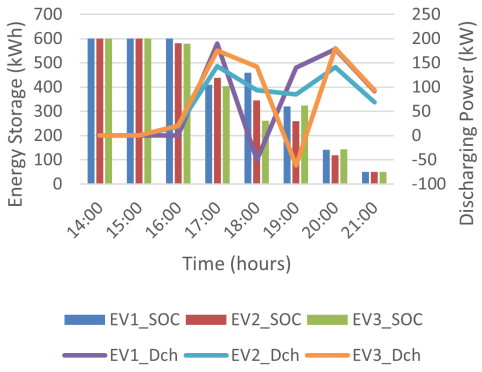

(b) Variation of SOC & charging power of FEVs

Figure 2.10: Results for fault Scenario-2 Case-4

error defined as

$$Gap = max_{\forall(i,j)} \left| p_{ij}^2 + q_{ij}^2 - (l_{ij} u_i) \right| \tag{2.66}$$

The SOC gap for the case is in the order of 10^{-9} MW. Simulations were carried out on an Apple Macbook with an Apple M2 Pro CPU, 12 cores, and 32 GB RAM. The problem was modeled utilizing MATLAB with YALMIP and Gurobi. The MIP GAP and the solution time of all simulated cases are shown in Table 2.4.

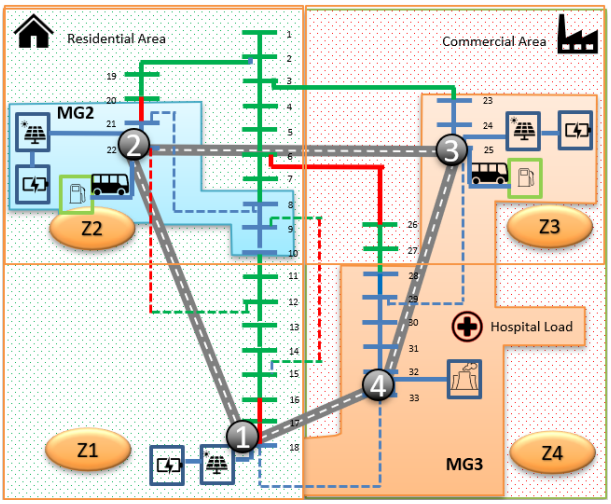

Figure 2.11: Grid service restoration in fault Scenario-2 Case-5

Figure 2.12: Objective function of Cases 0 -5

2.5 Comparing Computational Complexity

2.6 Conclusion & Future Works

The present study provides a comprehensive assessment of a two-stage stochastic model for optimizing the location of FEVCS within a distribution network. This innovative approach aims to improve network resilience and reliability, particularly during operational faults or disaster management scenarios. The model was thoroughly tested on a modified IEEE-33 node distribution network and a 4-node transportation network, which included various types of loads and distributed generators.

Table 2.3: Mobility & SOC of fleet vehicles in the transportation network-Case 5

Time	**15:00**	**16:00**	**17:00**	**18:00**	**19:00**	**20:00**	**21:00**
EV#1	*1-4*	*4-3*	**3-3**	***3-3***	***3-2***	***2-2***	***2-2***
EV1_SOC	600.0	600.0	**350.0**	**100.0**	100.0	**81.8**	**56.3**
EV#2	*2-3*	**3-3**	***3-2***	**2-2**	***2-3***	**3-3**	**3-3**
EV2_SOC	600.0	350.0	350.0	555.8	555.8	305.8	55.8
EV#3	**2-2**	**2-2**	*2-3*	**3-3**	**3-3**	**3-3**	*3-4*
EV3_SOC	513.3	600.0	600.0	427.6	216.8	50.0	50.0

Table 2.4: MIP gap & solution time

Case	**MIP GAP**	**Solution Time (hours)**
0	0	0.004
1	0	0.261
2	0.001	17.534
3	0	0.597
4	0.078	55.437
5	0.13	70.579

The optimal location of the FEVCS, as identified by the model, was at node 25. This node was selected due to its potential to act as energy storage for powering the node and its influence on zones Z3 and Z4 with higher VoLL. Furthermore, the second-best location was determined to be node 22, which added an active node to the network and reduced VoLL compared to the first case. This scenario also showed a strategic utilization of the mobility and storage capabilities of the fleet vehicles, providing energy supply demand balance.

In addition, renewable generators supported by BESS were also considered. The model demonstrated an increased number of active nodes in the restored distribution network, with the optimal FEVCS location remaining at node 25. The presence of the BESS allowed for greater flexibility in the network, allowing the vehicles to charge during periods of surplus energy and support the grid during other hours. When two FEVCS were present alongside BESS-backed renewables, the model prioritized loads

with higher VoLL, resulting in powering a fewer number of nodes, but catering to more critical loads.

The proposed stochastic model presents a potential path for strategic planning and optimization of FEVCS in a distribution network, enhancing the resilience and reliability of the network. The results highlight the valuable role of FEVCS, particularly when combined with BESS, in responding to network faults and managing supply demand balances. Future work may further explore other factors that influence the model and test the model on larger or more complex network configurations.

While the strategic deployment of FEVCS has demonstrated clear benefits in enhancing grid resilience, it is critical to recognize that these charging stations, due to their bidirectional energy transfer capabilities, can also serve as active market participants in the electricity markets. Chapter 3 will expand upon this by exploring how FEVCS, integrated with other DERs, can strategically influence the wholesale energy and reserve markets. This not only emphasizes the technical capabilities, but also highlights the economic and operational impacts of these systems in market dynamics.

CHAPTER 3: AGGREGATING FLEET EVS TO PROVIDE ENERGY AND ANCILLARY SERVICE IN WHOLESALE MARKETS

Building on the foundation laid in the previous chapter regarding the resilience benefits of strategically deploying FEVCS, this chapter shifts focus to modeling FEVCS providing energy and ancillary services in the wholesale markets. FEVCS, when aggregated with other DERs, offers unique opportunities to engage in wholesale markets, leveraging their ability to provide energy and ancillary services. This chapter will examine how FEVCS, as a part of DER aggregators, can contribute to grid stability and play a strategic role as price-makers in the energy and reserve markets.

The growing demands for energy and the awareness of the environment have accelerated the worldwide adoption and deployment of renewable energy generation. This transformation has catalyzed the augmentation of DERs such as distributed solar and wind, energy storage systems (ESS), and FEVCS. With the integration of DERs, the role of traditional distribution networks as Load Serving Entities (LSEs) that purchase energy from the wholesale electricity markets is evolving toward ADNs, which can be proactive market players in the ISO market to buy and sell energy and ancillary services.

FEVCSs are unique DERs that are highly dense in terms of power and energy, offering the bidirectional energy transfer capability of the grid through V2G services. Additionally, they can provide reactive power support and ancillary services. This flexibility enables aggregated FEVCS to influence market prices in the day-ahead ISO energy and reserve markets. With FERC Order 2222 allowing DERs to participate alongside traditional generators, FEVCS can no longer be viewed solely as passive consumers, but as active price-makers (PMs) capable of bidding strategically.

This chapter explores how FEVCS, as a part of DER aggregation, can act strategically in the ISO day-ahead energy and reserve market. A stochastic bi-level optimization framework is proposed to model the ADN's interaction with the ISO market, focusing on price-making capabilities and ancillary service provision by FEVCS. The reactive power support and market flexibility provided by the FEVCS not only enhances market participation, but also contributes to the stability of the ADN, addressing critical challenges in both market economics and operational resilience.

3.1 Literature Review & Contributions

The strategic behavior of an individual DER has the least impact on the electricity market because of its relatively small size compared to conventional generators connected to the transmission system. Aggregation of DERs can allow market players at the distribution level to strategically influence the market prices. Research related to aggregated DERs has emerged lately. Some existing works have modeled an ADN as a price-taker in the wholesale market, which aims to maximize its profit by responding to market prices set by the ISO. Asimakopoulou et al. proposed a bilevel optimization model in [35] to maximize the economic benefits of DER aggregation that increase with the flexibility of load. [36] investigated the optimal operation of distribution companies (DisCos) in a competitive electricity market. The results indicate that DisCo operates optimally by varying DER outputs according to market prices. Sarkhani et al. [37] analyzed the impact of distributed generation (DG) and interruptible load (IL) on strategic bidding of a DisCo in the day-ahead market. [38] models the optimal bidding strategy of a DER aggregator in a day-ahead energy market in the presence of flexible demand as a stochastic mixed-integer linear programming (MILP) problem. A bidding strategy for microgrids in joint energy, reserve and regulation market is presented in [39]. In [40], a stochastic framework for DisCo's decision-making in day-ahead and real-time market is presented. [41] modeled distribution networks with DERs as a virtual power plant (VPP) for integration with the

existing power grid. Strategic bidding of a VPP as a price-taker in the day-ahead and real-time market is modeled as a two-stage problem in [42]. A VPP is modeled as a service-centric aggregator which can provide ancillary services on demand from the ISO in [43]. A conditional value-at-risk (CVaR) based model for electricity purchase decisions of retailers in day-ahead market was presented in [44]. The aforementioned models treat DER and distribution networks as a price-taker to maximize the aggregator profit by responding to market prices. However, as DER penetration is increasing, recent work has identified that an ADN can influence the day-ahead energy and reserve market prices of the ISO market. It can also provide ancillary services requested by the ISO[45, 46, 47, 48]. Uncertainty of renewable energy sources have been incorporated in generation dispatch models in [49, 50, 51, 52, 53]. In [54], Li et al. presented a price-maker model for DisCo in the wholesale energy market. In [55], the strategic bidding of DisCo in day-ahead and real-time markets was modeled by Zhang et al. Bahramara et al. in [56] has modeled the strategic behavior of a DisCo in wholesale energy and reserve market as a bilevel problem. It considers the DisCo as a strategic player; however, it fails to consider the network models and operation constraints of distribution and transmission systems thus cannot reflect the network congestion, voltage conditions, and market prices at different locations and cannot guarantee the system operational security. A strategic bidding model for the ADN as a price-maker in the ISO energy and reserve market was proposed in [57].

With more DERs being integrated into distribution networks, ADNs will play a more important role in the future power grid operation and markets. In this chapter, a stochastic bilevel optimization approach to model and analyze the strategic participation of an ADN and its DERs to provide energy and ancillary services in the wholesale electricity markets is proposed. To explore the ADN's potential as a price-maker in the day-ahead ISO market, ADN is modeled as the upper-level model. Hence, ISO day-ahead energy and reserve market clearing problem is modeled as the

lower-level problem. In the upper-level problem, a stochastic optimization model is formulated for the ADN to optimally dispatch the DERs and make optimal decisions on the bidding of energy and reserve considering the availability, uncertainties, and flexibility of DERs. The lower-level problem is an optimization model for joint market-clearing of energy and reserve in the ISO market. Using strong duality theory and Karush-Kuhn Tucker (KKT) conditions, the proposed bilevel optimization problem is reformulated as a mathematical programming with equilibrium constraints (MPEC) problem and further converted into a computationally-solvable mixed integer second-order cone programming (MISOCP) model. The main contributions of this chapter are summarized as follows.

1. A stochastic bilevel optimization approach is proposed to model and analyze the strategic participation of an ADN with high penetration of DERs, including FEVCSs, in wholesale markets. The capability of DERs in providing both energy and ancillary services is modeled.

2. The availability, flexibility, and uncertainties of DERs, including FEVCSs, are accounted for in the transmission and distribution system and market operations. The DERs will contribute to local voltage regulation in ADN operation while strategically participating in the wholesale market.

3. The interactions between ADN and DER operation and the ISO energy and ancillary service markets are analyzed. The model simulations present the impact of a network-constrained strategic ADN's influence on the locational marginal prices (LMPs) and reserve price of the ISO market.

4. An FEVCS model representing the V2G and reactive power support capability of aggregated EVs' interaction with the ISO network is modeled in this chapter.

The rest of the chapter is organized as follows. The problem description is presented

in Section II. The mathematical formulation of the model is described in Section III. Numerical results are presented in Section IV. Section V concludes this chapter.

3.2 Problem Statement

The enhanced visibility and controllability of DERs allow the ADN to actively control DERs to strategically bid into the ISO's energy and reserve markets. As shown in Figure 3.1, an ADN consists of DERs such as distributed solar generators (DGs), wind DGs, energy storage systems (ESSs), and electric vehicle charging stations (FEVCSs). A substation connects an ADN to the transmission network. The

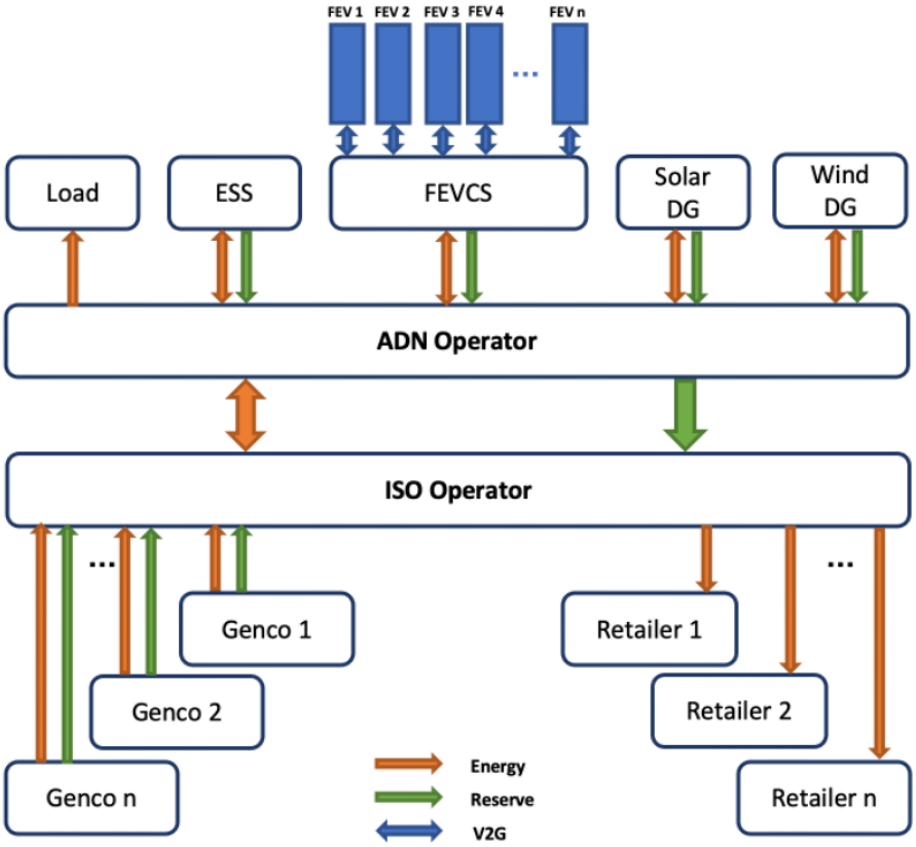

Figure 3.1: FEVCS's role within a DER aggregator bidding in the ISO market

ADN needs to bid in the wholesale market and trade energy and ancillary services with the ISO. Traditionally, distribution companies do not have much elastic load and are risk-averse, the distribution system operator (DSO) only bids for the total load de-

mand. However, with more DERs integrated into the distribution network, the ADN can provide energy and ancillary services back to the wholesale market. This turns the ADN into a prosumer and enhances the potential of the ADN to strategically play in the wholesale market and impact LMP and reserve prices in the transmission network to minimize its own operation costs by intentionally dispatching the DERs. The ISO market will accept offers and bids from the market players. Generation companies (GenCos) offer to sell energy and reserves to the ISO market. Retailers or LSEs bid to buy energy and reserves from the ISO market. The ADN can either buy or sell energy and reserves to the ISO market. The ISO optimally dispatches available resources to maximize social welfare. In this work, the strategic behavior of a price-maker ADN is modeled, and its behavior in a competitive wholesale market is analyzed. Other market participants are modeled as non-strategic players.

In this chapter, the strategic bidding of an ADN is modeled as a stochastic bilevel optimization problem considering the uncertainties of DERs. The structure of the bilevel optimization model is shown in Figure 3.2. At the upper level, the ADN optimizes the dispatch of active/reactive power of DERs in the distribution network and develops the bidding strategies considering the uncertainties of DERs. The ADN utilizes the DERs to impact the LMPs and the reserve prices in the wholesale market to minimize the total operation cost. The DERs are the key components that are to be optimized such that they can help the ADN achieve the desired market prices and provide ancillary services in the wholesale market. The uncertainty of DERs' available generation is crucial in the ADN's decision-making process. The uncertainties considered in the model include solar DG output, wind DG output, occupancy of the FEVCS, and the change in the aggregated SOC of the FEVCS due to the arrival or departure of EVs ($SOC^{FEVCS,\Delta}$).

In the lower-level problem, the ISO jointly clears the day-ahead energy and reserve market and broadcasts the LMPs and reserve prices. The ISO market clearing

problem optimizes the offers and bids from all market participants, considering social welfare maximization as the objective, and then determines the energy and reserve prices. In the upper-level problem, based on the input of LMP and reserve prices from the ISO, the ADN solves an ACOPF problem to optimally dispatch the DERs to determine the amount of energy and ancillary services to be traded in the ISO market. The bids and offers submitted to the ISO market will impact the LMP and reserve prices, and, in turn, the ISO market clearing results will impact the optimal dispatch of the ADN. The data and information exchange between the two models are illustrated in Figure 3.2. The ISO market clearing model requires the offers/bids of the ADN for energy and reserve in the ISO market. Considering the inputs from ADN, GenCos, and the non-strategic retailers/LSEs, the ISO market model will clear the day-ahead energy and reserve market and determine the amount of energy and reserve bought/sold from/to the ADN and the ISO market prices. The ADN needs the market clearing results, including the LMPs and reserve prices, to optimally dispatch its DERs for providing reserve and energy. To facilitate the computation of the optimal bidding strategy of the ADN, the bilevel optimization model is reformulated as a single-level model by converting the follower problem into its MPEC equivalent using KKT conditions and strong duality, resulting in a MISOCP model. The mathematical formulation is presented in the next section.

3.2.1 Rationale for Model Selection

A bilevel optimization model is well suited for problems where two distinct decision-making entities, with hierarchical interdependencies, such as interactions between the ADN and the ISO. The ADN, being modeled as the price-maker, is selected as the upper-level model, while the ISO is modeled as the lower-level since it reacts to the bids from the ADN by clearing the market. The key reasons for using a bilevel model include hierarchical decision-making, strategic interaction, and coordination of energy and ancillary services. MPEC is used to convert the bilevel model into a single-level

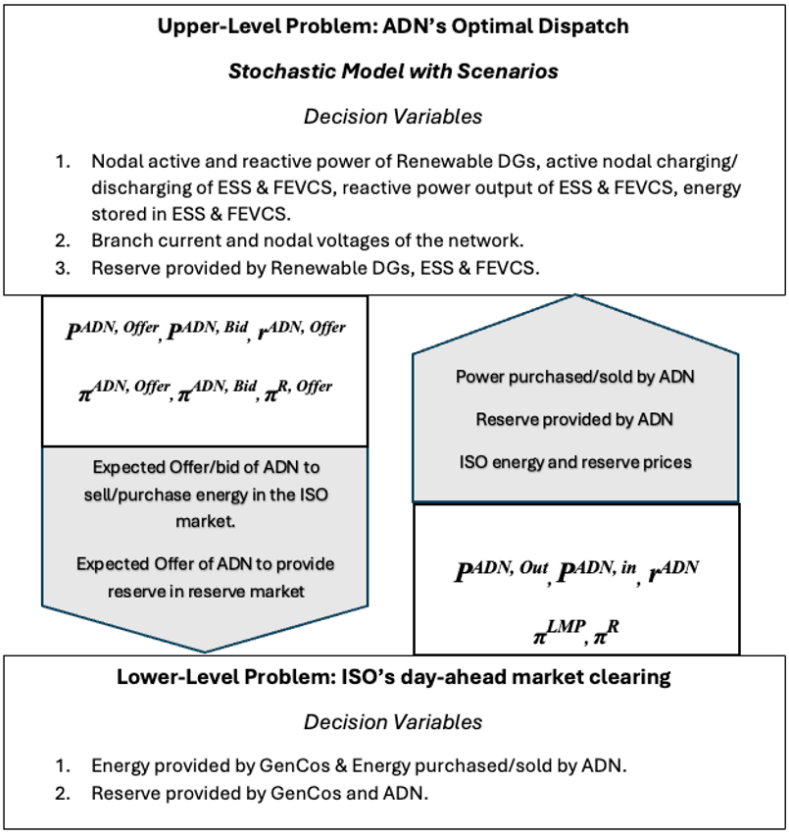

Figure 3.2: Model of the bilevel problem

optimization problem since the bilevel model, in its original form, is non-convex and difficult to solve.

3.3 Modeling

3.3.1 Upper-Level Problem: Optimal Dispatch of DERs in the ADN

At the upper-level, the ADN will develop an optimal bidding strategy based on the DER capacity/generation and distribution network operations to maximize total profit or minimize total operational cost. As a market player, the ADN expects its bidding to impact the energy and reserve prices in the ISO market so that it can gain more profit from the ISO market transactions. The objective function of the upper-level optimization model is to minimize the total expected operational cost of the ADN, including the cost of active and reactive power and reserve from the

renewable-based DERs, cost of purchasing power, and revenue from providing reserve in the ISO market, as shown in Eq. (3.1).

$$
\begin{aligned}
&min\ F(X^{LP}) \\
&= \sum_{t}\sum_{\gamma}\Gamma_{\gamma}\Bigg(\sum_{s} C_{s}^{PV,P}P_{s,\gamma,t}^{PV} + C_{s}^{PV,P}\alpha_{t}^{RM}r_{s,\gamma,t}^{PV} + \sum_{w} C_{w}^{WE,P}P_{w,\gamma,t}^{W} + C_{w}^{WE,P}\alpha_{t}^{RM}r_{w,\gamma,t}^{W} \\
&\quad + \sum_{e} C_{e}^{deg}(P_{e,\gamma,t}^{ES,ch}\eta_{e}^{ES,ch}\Delta t + \frac{P_{e,\gamma,t}^{ES,dch}}{\eta_{e}^{ES,dch}}\Delta t + \alpha_{t}^{RM}r_{e,\gamma,t}^{ES}) \\
&\quad + \sum_{f} C_{f}^{deg}(P_{f,\gamma,t}^{FEVCS,ch}\eta_{ch}^{FEVCS}\Delta t + \frac{P_{f,\gamma,t}^{FEVCS,dch}}{\eta_{dch}^{FEVCS}}\Delta t + \alpha_{t}^{RM}r_{f,\gamma,t}^{FEVCS})\Bigg) \\
&\quad - \sum_{t}(P_{t}^{ADN,Out} - P_{t}^{ADN,in})\pi_{t,k}^{LMP} - \sum_{t}(r_{t}^{ADN}\pi_{t}^{R} + \Pi_{t}^{inc}\alpha_{t}^{RM}r_{t}^{ADN})
\end{aligned}
\tag{3.1}
$$

The first term in Eq.(3.1) represents the cost of active power and reserve for solar DGs, where $C_s^{PV,P}$ represents the cost of active power generation for PV unit s, $P_{s,\gamma,t}^{PV}$ is the active power generated by PV unit s, α_t^{RM} is the ISO reserve market's probability of calling reserve, and $r_{s,\gamma,t}$ is the reserve from PV unit s. The second term presents the cost function of wind DG. The third term includes the cost of degradation of battery for ESS in the model. The fourth term includes C_f^{deg} as the cost of degradation of batteries of the EVs. The fifth term is the ADN's profit from sale of energy to the ISO market where $\pi_{t,k}^{LMP}$ is the ISO market's LMP at the ADN's substation which comprises marginal costs of energy and congestion. Uncertainty from the DERs is modeled in the upper level model using scenarios and stochastic programming. The parameter Γ_γ decides the probability of the scenario γ to happen. The variables $P_t^{ADN,Out}$, $P_t^{ADN,in}$ and r_t^{ADN} represent the expected power and reserve exchanged with the ISO which is the weighted sum of the scenario-specific value dependent on the probability of each scenario. The above-mentioned expected variables link the stochastic upper-level model to the lower-level model. The sixth term is the reserve sold to the ISO market at a price π_t^R with an incentive Π_t^{inc} for providing re-

serve. Constraints (3.2)-(3.6) of the ADN's optimal dispatch model utilize convex AC power flow in a radial distribution network. Second-order cone programming (SOCP) relaxation is employed to maintain the convexity of the power flow constraints[58], [59]. Eq. (3.1) is subjected to the following constraints:

3.3.1.1 Nodal power flow constraints

Nodal active power balance constraint

$$\sum_{i\in N1(j)}(p_{ij,\gamma,t}-l_{ij,\gamma,t}r_{ij})-\sum_{i\in N2(j)}p_{ij,\gamma,t}+p^{PV}_{j,\gamma,t}+p^{W}_{j,\gamma,t}-\frac{p^{ES,ch}_{j,\gamma,t}}{\eta^{ES,ch}}+p^{ES,dch}_{j,\gamma,t}\eta^{ES,dch}$$
$$-p^{d}_{j,t}-\frac{p^{FEVCS,ch}_{j,\gamma,t}}{\eta^{FEVCS,ch}}+p^{FEVCS,dch}_{j,\gamma,t}\eta^{FEVCS,dch}-p^{ADN,Out}_{j,\gamma,t}+p^{ADN,in}_{j,\gamma,t}=0 \tag{3.2}$$

Nodal reactive power balance constraint

$$\sum_{i\in N1(j)}(q_{ij,\gamma,t}-l_{ij,\gamma,t}x_{ij})-\sum_{i\in N2(j)}q_{ij,\gamma,t}+q^{PV}_{j,\gamma,t}+q^{W}_{j,\gamma,t}+q^{ES,dch}_{j,\gamma,t}+q^{FEVCS,dch}_{j,\gamma,t}-q^{d}_{j,t}=0 \tag{3.3}$$

Apparent power limit constraint

$$\|2p_{ij,\gamma,t}\ \ 2q_{ij,\gamma,t}\ \ (l_{ij,\gamma,t}-u_{i,\gamma,t})\|\leq(l_{ij,\gamma,t}+u_{i,\gamma,t}) \tag{3.4}$$

Voltage drop equation

$$u_{j,\gamma,t}=u_{i,\gamma,t}-2(r_{ij}p_{ij,\gamma,t}+x_{ij}q_{ij,\gamma,t})+((r_{ij})^2+(x_{ij})^2)l_{ij,\gamma,t} \tag{3.5}$$

Nodal voltage limit

$$(V_{(i,min)})^2 \leq u_{i,\gamma,t} \leq (V_{(i,max)})^2 \tag{3.6}$$

Each constraint in the nodal power flow constraints is regarding node j in the distribution network. Eq. (3.2) depicts the nodal active power balance constraint. The incoming active power at the node j is equal to the outgoing power from the node. Eq. (3.3) represents the nodal reactive power balance. Eq. (3.4) represents the relation between active and reactive power flows at each node. Voltage drop is defined in Eq. (3.5). Nodal voltage constraint is defined in Eq. (3.6).

3.3.1.2 Reserve balance constraint

$$r_{t,\gamma}^{ADN} = \sum_{s} r_{s,\gamma,t}^{PV} + \sum_{w} r_{w,\gamma,t}^{W} + \sum_{e} r_{e,\gamma,t}^{ES} + \sum_{f} r_{f,\gamma,t}^{FEVCS} \tag{3.7}$$

Eq. (3.7) defines the equality constraint of the ADN's reserve bid as the sum of reserves provided by the renewable DERs, ESS and FEVCS in the ADN.

3.3.1.3 Solar DG constraints

$$P_{s,\gamma,t}^{PV} + r_{s,\gamma,t}^{PV} \leq P_{s,t}^{PV,Forecast} \tag{3.8}$$

$$0 \leq P_{s,\gamma,t}^{PV} \tag{3.9}$$

$$0 \leq r_{s,\gamma,t}^{PV} \tag{3.10}$$

$$Q_{s,t}^{PV,min} \leq Q_{s,\gamma,t}^{PV} \leq Q_{s,t}^{PV,max} \tag{3.11}$$

$$\left\| P_{s,\gamma,t}^{PV} + r_{s,\gamma,t}^{PV},\ \ Q_{s,\gamma,t}^{PV} \right\| \leq S_{s}^{PV,max} \tag{3.12}$$

Eqs. (3.8)-(3.10) define the maximum and minimum limits of solar PVs' active power generation and reserve outputs at time t. Eq. (3.11) defines the minimum and maximum limits of solar PVs' reactive power outputs at time *t*. Eq. (3.12) defines the capacity limit on the active and reactive power outputs of the Solar PV at time *t*. The wind unit utilizes a model similar to the solar PV model. The forecast data utilized will define the difference in the nature of solar and wind DGs.

3.3.1.4 Energy Storage Constraints

$$0 \leq P_{e,\gamma,t}^{ES,ch} \leq P_{e}^{ES,max} \tag{3.13}$$

$$0 \leq P_{e,\gamma,t}^{ES,dch} \leq P_{e}^{ES,max} \tag{3.14}$$

$$E_{e}^{ES,min} \leq e_{e,\gamma,t}^{ES} \leq E_{e}^{ES,max} \tag{3.15}$$

$$(P_{e,\gamma,t}^{ES,dch} + r_{e,\gamma,t}^{ES})/\eta_{e}^{ES,dch} \leq e_{e,\gamma,t}^{ES} \tag{3.16}$$

$$r_{e,\gamma,t}^{ES} - P_{e,\gamma,t}^{ES,ch} + P_{e,\gamma,t}^{ES,dch} \leq P_{e}^{ES,max} \tag{3.17}$$

$$0 \leq r_{e,\gamma,t}^{ES} \leq P_e^{ES,max} \tag{3.18}$$

$$e_{e,\gamma,t}^{ES} = e_{e,\gamma,t-1}^{ES} + P_{e,\gamma,t}^{ES,ch}\eta_e^{ES,ch} - \frac{P_{e,\gamma,t}^{ES,dch}}{\eta_e^{ES,dch}} \tag{3.19}$$

$$Q_e^{ES,min} \leq Q_{e,\gamma,t}^{ES} \leq Q_e^{ES,max} \tag{3.20}$$

$$\left\| P_{e,\gamma,t}^{ES,ch} - P_{e,\gamma,t}^{ES,dch} + r_{e,\gamma,t}^{ES}, Q_{e,\gamma,t}^{ES} \right\| \leq S_e^{ES,max} \tag{3.21}$$

Eqs. (3.13)-(3.15) represent the boundary constraints for charging power, discharging power, and energy stored for the ESS, respectively. Eqs. (3.16) -(3.18) define the relation between the scheduled power discharge and scheduled reserve. In Eq. (3.16), the energy stored at time t limits the sum of scheduled power discharge and reserve for time t. Moreover, Eq. (3.17) limits the reserve and power scheduled for a time interval t by the maximum power output of the ESS. Equation (3.19) defines how the power interactions of the ESS with the ADN at the time *t-1* will affect the stored energy during the time interval t. Eq. (3.21) shows the relation between the active and reactive power discharge limited by the inverter capacity of the ESS.

3.3.1.5 Fleet Charging Station

The FEVCS model presented in this chapter is assuming that all the EVs connected to the FEVCS can be controlled by the FEVCS. The FEVCS provides the data of the available number of EVs and the dispatchable energy block in the individual EVs to the ADN. Each time an EV arrives, there is an increment in FEVCS capacity which is equivalent to the rating of the charging port available at the FEVCS and vice versa when an EV departs the FEVCS. Similarly, the SOC of the FEVCS increases

depending on the SOC of the vehicle arriving. Whereas, there is a decrement in the FEVCS's SOC, which is equivalent to the 100% SOC of an EV. In the presented model, the active, reactive and apparent power capacity of the FEVCS is controlled by the occupancy of the FEVCS represented by O. $SOC^{FEVCS,\Delta}$ is utilized in the FEVCS model to include the variation of SOC of the FEVCS due to the arrival or departure of vehicles. An FEVCS model, which represents the aggregated capacity of the EVs connected to the FEVCS at each period, is modeled in this chapter using equations (3.22)-(3.31).

$$0 \leq P_{f,\gamma,t}^{FEVCS,ch} \leq O_{f,\gamma,t} \times P_{unit}^{EV,max} \times B1_{f,\gamma,t} \tag{3.22}$$

$$0 \leq P_{f,\gamma,t}^{FEVCS,dch} \leq O_{f,\gamma,t} \times P_{unit}^{EV,max} \times B2_{f,\gamma,t} \tag{3.23}$$

$$B1_{f,\gamma,t} + B2_{f,\gamma,t} \leq 1 \tag{3.24}$$

$$SOC_{unit}^{EV,min} \times O_{f,\gamma,t} \leq SOC_{f,\gamma,t}^{FEVCS} \leq SOC_{unit}^{EV,max} \times O_{f,\gamma,t} \tag{3.25}$$

$$(P_{f,\gamma,t}^{FEVCS,dch} + r_{f,\gamma,t}^{FEVCS})/\eta_{f}^{FEVCS,dch} \leq SOC_{f,\gamma,t}^{FEVCS} \tag{3.26}$$

$$r_{f,\gamma,t}^{FEVCS} - P_{f,\gamma,t}^{FEVCS,ch} + P_{f,\gamma,t}^{FEVCS,dch} \leq P_{unit}^{EV,max} \times O_{f,\gamma,t} \tag{3.27}$$

$$0 \leq r_{f,\gamma,t}^{FEVCS} \leq P_{unit}^{FEVCS,max} \times O_{f,\gamma,t} \tag{3.28}$$

$$SOC_{f,\gamma,t}^{FEVCS} = SOC_{f,\gamma,t-1}^{FEVCS} + P_{f,\gamma,t}^{FEVCS,ch}\eta_{ch}^{FEVCS} - \frac{P_{f,\gamma,t}^{FEVCS,dch}}{\eta_{dch}^{FEVCS}} + SOC_{f,\gamma,t}^{FEVCS,\Delta} \tag{3.29}$$

$$Q_{unit}^{FEVCS,min} \times O_{f,\gamma,t} \leq Q_{f,\gamma,t}^{FEVCS} \leq Q_{unit}^{FEVCS,max} \times O_{f,\gamma,t} \tag{3.30}$$

$$\left\| P_{f,\gamma,t}^{FEVCS,ch} - P_{f,\gamma,t}^{FEVCS,dch} + r_{f,\gamma,t}^{FEVCS}, Q_{f,\gamma,t}^{FEVCS} \right\| \leq S_{unit}^{FEVCS,max} \times O_{f,\gamma,t} \tag{3.31}$$

Eqs. (3.22)-(3.24) defines the charging and discharging capability of the FEVCS being controlled by the occupancy. The FEVCS either charges or discharges at a point of time. Eq. (3.25) represents the SOC of the FEVCS controlled by the occupancy of the FEVCS. Eqs. (3.26)-(3.28) defines the constraints on FEVCS's discharging power and reserve contribution to the ADN. Eq. (3.29) defines the relation between the SOC, discharging/charging power and the stochastic parameter $SOC_{f,\gamma,t}^{FEVCS,\Delta}$. Eq. (3.30) and (3.31) define the constraints for reactive power and apparent power of the FEVCS.

The upper-level problem is as presented in Eqs. (3.1)-(3.21). The solution to the

upper-level optimization problem yields the energy bid (EB), energy offer (EO), and reserve offer (RO) of the ADN, which depend on the DER uncertainties, the expected energy, and reserve prices in the ISO market.

3.3.2 Lower Level Problem: ISO's Day-ahead Market Clearing

The ISO performs market clearing for the bids and offers from GenCos and the ADN to meet the total demand and maximize social welfare. Equivalently, the objective function (3.32) of the lower-level problem is to minimize the total operation cost of the ISO energy and reserve market.

$$\begin{aligned} &min\ F(X^{FP}) \\ &= \sum_t \left(\sum_g \Pi_{g,t}^{gen,offer} P_{g,t}^{gen} + \pi_t^{\overline{ADN,offer}} P_t^{ADN,out} - \pi_t^{\overline{ADN,bid}} P_t^{ADN,in} \right. \\ &\quad \left. + \sum_g (\Pi_{g,t}^{gen,res} r_{g,t}^{gen} + \Pi_t^{inc} \alpha_t^{RM} r_{g,t}^{gen}) + \pi_t^{\overline{ADN,res}} r_t^{ADN} + \Pi_t^{inc} \alpha_t^{RM} r_t^{ADN} \right) \end{aligned} \tag{3.32}$$

3.3.2.1 Energy & Reserve Balance Constraints

$$\sum_g P_{g,t}^{gen} - \sum_r P_{r,t}^{Ret} - P_t^{ADN,in} + P_t^{ADN,out} = 0 : \pi_t^E \tag{3.33}$$

$$\sum_g r_{g,t}^{gen} + r_t^{ADN} = R_t^{sys} : \pi_t^R \tag{3.34}$$

Eqs. (3.33) and (3.34) define the energy and reserve balance in the ISO market clearing framework respectively.

3.3.2.2 Transmission branch flow constraint

$$-PL_{j,max}^{TSO} \leq \sum_{g} GSF_{j-g}^{TSO} P_{g,t}^{gen} - \sum_{r} GSF_{j-r}^{TSO} P_{r,t}^{Ret} + GSF_{j,k}^{TSO}(P_t^{ADN,out} - P_t^{ADN,in}) \leq PL_{j,max}^{TSO} : \mu_{j,t}^{TSO,min/max} \tag{3.35}$$

Eq. (3.35) represents the transmission branch flow constraint.

3.3.2.3 GenCo's constraints

$$0 \leq p_{g,t}^{gen} : \mu_{g,t}^{gen,min} \tag{3.36}$$

$$P_{g,t}^{gen} + r_{g,t}^{gen} \leq P_g^{gen,max} : \mu_{g,t}^{gen,max} \tag{3.37}$$

$$0 \leq r_{g,t}^{gen} \leq R_g^{gen,max} : \mu_{g,t}^{gen,minres}, \mu_{g,t}^{gen,maxres} \tag{3.38}$$

Eqs. (3.36)-(3.38) define the upper and lower bounds of the reserve and energy provided by the GenCos.

3.3.2.4 ADN's constraints

$$0 \leq p_t^{ADN,out} : \mu_t^{ADN,out} \tag{3.39}$$

$$P_t^{ADN} + r_t^{ADN} \leq P^{ADN,max} : \mu_t^{ADN,max} \tag{3.40}$$

$$0 \leq P_t^{ADN,in} \leq P^{ADN,max} : \mu_t^{ADN,minin}, \mu_t^{ADN,maxin} \tag{3.41}$$

$$0 \leq r_t^{ADN} \leq R^{ADN,max} : \mu_t^{ADN,minres}, \mu_t^{ADN,maxres} \tag{3.42}$$

Eqs. (3.39)-(3.42) define the upper and lower bounds of reserve and energy provided by the ADN. The lower-level problem is incorporated into the upper-level problem

and linearized using KKT conditions and the duality theorem in [60]. We will reformulate the bilevel optimization model as a single-level MPEC presented in the next subsection.

3.3.3 Mathematical Program with Equilibrium Constraints

The MPEC is obtained from the KKT conditions of the Lagrange equation of the lower-level problem. Stationary constraints are obtained from the partial differential of the Lagrange function with respect to the decision variables.

3.3.3.1 Stationary constraints

$$\Pi_{g,t}^{gen,offer} - \pi_t^E - \sum_{j=1}^{Nl} \mu_{j,t}^{TSO,min} \sum_g GSF_{j-g}^{TSO} + \sum_{j=1}^{Nl} \mu_{j,t}^{TSO,max} \sum_g GSF_{j-g}^{TSO} - \mu_{g,t}^{gen,min} + \mu_{g,t}^{gen,max} = 0 \quad (3.43)$$

$$\Pi_{g,t}^{gen,res} + \Pi_t^{inc} \alpha_t^{RM} - \pi_t^{RM} + \mu_{g,t}^{gen,max} - \mu_{g,t}^{gen,minres} + \mu_{g,t}^{gen,maxres} = 0 \quad (3.44)$$

$$\pi_t^{\overline{ADN,offer}} - \pi_t^E - \mu_t^{ADN,minout} + \mu_t^{ADN,maxout} - \sum_{j=1}^{Nl} \mu_{j,t}^{TSO,min} GSF_{j,k}^{TSO} + \sum_{j=1}^{Nl} \mu_{j,t}^{TSO,max} GSF_{j,k}^{TSO} = 0 \quad (3.45)$$

$$-\pi_t^{\overline{ADN,bid}} + \pi_t^E - \mu_t^{ADN,minin} + \mu_t^{ADN,maxin} + \sum_{j=1}^{Nl} \mu_{j,t}^{TSO,min} GSF_{j,k}^{TSO} - \sum_{j=1}^{Nl} \mu_{j,t}^{TSO,max} GSF_{j,k}^{TSO} = 0 \quad (3.46)$$

$$\pi_t^{\overline{ADN,res}} + \Pi_t^{inc}\alpha_t^{RM} - \mu_t^{ADN,minres} + \mu_t^{ADN,maxres} = 0 \tag{3.47}$$

3.3.3.2 Complementary Constraints

$$0 \leq \sum_g GSF_{j-g}^{TSO} P_{g,t}^{gen} - \sum_r GSF_{j-r}^{TSO} P_{r,t}^{Ret} + GSF_{j,k}^{TSO}\left(P_t^{ADN,out} - P_t^{ADN,in}\right) + PL_{j,max}^{TSO} \perp \mu_{j,t}^{TSO,min} \geq 0 \tag{3.48}$$

$$0 \leq \sum_g GSF_{j-g}^{TSO} P_{g,t}^{gen} - \sum_r GSF_{j-r}^{TSO} P_{r,t}^{Ret} + GSF_{j,k}^{TSO}\left(P_t^{ADN,out} - P_t^{ADN,in}\right) + PL_{j,max}^{TSO} \perp \mu_{j,t}^{TSO,max} \geq 0 \tag{3.49}$$

$$0 \leq P_{g,t}^{gen} \perp \mu_{g,t}^{gen,min} \geq 0 \tag{3.50}$$

$$0 \leq (P_{g,t}^{gen,max} - P_{g,t}^{gen} - r_{g,t}^{gen}) \perp \mu_{g,t}^{gen,max} \geq 0 \tag{3.51}$$

$$0 \leq r_{g,t}^{gen} \perp \mu_{g,t}^{gen,minres} \geq 0 \tag{3.52}$$

$$0 \leq (R_{g,t}^{gen,max} - r_{g,t}^{gen}) \perp \mu_{g,t}^{gen,maxres} \geq 0 \tag{3.53}$$

$$0 \leq P_t^{ADN,out} \perp \mu_t^{ADN,minout} \geq 0 \tag{3.54}$$

$$0 \leq (P^{ADN,max} - P_t^{ADN,out} - r_t^{ADN}) \perp \mu_t^{ADN,maxout} \geq 0 \tag{3.55}$$

$$0 \leq (P^{ADN,max} - P_t^{ADN,in}) \perp \mu_t^{ADN,maxin} \geq 0 \tag{3.56}$$

$$0 \leq P_t^{ADN,in} \perp \mu_t^{ADN,minin} \geq 0 \tag{3.57}$$

$$0 \leq (R^{ADN,max} - r_t^{ADN}) \perp \mu_t^{ADN,maxres} \geq 0 \tag{3.58}$$

$$0 \leq r_t^{ADN} \perp \mu_t^{ADN,minres} \geq 0 \tag{3.59}$$

The complementary slackness constraints (3.48)-(3.59) are transformed as below in the model[56].

$$0 \leq x \perp y \geq 0 \Longrightarrow x \geq 0, y \geq 0, x \leq H_1 U, y \leq H_2(1-U) \tag{3.60}$$

U is a binary variable and H_1 & H_2 are large numbers.

3.3.4 Mixed-Integer Second-Order Cone Programming Model

The energy and reserve prices of the ISO market in Eq. (3.1) are unknown variables for the upper-level problem. The quantities of energy and reserve that have to be offered/bought are also unknown, leading to a non-linearity in Eq. (3.1). This non-linearity is linearized employing KKT conditions and strong duality theory to obtain the below objective function[61],[62].

$$\begin{aligned}
&MinF\left(X^{MP}\right) = \\
&\sum_t \Bigg[\sum_\gamma \Gamma_\gamma \Bigg(\sum_s C_s^{PV,P} P_{s,\gamma,t}^{PV} + C_s^{PV,P} \alpha_t^{RM} r_{s,\gamma,t}^{PV} + \sum_w C_w^{WE,P} P_{w,\gamma,t}^{W} \\
&+ C_w^{WE,P} \alpha_t^{RM} r_{w,\gamma,t}^{W} + \sum_e C_e^{deg} (P_{e,\gamma,t}^{ES,ch} \eta_e^{ES,ch} \Delta t + \frac{P_{e,\gamma,t}^{ES,ch}}{\eta_e^{ES,dch}} \Delta t + \alpha_t^{RM} r_{e,\gamma,t}^{ES}) \\
&+ \sum_f C_f^{deg} (P_{f,\gamma,t}^{FEVCS,ch} \eta_{ch}^{FEVCS} \Delta t + \frac{P_{ef,\gamma,t}^{FEVCS,ch}}{\eta_{ch}^{FEVCS}} \Delta t + \alpha_t^{RM} r_{f,\gamma,t}^{FEVCS}) \Bigg) \\
&- \Pi_t^{inc} \alpha_t^{RM} r_t^{ADN} + \sum_g \Pi_{g,t}^{gen,offer} P_{g,t}^{gen} + \sum_g (\Pi_{g,t}^{gen,res} r_{g,t}^{gen} + \Pi_t^{inc} \alpha_t^{RM} r_{g,t}^{gen}) \\
&+ \sum_g (P_g^{gen,max} \mu_{g,t}^{gen,max} + R_g^{gen,max} \mu_{g,t}^{gen,maxres}) - R_t^{Sys} \pi_t^{RM} \\
&+ PL_{j,max}^{TSO} \mu_{j,t}^{TSO,min} + PL_{j,max}^{TSO} \mu_{j,t}^{TSO,max} \Bigg]
\end{aligned} \tag{3.61}$$

subject to constraints (3.2)-(3.21), (3.43)-(3.60).

The transformed problem will have the original constraints (3.2)-(3.21) of the

upper-level problem. In addition to that, the model will have stationary and complementary slackness constraints of the lower-level problem. The bilevel problem has been transformed into a MISOCP model. Data used for simulation and results obtained from the model are presented in the next section.

3.4 Numerical Results

In this section, the proposed model was tested on two test cases. A 9-bus distribution network connected to a modified PJM 5-bus transmission system (ISO5-ADN9) and an IEEE 33-bus distribution system connected to an IEEE-30 bus transmission system (ISO30-ADN33) were used for testing the performance of the model.

3.4.1 Case ISO5-ADN9

3.4.1.1 Case Data and Assumptions

The ISO market represented by a PJM 5-bus system has 5 GenCos and one ADN connected to node 1 as market participants. Retailers are considered to be conventional distribution networks with no flexibility in consumer demand. All data related to the modified 9-node distribution network case and the modified PJM 5-bus case are provided in [63]. The ADN has a radial topology with high penetration of renewable DERs. The peak load in the ADN is 53 MW. The 9-node distribution network has been modified so that it will have enough DER capacity to influence the PJM-5 bus representing the transmission network, which hosts a peak load of 1070 MW. It is assumed that the ADN has control of all the DERs that are connected to its network. The probability of calling reserve and incentive for providing reserve can be found in [56]. For modeling uncertainty of solar DG, wind DG, and FEVCS, 365 scenarios were generated for solar DG output, wind DG output, occupancy of the FEVCS and change in aggregated SOC of FEVCS due to arrival or departure of EVs. The scenarios for solar and wind generation were derived were obtained from National Renewable Energy Laboratory (NREL) [**?**] and [64]. Similarly, 365 scenarios for vari-

ation of occupancy and SOC of the FEVCS were generated. The ADN is assumed to have control over the FEVCS. Hence, the data of occupancy and change in SOC of FEVCS are generated using a case of a medium-duty fleet charging station for 20 EVs of 200 kWh storage each. Usable storage of 150 kWh is considered for each EV. The FEVCS has 20 chargers of 150 kW to charge these EVs. The time of arrival and time of departure for a fleet charging station can be assumed to follow a normal distribution, since medium-duty vehicles are often utilized for delivering goods. A mean of 7 and a standard deviation of 1 hour were used for generating the time of departure of EVs from the FEVCS. A mean of 19 and a standard deviation of 1 were used to generate the time of arrival of EVs to the FEVCS. The SOC of vehicles arriving was also generated based on a normal distribution with a mean of 45 kWh and a standard deviation of 5. Using the provided data, scenarios for occupancy and $SOC^{FEVCS,\Delta}$ were generated. These scenarios were reduced to 3 scenarios by the fast-forward scenario reduction method based on Kantorovich distance [34]-[65]. Figure 3.3 presents the scenarios for the occupancy of the FEVCS. The reduced scenarios are shown as line plots in black. The scenarios and reduced scenarios for $SOC^{FEVCS,\Delta}$ is shown in Figure 3.4. The cost of degradation of battery for BESS and EV are assumed to be 30$/MWh and 50$/MWh respectively. The efficiency considered for BESS and EV are 98% and 95% respectively [66], [67]. Two cases for the ISO5-ADN9 with different DER generation costs were used to analyze the impact of DER generation cost on the strategic behavior of the ADN. The generation costs of DERs are set to be 0 $/MWh for both active and reactive power in Case 0 and a nonzero cost of DER generation is considered in Case 1.

3.4.1.2 Simulation Results and Analysis

An ADN with a strategic bidding approach will use the available generation in a time period to control the energy and reserve bidding prices to increase its profit. The ISO energy market clearing can be observed in Figure 3.5. In the energy market,

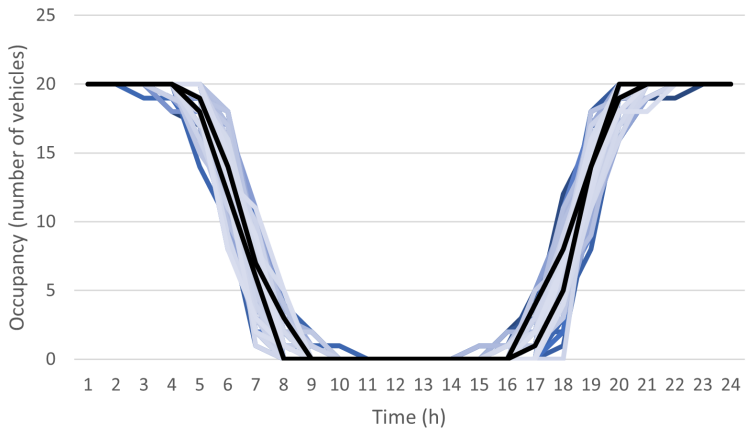

Figure 3.3: Scenarios and reduced scenarios for occupancy of the FEVCS

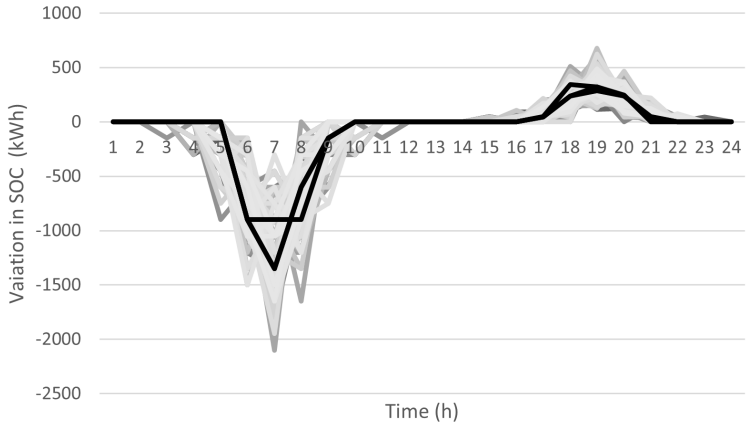

Figure 3.4: Scenarios and reduced scenarios for variation of SOC of the FEVCS

ADN acts as a strategic consumer in most of the hours. The marginal players in the ISO energy market at each point in time are presented in Figure 3.5. GenCo#2, GenCo#3, and GenCo#5 are the marginal players in the energy market. GenCo#5 is the marginal player throughout the day. GenCo#3 is the marginal player in periods 1-4 and 10-24. Meanwhile, GenCo#2 is the marginal player in periods 15 and 16 only. For n congested lines, there will be $n + 1$ marginal generators. There is congestion on branches 1-5 during periods 1-4 and 10-24. There is congestion on branches 2-3 during periods 15 and 16. The ADN bids for energy strategically to reduce the LMP at node 1 so that it can reduce the cost of purchasing energy from the ISO market.

The ADN achieved so by reducing congestion in the ISO network.

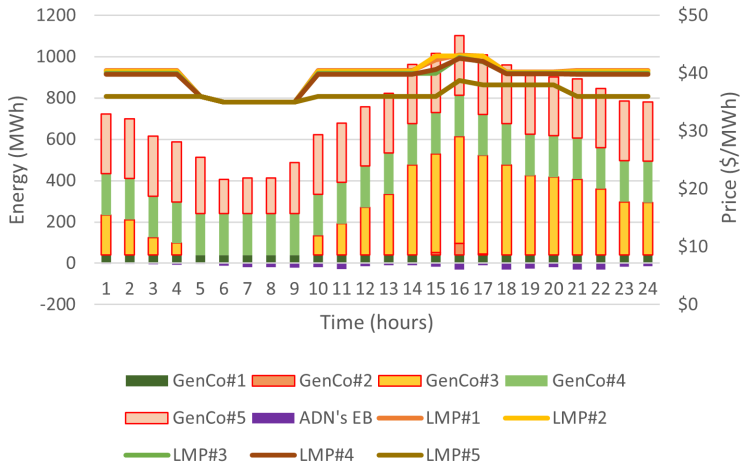

Figure 3.5: ISO energy market clearing - ISO5-ADN9

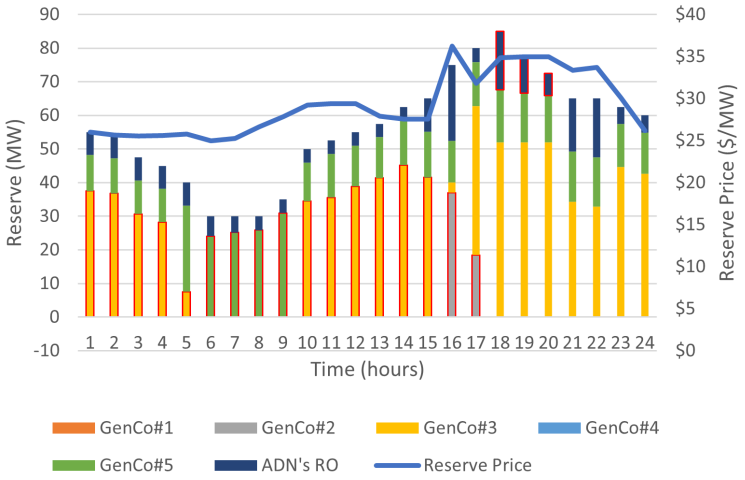

Figure 3.6: ISO reserve market clearing - ISO5-ADN9

The power exchange between the ADN and the ISO market compared to the total load of the system is small. However, the reserve provided by the ADN is sizeable when compared to the total reserve requirement of the system. GenCo#2, GenCo#3, GenCo#5, and the ADN are the marginal units at different time periods in the ISO reserve market. GenCo#3 is the marginal player in periods 1-5, 10-15, and 21-24. GenCo#5 is the marginal player in periods 6-9. GenCo#2 is the marginal player in periods 16 and 17. The ADN is the marginal player in periods 18-20. The strategic

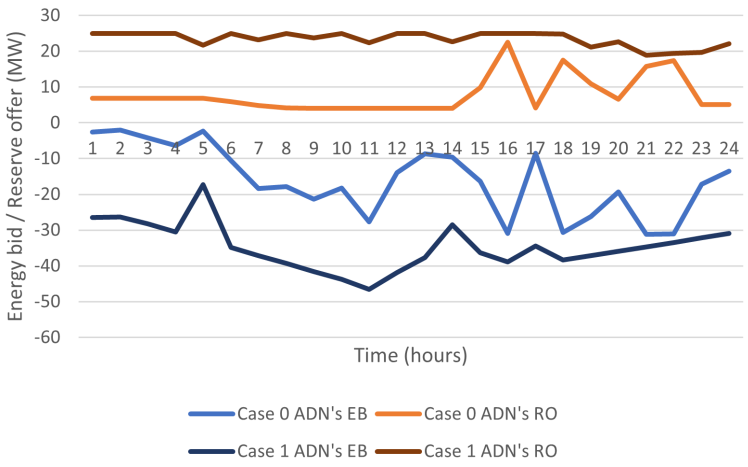

Figure 3.7: ADN's behavior in the ISO market for Case-0 and Case-1

behavior of the ADN in the reserve market is shown in Figure 3.6. The columns with a red outline represent the marginal players in Figure 3.5 and Figure 3.6. With the DERs, the ADN is able to provide reserve to the ISO reserve market. The ADN attempts to gain more profits from the reserve market by increasing the reserve price through its strategic bidding. The ADN acts as the marginal unit in the reserve market for periods 18-20. The ADN's optimal reserve offers raised the ISO's reserve price from the marginal reserve price of GenCo#3 to the marginal price of GenCo#2 even though GenCo#2 is not providing any reserve to the reserve market in periods 18-20. Without the strategic bidding of the ADN, the reserve price of the system is the reserve offer price of GenCo#3. However, with the strategic reserve offering of the ADN, the system's reserve price is raised to the reserve bidding price of GenCo#2's, thus increasing the ADN's profit from the sale of reserves. Irrespective of the relatively small size in both markets, the ADN has the potential to be a strategic player in the ISO market because of the low cost of the renewable DERs when compared to conventional sources.

The strategic nature of ADN changes in behavior when the cost of DERs is considered in the model. The change in behavior can be analyzed by comparing the energy and reserve transactions of the ADN in the ISO market. Figure 3.7 features

the comparison between Case 0 and Case 1. In Case 1, the amount of reserve that the ADN provides to the ISO market increases while the energy purchased from the ISO market increases. This behavior is motivated by the ADN's objective to decrease the total generation cost of the DERs. The ADN allocates more of the available DER generation capacity to the reserve market than to the energy market.

The ADN's active and reactive power dispatches are presented in Figure 3.8. From Figure 3.8, it is clear that solar DGs, wind DGs, ESSs, and FEVCS are utilized in providing reserves in the ISO market. The ESSs are charged to their full SOC at the first time period and are utilized as reserves as part of ADN's strategy of maximizing profit from the day ahead reserve market. The active power of the DERs is dispatched based on the strategic behavior required to participate in the ISO market. The reactive power is provided by the DERs for voltage regulation in the ADN. Hence, as presented in Figure 3.9, the nodal voltages are within the tolerance range of +/- 0.05 per unit.

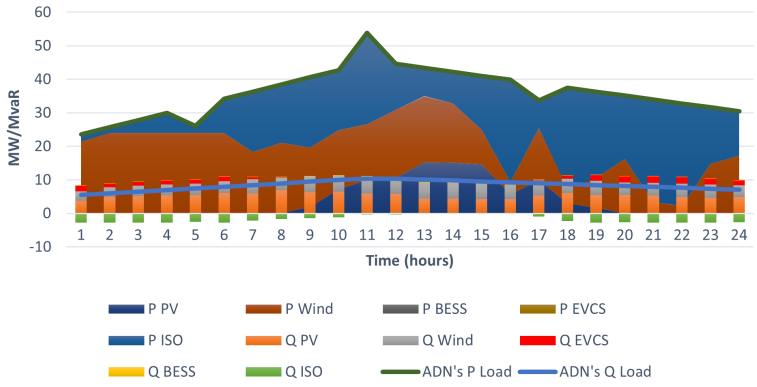

Figure 3.8: ADN's power generation and demand - ISO5-ADN9

Modeled as a price-maker, the ADN needs to balance the DER dispatch for providing energy and reserve so that it can gain the maximum profits from the ISO markets. It will try to minimize the cost of energy purchases from the ISO energy market and maximize the revenue of providing reserve in the ISO's ancillary service market. The proposed price-maker model was compared with the conventional dis-

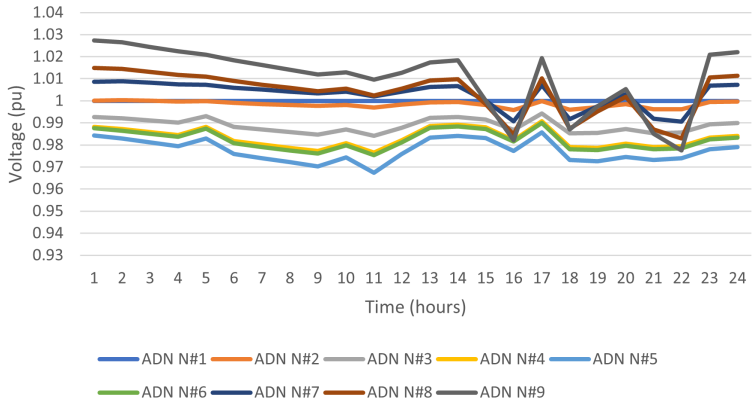

Figure 3.9: ADN's nodal voltages in ISO5-ADN9

Table 3.1: Comparison between the cost of price-maker and price-taker ADNs from ISO interactions for ISO5-ADN9

Test case	**Payment to the ISO market ($)**	
	PM-ADN	**PT-ADN**
ISO5-ADN9	8720	21211

tribution network modeled as a price-taker, i.e., strategic ADN v.s. non-strategic ADN. Both models were run for a 24-hour time period to obtain the ISO energy and reserve prices for both test cases. In the ISO5-ADN9 test case, both PM-ADN and the PT-ADN are net consumers in the ISO energy market. As presented in Table 3.1, the PM-ADN reduced the cost to buy energy from the ISO market by 58.8% when compared to the PT-ADN.

3.4.2 Case ISO30-ADN33

3.4.2.1 Case Description

The second test case consists of an IEEE 30-bus transmission network and an IEEE 33-node distribution system. In the transmission case, the peak load is 168 MW. The maximum reserve capacity of each GenCo is set to 15% of its generation capacity. The generation costs of GenCo#1, GenCo#2, GenCo#3, GenCo#4, GenCo#5 and GenCo#6 are set to 35, 15, 17, 20, 25, and 30 $/MWh respectively. The cost of providing reserve was considered to be 70% of the cost of energy. For the IEEE

33-node distribution network that represents an ADN with high penetration DERs, it has 3 MW wind power, 2.2 MW ESS, and FEVCS with 3 MW capacity in the network. All other data were kept the same as in the standard case.

3.4.2.2 Simulation Results and Analysis

The case considers an ADN with extremely high DER penetration. When compared to the Case ISO5-ADN9 where the net load of the ADN network is never negative, this case has the DER capacity to sell power to the ISO market. The capability of the ADN to control DER generation allows the ADN to be a net producer or consumer, which is well reflected by the energy exchange between the PM-ADN and the ISO market in Figure 3.11. As presented in Figure 3.11, periods 9, 13, and 16 showed a decrease in the energy price at node 1 where the ADN is connected to the ISO network. The PM-ADN acts as a strategic consumer during these periods, reducing the LMPs for all the nodes when there is no congestion in the ISO30-ADN33 network in these periods. Figure 3.11 also illustrates the reserve prices of the PM-ADN and the PT-ADN. In the reserve market, the PM-ADN purchases energy from the ISO energy market and provides reserve in the ISO reserve market, whereas the PT-ADN generates maximum energy and sells energy in the ISO market. Similar to the ISO5-ADN9 case, the ADN is capable of influencing the ISO reserve market to increase the price in the periods 20 and 21 to the reserve price of the next marginal reserve. In Case ISO30-ADN33, the profit from the ISO market increased when compared to the PT-ADN. The comparison of the PM-ADN and the PT-ADN is presented in Table 3.2. The nodal voltage for the test case I30-A33 was in the security range.

The behavior of wind generation, ESS, and EVCS in the strategic ADN model is as shown in Figure 3.10. The figure shows the optimal dispatch of the ADN for scenario 3 in the stochastic model. The available wind energy is utilized to bid in both energy and reserve markets. Whereas both ESS and EVCS are primarily used in the reserve market to reduce the cost of degradation of the battery. The cost of providing

Table 3.2: Comparison between the cost of price-maker and price-taker ADNs from ISO interactions for ISO30-ADN33

Test case	Payment to the ISO market ($)	
	PM-ADN	PT-ADN
ISO30-ADN33	-1300	193.41

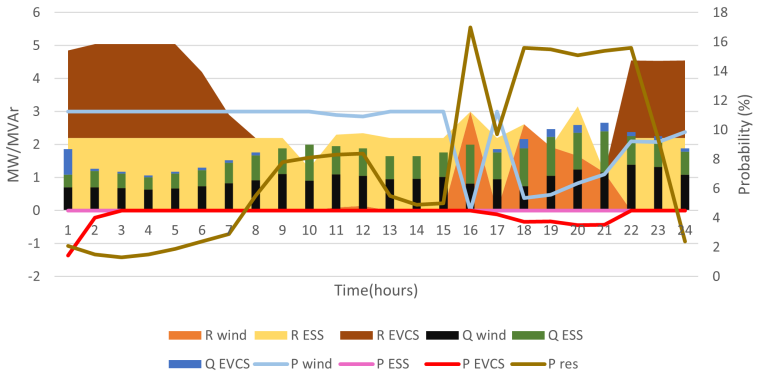

Figure 3.10: Behavior of DERs in the strategic ADN

reserve for EVCS and ESS is dependent on the cost of degradation of the battery. The probability of calling reserve is high in periods 16, 18, 19, and 20. Since the cost of generation of wind generation is considered 0, the model utilizes wind energy in providing reserves in periods 16 and 18-21. During period 16, 3MW wind energy is curtailed to provide 3MW in the reserve market. Similarly, energy is curtailed in periods 18-21. The comparable price of energy and reserve in the ISO market during this period is also the reason for this behavior. Similarly, even though the initial SOC of the FEVCS is set at 50% of the total SOC, the FEVCS charges the connected vehicles to their maximum capacity and then uses the stored energy to bid in the reserve market. The reserve from the FEVCS (R-EVCS) is reduced during hours 8-17 since the occupancy of the FEVCS is 0. After period 17, the charging power from FEVCS increases as the occupancy increases. The EVs are charged as they arrive to the FEVCS. FEVCS is the third choice of reserve, as the cost of battery degradation in EVs is higher than that of ESS. The DERs which are not used for reserve or energy

are used for reactive power support since the reactive power load is higher during the period 18-22.

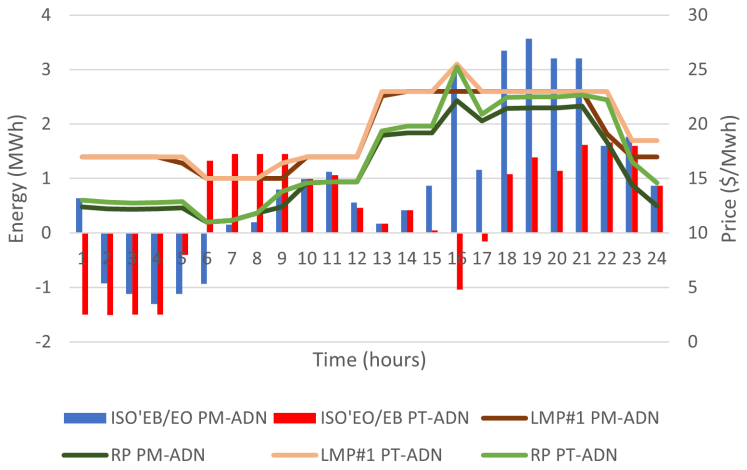

Figure 3.11: Comparison of PM-ADN with PT-ADN in the ISO30-ADN33 case

The strategic ADN model was tested at 40%, 70%, and 100% DER penetration to understand the impact of DER penetration on the strategic behavior of the ADN. The strategic behavior of the ADN with 40% and 100% DER penetration is shown in Figure 3.12. At 40% penetration, the ADN was able to set the price in the reserve market for period 18. The strategic behavior for the ADN with 40% DER penetration is shown as the black marker in Figure 3.12 At 70% DER penetration, the ADN was able to set reserve prices for periods 14, 16, and 17. At 100% DER penetration, the ADN was able to set prices in periods 10, 14, 15, 16, and 17. The strategic behavior for the ADN with 100% DER penetration is shown as red markers in Figure 3.12. With an increase in DER penetration, there is an increase in the strategic behavior of the ADN. This is due to the increase in the resources that can be optimally dispatched in both energy and reserve markets.

3.4.3 Impact of Uncertainty's in the ADN's Decision-making

As mentioned in section II, the uncertainty of DERs has been included in the ADN's model utilizing scenarios for solar DG output, wind DG output, occupancy of the FEVCS, and, $SOC^{FEVCS,\Delta}$. Optimal scenario reduction for multivariate data from

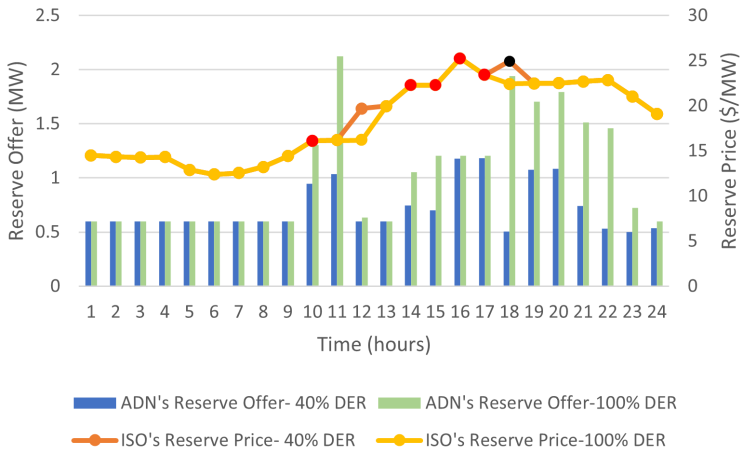

Figure 3.12: Strategic behavior of ADN with in increase in DER penetration

[34] is utilized for scenario reduction. As presented in [68], a set of scenarios is reduced to a scenario tree. The tree structure is modified by bundling similar scenarios to reduce the number of nodes of a fan of an individual scenario. The reduced scenarios represent the most probable scenarios, each with a probability value linked to it. In the case studies provided in this chapter, we have reduced 365 scenarios to the 3 most probable scenarios, which are then utilized in the stochastic model to obtain the expected value of energy offer/bid and reserve offer to the ISO market. The probabilities linked to Scenario 1, Scenario 2, and Scenario 3 are 0.4466, 0.3726, and 0.1808 respectively. Figure 3.13 shows the EB/EO and RO values in each scenario and the expected value. The expected value of energy and reserve is optimized by the model utilizing the integrated ISO market-clearing model.

3.4.4 SOCP Relaxation Analysis and Simulation Setup

The accuracy of SOCP relaxation was tested to compare the power flow obtained from conic relaxation with the original non-convex model by evaluating the relaxation error defined as

$$Gap = max_{\forall(i,j)} \left| p_{ij}^2 + q_{ij}^2 - (l_{ij} u_i) \right| \tag{3.62}$$

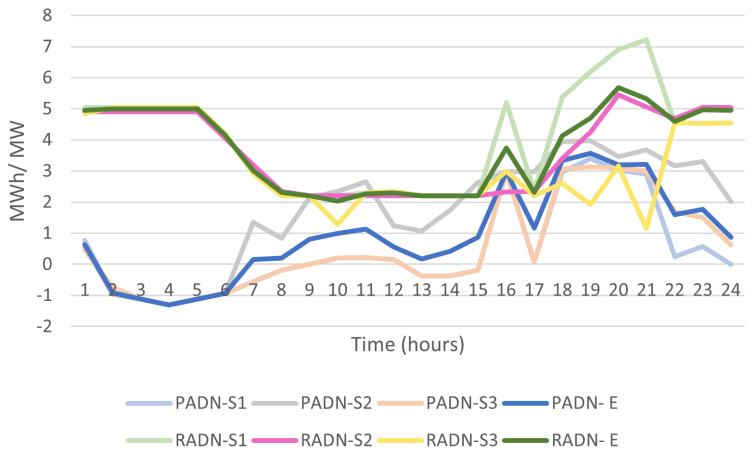

Figure 3.13: Expected value of ADN's energy and reserve bids

The SOC gap for the ISO5-ADN9 case is $1.5 \cdot e^{-4}$ MW. The SOC gap for ISO30-ADN33 is $6.3e^{-6}$ MW. The gaps obtained for both cases are small enough and do not impact the optimal solution of the proposed model.

Simulations were carried out on a 64-bit Windows Laptop with Intel Core i5 CPU, 2.5 GHz, and 16 GB RAM. The problem was modeled utilizing MATLAB with YALMIP and Gurobi. The stochastic model for the ISO5-ADN9 case with 6495 continuous variables and 168 binary variables was solved in 60 seconds. The stochastic model for the ISO30-ADN33 case with 65928 continuous and 2832 binary variables was solved in 147 seconds.

3.5 Conclusion & Future Works

In this chapter, the strategic bidding and behaviors of an ADN with high penetration DERs in wholesale electricity markets are modeled and investigated. Considering the interactions between the ADN and the ISO, the DERs are optimized by the ADN to coordinate the energy and reserve provision to the wholesale market to minimize the total cost of the ADN considering network operation constraints and uncertainties of solar and wind. The strategic behavior of the ADN with DERs in the ISO market is formulated as a bilevel optimization problem, which is converted to a single-level

MPEC problem and further reformulated as a computationally solvable MISOCP model. The proposed model was tested using two cases and compared with a conventional price-taker ADN model. The results indicate that a price-maker ADN can increase the profit of an ADN while decreasing the LMPs of the ISO network during peak load hours. An increase in the generation cost of DERs resulted in an increase in reserve allocation of ADNs. With the increase in DER penetration, the ability of the ADN to be a price-maker increase. This model can be utilized to study the behaviors of an ADN and DERs in providing energy and reserve under the competitive ISO markets. In future work, the DER control can be modeled in a decentralized manner to incorporate the rapid restructuring and privatization of the power grid.

In conclusion, the results from the strategic market participation model have demonstrated the significant influence that DER aggregators, specifically FEVCS, can exert on market dynamics, such as LMPs and reserve prices. While the bilevel optimization framework offers valuable insights into the operational strategies and market interactions of FEVCS, these strategies are inherently centralized. To further improve grid stability, particularly in a system with high DER penetration, decentralized control mechanisms must be explored. As the complexity of managing FEVCS grows, especially in distributed networks, decentralized control schemes such as those provided by multi-agent reinforcement learning (MARL) frameworks become increasingly important. The next chapter introduces a novel Federated Learning-Enhanced Conflict-Aware Multi-Agent Reinforcement Learning (FLE-CA-MARL) framework, aimed at addressing these challenges.

CHAPTER 4: FEDERATED REINFORCEMENT LEARNING AND MULTI-AGENT DISTRIBUTED CONTROL FOR FLEET EV GRID SERVICES

Building upon the insights gained from the centralized market optimization model in the previous chapter, this chapter delves into the decentralized control of FEVCS. The proposed FLE-CA-MARL framework integrates FL and MARL to optimize the voltage and reactive power support provided by FEVCS. This framework allows FEV agents to make decentralized decisions, ensuring not only local grid stability but also improving overall system resilience.

The growing integration of FEVCS into the power grid demands real-time, adaptive, and intelligent control mechanisms to ensure grid stability. With the increasing number of FEVs, traditional methods struggle to manage the complexity of DERs and bidirectional power flows. ML techniques have emerged as a promising solution, particularly RL, which provide adaptive control for FEVCS by managing key grid challenges, including voltage regulation and operational uncertainty.

As the grid becomes more decentralized and volatile due to the integration of DERs, RL's ability to learn optimal actions through interaction with the environment is crucial to the power grid control. RL's applications span across power system optimization and control tasks such as energy management, demand response, and voltage control, where RL enables the system and DER devices to operate autonomously with minimal oversight.

4.1 Literature Review & Contributions

RL models offer a human-like approach to learning control strategies through the RL agent's interaction with the environment, using rewards and feedbacks. Integrat-

ing deep neural networks into RL to create deep RL (DRL) has also enhanced the exploration, convergence, and stability of the RL models. Optimization, planning, management, and control problems can be formulated as RL problems and solved using algorithms like Q-learning, deep deterministic policy gradient (DDPG) and soft actor-critic (SAC).

Power system applications for energy management, demand response, operational control, cybersecurity, economic dispatch, edge computing, etc. have been modeled using the RL framework [69]. RL approaches can be single-agent or multi-agent (MA) based on the number of agents learning from the same environment. Although single-agent RL models have a single objective represented by a single reward function that includes all rewards and penalties being considered, MARL models can have multiple objectives with agents working alongside or against each other. As EV charging stations often involve multiple chargers or FEVs, MARL is effective in managing the collective behaviors of FEV agents, leading to more efficient and coordinated optimization. [70] presents a MARL approach for controlling the charging of a large population of EVs. In this paper, an MA-DDPG algorithm operating in a mixed cooperative-competitive setting is implemented using centralized training and decentralized execution. However, the centralized training approach presents challenges in scalability, particularly in distributed large-scale environments. Furthermore, agents are trained in a cooperative environment, leading to the possibility of suboptimal actions when multiple agents interact. An MARL framework for providing grid services such as valley filling and minimizing power loss is presented in [71]. However, the authors used a simplified grid model, ignoring reactive power from the action space. [72] presented a MARL framework featuring DDPG algorithm and a parameter sharing framework to solve the EV's coordinated active and reactive power control problem, addressing demand-side response and voltage regulations. This is a centralized approach with parameter sharing that produces a unified control policy for all agents

without considering their heterogeneity. [73] introduces Fleet RL, the first customizable RL environment specifically designed to optimize the charging of commercial EV fleets. Although it provides a flexible and customizable environment for EV fleet operations, it lacks provisions for reactive power support, which is critical in voltage regulation. A cooperative charging control strategy for EVs using a MARL approach is presented in [74]. This model does not support reactive power management. Additionally, the use of a collective-policy model introduces the possibility of suboptimal behaviors from the individual vehicle's perspective. Cheng et al. in [75], propose a delay adaptive Volt/VAR control (VVC) framework for ADNs with massive PV devices. The authors address the challenge of communication latency in the distribution network (DN).

In general, the literature reveals that while the RL and MARL approaches have been applied to the optimization of FEVCS, key limitations remain: many works rely on centralized training, lack scalability, or omit critical elements such as reactive power management and conflict resolution between agents.

Most single-agent and multi-agent models require centralized training or centralized control to implement a coordinated response from the agents that are most likely distributed in different locations on the transmission or distribution grid. Using an agent trained in the local area alone provides optimal results based on the historical experience of the agent, but limits the agent's exposure to unfamiliar scenarios. Any attempt to implement a much more global model increases the toll on the communication system exponentially. A hybrid approach to centralized and distributed control is the way forward for efficient control of power distribution networks. Federated learning (FL) addresses these concerns by enabling decentralized, privacy-preserving collaborative learning across agents. FL is a form of distributed learning technique introduced by Google AI in 2016, where data processing is decentralized, parallel and collaborative among numerous client devices [76]. RL agents deployed in FL

framework forms federated RL (FRL) framework. FRL frameworks are emerging as powerful tools for power system applications, offering solutions that preserve data privacy and enhance scalability. Power system applications such as information security [77], predictive maintenance[78], EV charging scheduling, transformer protection, VVO have been implemented employing FDRL frameworks. Qian et al. have proposed an FDRL algorithm, FedSAC, for multi-EV charging control on a DN [79]. Although FedSAC addresses active power control, fleet EV charging systems must also handle reactive power to maintain voltage stability, which FedSAC does not address. Building on this foundation, Danish et al. introduce a blockchain-based FL approach to enhance privacy and security in EV load forecasting. However, these models focus on prediction rather than real-time decision-making, leaving a gap in adaptive control strategies for fleet-level charging optimization [80]. [81] proposes an FL framework using the proximal algorithm and the transformer model to address the challenges of non-IID data in the dispatch of V2G. Even though a system of periodic retraining with new data can update the transformer model to new data, the above system lacks the self-learning capability of RL. These studies demonstrate the potential of FDRL in power system applications, yet there remain gaps in providing comprehensive solutions for FEVCS. Notably, none of the existing works incorporate both active and reactive power control, with a focus on volt-VAR control using an FRL architecture.

Existing work focuses primarily on active power optimization in multi-agent settings but lacks integrated frameworks that handle both active and reactive power control, which is essential for voltage stability in fleet EV charging stations [71],[73], [82],[83]. Moreover, these frameworks often rely on centralized decision-making, which limits their scalability [70],[72]. Although these studies demonstrate significant progress in DRL, FL, and FDRL for grid management, crucial gaps remain, particularly in the area of decentralized reactive power support mechanisms for FEVCS.

Additionally, most studies focus on light-duty EVs or residential applications, overlooking the unique challenges posed by commercial and industrial fleets, which have higher power demands, more stringent operational constraints, and typically centralized depot-based charging strategies. Unlike residential EVs, FEVs must coordinate their charging schedules to not only meet operational demands, but also to support grid services like voltage control. This introduces a dual-layer complexity where both the FEVCS level and the DN level must be modeled and coordinated for effective control.

Hence, this chapter seeks to address these gaps by developing an adaptive, scalable, decentralized framework that integrates both active and reactive power management at the FEVCS level while ensuring that grid-wide voltage stability is maintained at the DN level. This framework aims to provide a more comprehensive solution that can be applied to commercial fleet EVs, which have been not explored in the existing literature.

This work presents a novel FDRL framework for grid-managed distributed EV charging for Volt/VAR control in distribution systems, with the following key contributions that advance the state-of-the-art:

1. This paper proposes a Federated Learning-Enhanced Conflict-Aware Multi-Agent Reinforcement Learning (FLE-CA-MARL) control framework specifically designed for FEV-level collaborative learning within a DN. By enabling decentralized decision-making among FEV agents, the framework ensures that both local voltage regulation and global voltage control are optimized, demonstrating scalability and adaptability across diverse network configurations.

2. A novel conflict-aware MARL (CA-MARL) environment is utilized, to model the coordinated reactive-power support of multiple active FEV agents connected within an FEVCS. This mechanism effectively penalizes conflicting, and incorrect actions associated with the reactive power injections, ensuring that the

agents collectively contribute to the optimal control of charging in the FEVCS while maintaining local voltage stability, avoiding convergence to suboptimal policies.

3. This work incorporates a POMDP model for an FEV agent, enabling decentralized optimization with limited grid state information, a crucial advancement in managing real-world uncertainty and improving grid stability, as agents make decisions with incomplete knowledge of the overall grid state.

4. The framework is tested across scenarios involving both localized (single FEVCS) and distributed (multiple FEVCSs) agent configurations. These tests validate the frameworkâs effectiveness in coordinating agent actions, ensuring robust voltage regulation and grid stability across varying conditions and load profiles.

4.2 Problem Statement

As the integration of FEVs into DNs accelerates, the management of the charging load poses significant challenges for Volt/VAR control. The challenges are present in multiple layers of controls at individual FEV level, the FEV charging station level, and the system level in modern DNs, as shown in Figure 4.1.

At the FEV level, each FEV agent manages its charging and VAR injection in a decentralized manner while considering the local voltage of the point of interconnection on the grid. However, FEVs have limited visibility into the state of operation of the system, leading to decisions that may not be in line with the needs of the system. Since this work focuses on distributed optimization, each FEV is assumed to obtain a signal for the net voltage deviation of the neighboring nodes that form a subnetwork within the distribution network. The challenge is to ensure that even with limited information, each FEVâs action contributes to local and global voltage stability.

At the FEVCS level, multiple FEVs are connected to the same FEVCS. The FEVCS must avoid conflicting actions of individual FEV that may undermine the overall

ability to maintain local voltage. The lack of coordination can also influence the surrounding nodes in the DN. Hence, there is a need for a framework that can harmonize the actions of co-located agents, ensuring that their collective behavior supports the local voltage regulation without causing instability.

At the system level, multiple FEVCSs interact with the distribution network operator, each unique with its characteristics like duty cycle, energy demand, and peak demand. The FEVs at different FEVCSs at different nodes on the DN need to be coordinated for distributed voltage control to maintain system-wide voltage stability.

The complexity lies in coordinating these distributed agents to achieve grid-wide objectives. Given that FEVs operate under different conditions, a scalable solution with the capability to generalize across these varying conditions while ensuring that the decentralized decision-making of individual FEVs contributes positively to the overall stability of the DN.

This paper addresses these multilayered challenges by presenting a novel FLE-CA-MARL framework for distributed control of FEVCSs with individual FEV agents cooperatively for Volt/VAR optimization in the distribution network. Firstly, the individual FEV agent's optimal charging with VVO is modeled using a POMDP that allows for the learning of the FEV agents with limited grid visibility and operation states. Secondly, the CA-MARL design ensures the actions of multiple FEVs at the same FEVCS are harmonized to maintain local voltage regulation. Furthermore, individual FEV agents at different FEVCSs at different locations in the DN are deployed in a federate learning framework to enable collaborative learning while preserving data privacy. The proposed FLE-CA-MARL framework integrating federated learning and CA-MARL is scalable to handle numerous EV agents and is adaptive to different networks with different configurations of FEVCS, presenting a generalizable solution for implementation in diverse DNs. Under the proposed framework, each FEV contributes to the global system's objective while optimizing its local environ-

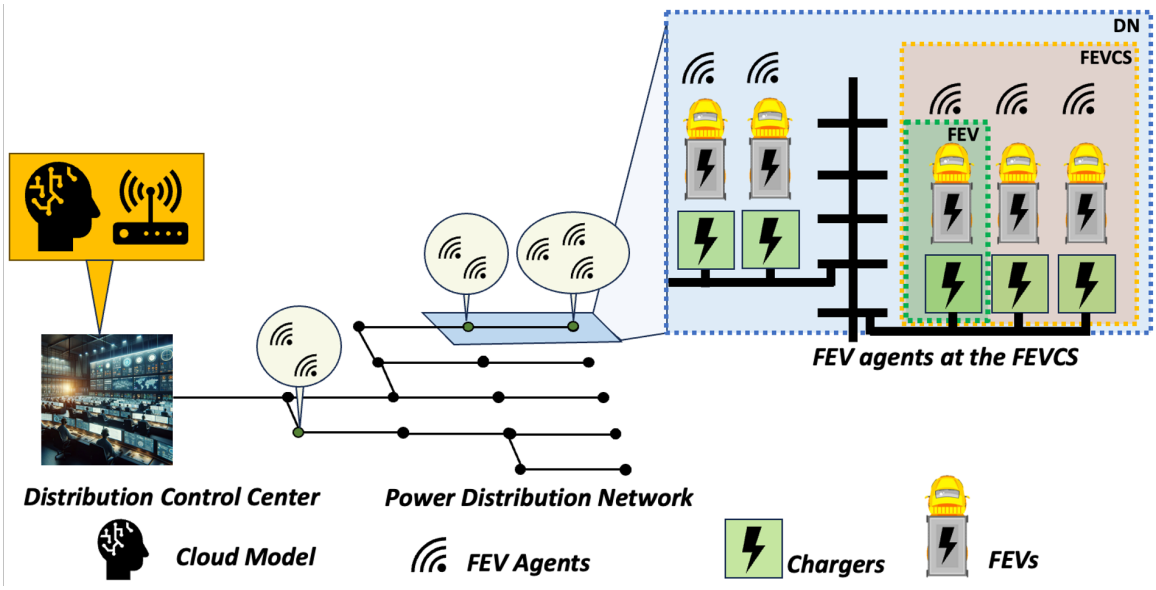

Figure 4.1: Layered challenges present in VVO of FEVCS

ment, resulting in a robust and flexible system for managing FEV charging across a distribution network.

4.2.1 Rationale for Model Selection

MARL was selected for modeling the interaction of FEVs in an FEVCS because it allows for decentralized decision-making in uncertain grid environments. The key advantage of having RL over other ML-based optimization methods is the adaptability that it offers, which can be advantageous for optimizing highly dynamic and uncertain environments. RL allows agents to adapt to the dynamics by learning from historical data and continuously updating their policies. In contrast, rule-based or static optimization methods cannot adjust to these rapid changes. Additionally, the horizontal nature of the proposed FL framework, FDRL enhances the adaptive nature of the RL by connecting several RL agents with diverse experiences, accelerating the learning of the global RL agent's policy. Moreover, FEVCSs operate at various locations with distributed agents, making centralized control both computationally heavy and slow. However, FDRL frameworks are highly suitable for implementing decentralized frameworks that require real-time adaptive control with periodic model

synchronizations. Additionally, by using MARL, multiple FEV agents can learn to act autonomously while coordinating their actions to support the grid. This coordination happens in a flexible manner, as the agents interact and learn through rewards based on their collective impact on the grid's stability. Finally, the most important factor is the scalability of the proposed approach. Since the states and actions in the framework remain constant for every agent, the model is highly scalable and generalizable from a fleet EV perspective. Moreover, with increasing agents in the FDRL framework, the policy becomes more optimal and generalized.

Model Predictive Control (MPC) is another powerful technique that could be considered for managing FEVCS, MPC works by solving an optimization problem at each step, predicting future system states, and making control decisions accordingly. Although MPC is well suited for handling constraints for short-term dynamics, it has limitations when applied to a multiagent system like FEVCS. MPC requires an accurate system model, which becomes difficult in complex multi-agent environments where the behavior of each FEV agent and the overall grid interaction is challenging to model. Moreover, while MPC excels in constrained optimization, it may struggle to adapt to real-time changes in system dynamics as efficiently as RL. In an environment where agents need to learn from, past interactions and adjust future actions based on dynamic conditions, RL provides better adaptability. Heuristic optimization-based techniques could be applied to optimize FEV scheduling and control tasks. However, they lack the flexibility of RL in dealing with dynamic decision-making. Hence, out of the existing ML-based optimization techniques, RL was chosen for optimization in the proposed FL framework.

4.3 Modeling

This work systematically addresses the challenges presented by individual FEV agents, multiple FEV agents at the same FEVCS, and the coordination of FEVCSs across the DN. The structure of the proposed FLE-CA-MARL framework is presented

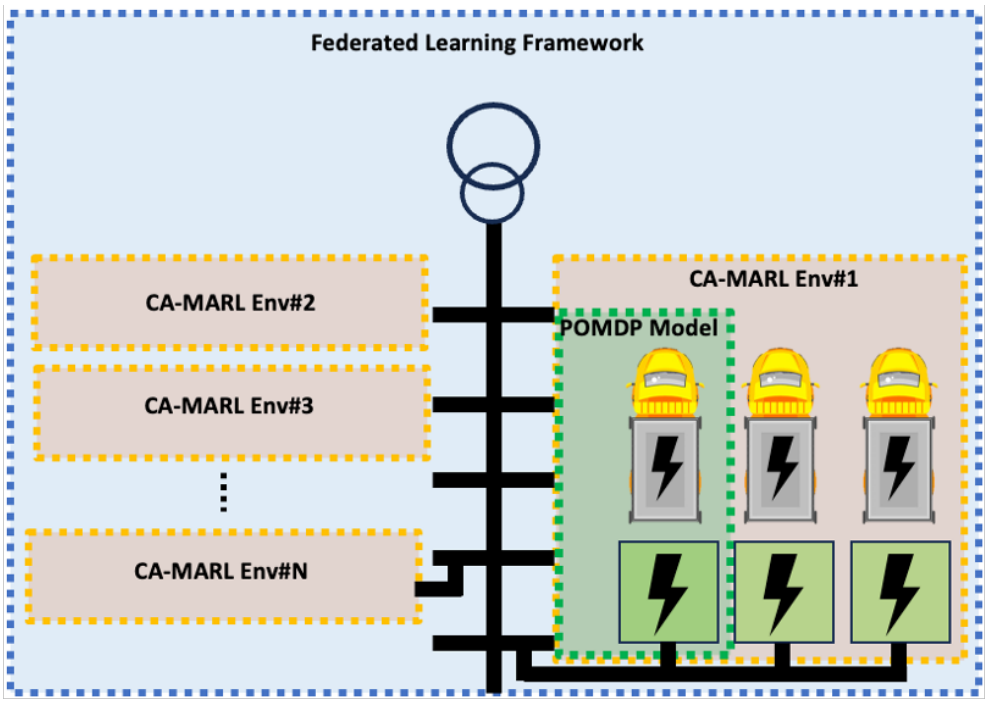

Figure 4.2: Proposed FLE-CA-MARL model

in Figure 4.2, consisting of (1) the POMDP model for the control of FEV agents, (2) the CA-MARL environment at the FEVCS level formed by multiple POMDP models of the FEV agents to harmonize the actions of multiple FEVs at the same FEVCS, and (3) the FL framework at the system level that connects all the RL agent's models of FEVs using a global RL model's synchronized aggregation and updates. Subsection 4.3.1 presents the conflict-aware RL model using POMDP for the control of each FEV agent. The CA-MARL environment for coordinating the controls of multiple FEV agents within an FEVCS is presented in subsection 4.3.2. Then, the FLE-MA-TD3 algorithm, employed to solve the model for the whole DN, is presented in subsection 4.3.3.

4.3.1 Modeling a Conflict-Aware FEV Agent

The first step in modeling the framework is to model the problem from the perspective of a single FEV agent. The decision-making process for FEV agents involves handling interactions between multiple agents operating in a shared environment.

Although each FEV agent can observe its variables, which includes the signal that provides the deviation of the neighboring nodes within it, it cannot observe the states of other FEV agents connected to the same charging station. This uncertainty makes the problem well-suited for modeling as a POMDP. Although the state transitions in the model are deterministic, the agent's partial observability creates a probabilistic perception of the environment, which POMDPs are designed to handle effectively. This framework captures uncertainty and helps to make optimal decisions despite incomplete knowledge of the full state of the system. The MDP is defined by a set of states S, a set of actions A, a reward function R, and a transition function of the state $\mathcal{T}$.

4.3.1.1 State Variables

The states represent the current state of the system, including the charging status, the state of charge, the time to departure, the power injected into the bus and the voltage deviations. The state $s \in S$ at the time t is defined as:

$$\begin{aligned} s(t): \quad & [C_t, C_{t-1}, \mathrm{SOC}_t, \mathrm{SOC}_{t-1}, \mathrm{TD}_t, P_{bus,t}, Q_{bus,t}, V_{bus,t}, \sum_{k \in K} |V_{k,t} - 1|, \\ & N_{agents,t}, p^{ch}_{t-1}, q^{dch}_{t-1}] \end{aligned} \tag{4.1}$$

where C_t and C_{t-1} indicate if the FEV is connected to the charger at the time t and $t-1$ respectively. SOC_t indicates the state of charge of the FEV at the time t. The departure time of the FEV is captured by the state TD_t. Active power, reactive power, and voltage at the agent bus are represented by $P_{bus,t}$, $Q_{bus,t}$, and $V_{bus,t}$ respectively. The state $\sum_{k \in K} |V_{k,t} - 1|$ represents the sum of voltage deviations of all buses in the subnetwork K . $N_{agents,t}$ presents the number of active agents available at the agent's node at time t. p^{ch}_{t-1} and q^{dch}_{t-1} are states that record previous actions of the agent.

4.3.1.2 Action Variables

As shown in Eq.(4.2), the actions of the FEV agent include active power charging, p_t^{ch} and reactive power injection q_t^{dch}. The set of actions A at the time t is defined as:

$$a(t): \quad [p_t^{ch}, q_t^{dch}] \tag{4.2}$$

The agent selects the actions based on the current observation and the policy of the DRL agent.

Additionally, to mitigate abrupt changes in the agents' actions, particularly in reactive power injections, a smoothing mechanism is introduced into the action space by applying a weighted moving average to the current and previous actions, ensuring smoother transitions. The smoothed action at time step t, a_t, is computed using the following equation:

$$a(t) = \alpha \cdot a(t)^{\text{new}} + (1 - \alpha) \cdot a(t-1) \tag{4.3}$$

where $a(t)^{\text{new}}$ is the new action selected by the FEV agent, and α is the smoothing factor that determines the weight of the current versus previous actions.

4.3.1.3 State Transition Equations

The state transition equations describe how the state variables evolve based on the actions taken. The state transition function $\mathcal{T} : S \times A \to S$ is defined as:

$$\text{SOC}_{t-1} = \text{SOC}_t \tag{4.4}$$

$$\text{SOC}_t = \text{SOC}_{t-1} - (p_t^{ch} \cdot \eta_{fv} \Delta t) \tag{4.5}$$

In Eq.(4.5), η_{fv} represents the charging efficiency factor and Δt is the time step size. In addition to the above transition equations, the agent's transition includes storing the previous actions as an observation for the next action using Eq. (4.6).

$$[p_{t-1}^{ch}, q_{t-1}^{dch}] = [p_t^{ch}, q_t^{dch}] \tag{4.6}$$

4.3.1.4 Reward Function

The reward function $R : S \times A \rightarrow R$ defines the objective of the optimization problem, penalizing deviations and undesirable outcomes. The reward $r(t)$ at time t is given by:

$$R_{\text{VF}} = \begin{cases} -C_{\text{VF}} \sum_{k \in K} |V_k - 1| & \text{if } C(t) = 1 \\ 0 & \text{otherwise} \end{cases} \tag{4.7}$$

$$R_{\text{VL}} = \begin{cases} -C_{\text{VL}} \, |V_{\text{bus}} - 1.05| & \text{if } V_{\text{bus}} > 1.05 \text{ and } C(t) = 1 \\ -C_{\text{VL}} \, |V_{\text{bus}} - 0.95| & \text{if } V_{\text{bus}} < 0.95 \text{ and } C(t) = 1 \\ 0 & \text{otherwise} \end{cases} \tag{4.8}$$

$$R_{\text{CR}} = \begin{cases} C_{\text{CR}} \cdot \exp\left(-\frac{(P_{\text{ch}} - P_{cr*} \cdot P_{\max})^2}{2 \cdot \sigma^2}\right) & \text{if } C(t) = 1 \\ & \text{and SOC}(t) < 1 \\ 0 & \text{otherwise} \end{cases} \tag{4.9}$$

$$R_{\text{SL}} = \begin{cases} -C_{\text{SL}} & \text{if } C(t) = 0 \text{ and } C(t-1) = 1 \\ & \quad \text{and SOC}(t-1) < 1 \\ 0 & \text{otherwise} \end{cases} \tag{4.10}$$

Eq. (4.7) defines the penalty applied to the agent for the voltage deviation of all the

nodes in the agent's subnetwork K. The penalty R_{VL}, defined to restrict the agent node's voltage within the acceptable range of 1 +/- 0.05 p.u is defined in Eq.(4.8). Both Eq.(4.7) and Eq.(4.8) are applied to the agent when the FEV is connected to the charger. Since the agent requires an incentive to charge the vehicle, Eq. (4.9) is defined to introduce the reward R_{CR} to motivate the agent to try charging at a recommended rate to increase the SOC to avoid the sparse penalty that is defined in Eq.(4.10). This approach is based on a Gaussian function, with σ controlling the range of recommended charging rate. The penalty R_{SL}, is introduced to penalize the agent if the vehicle is forced to leave the charging station with a state of charge of 100%. The reward function also includes a penalty for conflicts arising from multiple agents attempting to optimize their reactive power discharge simultaneously. The conflict-aware reward function, designed to penalize conflicts with the other active agents within the FEVCS and the incorrect actions of reactive power injections, can be expressed by Eq. (4.11).

$$R_{\mathrm{C}} = \sum_{f' \neq f}^{N} \begin{cases} -C_{\mathrm{C}} \cdot |q_{t-1}^{dch} - q_{f',t-1}^{dch}| & \text{if conflict detected} \\ -C_{\mathrm{A}} & \text{if incorrect polarity} \\ 0 & \text{otherwise} \end{cases} \tag{4.11}$$

where R_{C} represents the reward associated with the conflict-awareness feature of the agent, C_{C} represents the coefficient of penalty for a detected conflict with another agent in the same charging station, C_{A} represents the coefficient of penalty for incorrect polarity of reactive power injection, q_t^{dch} represents the reactive power discharged by the agent, and $q_{f',t}^{dch}$ represents the actions related reactive power injection of all the other agents.

$$R(t) = R_{\mathrm{VF}}(t) + R_{\mathrm{VL}}(t) + R_{\mathrm{CR}}(t) + R_{\mathrm{SL}}(t) + R_{\mathrm{C}}(t) \tag{4.12}$$

As shown in Eq.(4.12), the final reward for each time step is the summation of all

the rewards presented from Eqs.(4.7)-(4.11).

4.3.2 CA-MARL Environment

The CA-MARL environment integrates multiple POMDP models for FEV agents within a single FEVCS. Each agent f operates under the POMDP framework, where their interactions are managed collectively to ensure optimal voltage regulation at the charging station level.

4.3.2.1 State Aggregation

The aggregated state for the FEVCS at the time t is given by:

$$S_{\text{FEVCS}}(t) = \{s_1(t), s_2(t), \ldots, s_N(t)\} \tag{4.13}$$

where $s_f(t)$ represents the state of each agent f as defined in equation (4.1).

4.3.2.2 Action Aggregation

The aggregated action set for the FEVCS is:

$$A_{\text{FEVCS}}(t) = \{a_1(t), a_2(t), \ldots, a_N(t)\} \tag{4.14}$$

where $a_f(t)$ represents the action of each agent f as defined in Eq. (4.2).

4.3.2.3 State Transition Function

The state transition for the CA-MARL environment accounts for interactions among agents:

$$\begin{aligned}\mathcal{T}_{\text{FEVCS}}(S_{\text{FEVCS}}(t), A_{\text{FEVCS}}(t)) = \{&\mathcal{T}(s_1(t), a_1(t)),\ \mathcal{T}(s_2(t), a_2(t)),\\ &\ldots, \mathcal{T}(s_N(t), a_N(t))\}\end{aligned} \tag{4.15}$$

where $\mathcal{T}(s_f(t), a_f(t))$ is the individual state transition function of each agent f.

4.3.2.4 Reward Function

The reward for each individual agent f in the CA-MARL environment is defined independently, based on the specific conditions at the location of each agent and their interactions with other agents. The individual reward function for the agent f at time t is presented in Eq. (4.12). To express the aggregated reward across all agents at the FEVCS, we sum the individual rewards:

$$R_{\text{FEVCS}}(t) = \sum_{f=1}^{N} R_f(t) \tag{4.16}$$

This aggregated reward function reflects the combined performance of all agents in the FEVCS while maintaining the independence of each agent's decision-making process.

This CA-MARL environment ensures that all FEV agents in a single FEVCS work in coordination, managing both their individual objectives and the overall voltage regulation of the FEVCS.

4.3.3 Federated Learning-Enhanced MA-TD3 Algorithm

The proposed FLE-MA-TD3 algorithm introduces a personalized update mechanism to coordinate the learning of FEV agents at different charging stations. This framework allows each agent to benefit from global knowledge while retaining local adaptability. The architecture of the FLE-MA-TD3 algorithm in Figure 4.3 illustrates the CA-MARL environment for the FEV agents, the FL framework for the TD3 agents, and the communication between the TD3 agents.

Algorithm 1 Multi-Agent TD3 with Federated Learning

Initialize environment env, number of agents N, Replay Buffers B_i for each agent i
Initialize actor networks π_{θ_i} and target actor networks π'_{θ_i} for each agent i
Initialize critic networks Q_{ϕ_i}, Q'_{ϕ_i} and target critic networks Q'_{ϕ_i} for each agent i
Initialize central server for federated learning
for total steps $t = 1$ to T **do**
    Sample actions $a_i = \pi_{\theta_i}(s_i) + \epsilon$ for each agent i
    Execute actions a_i in environment, observe rewards r_i and next states s'_i
    Store transitions $(s_i, a_i, r_i, s'_i, d_i)$ in replay buffer B_i for each agent i
    if B_i is ready for training **then**
        for each agent i **do**
            Sample mini-batch of transitions from B_i
            Compute target actions $\tilde{a}_i = \pi'_{\theta_i}(s'_i) + \epsilon'$
            Compute target Q-values $y_i = r_i + \gamma(1 - d_i)\min(Q'_{\phi_i}(s'_i, \tilde{a}_i))$
            Update critic by minimizing loss $L(\phi_i) = \frac{1}{|B_i|}\sum(Q_{\phi_i}(s_i, a_i) - y_i)^2$
            if $\mathrm{mod}(t, \mathrm{policy\_delay}) == 0$ **then**
                Update actor by maximizing $J(\theta_i) = \frac{1}{|B_i|}\sum Q_{\phi_i}(s_i, \pi_{\theta_i}(s_i))$
                Update target networks: $\theta'_i \leftarrow \tau\theta_i + (1 - \tau)\theta'_i$
            end if
        end for
    end if
    if $\mathrm{mod}(t, \mathrm{sync\_interval}) == 0$ **then**
        Aggregate models across all agents at central server
        Distribute aggregated models back to agents
    end if
    if any episode ends **then**
        Reset environment
    end if
end for
Save the model at the end of training

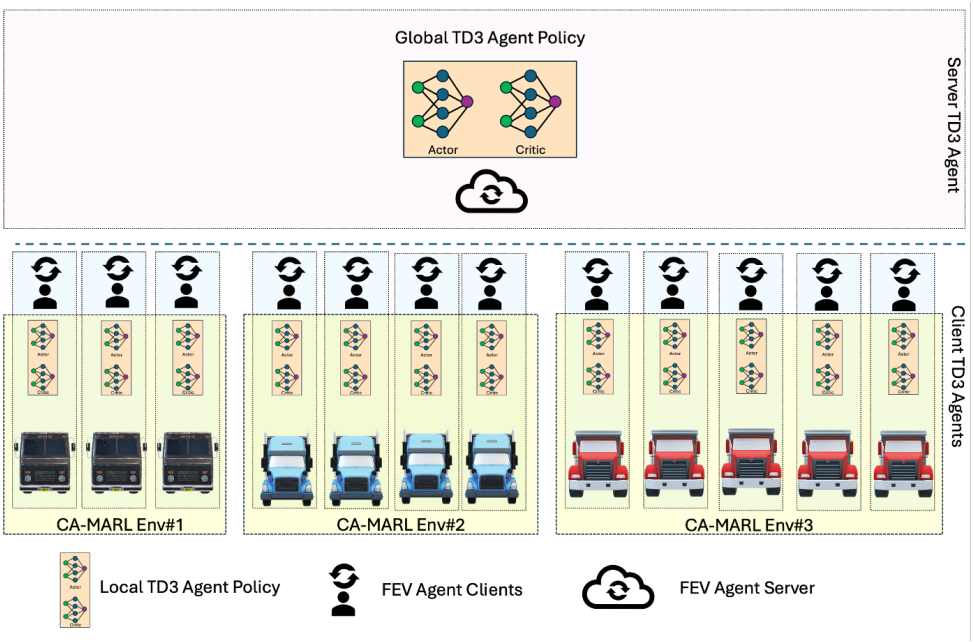

Figure 4.3: Architecture of the FLE-MA-TD3 algorithm

4.3.3.1 Global Model Aggregation

The global model parameters θ_g^t are computed by aggregating the local model parameters θ_f^t from each FEV f at iteration t:

$$\theta_g^t = \frac{1}{N} \sum_{i=1}^{N} \theta_f^t \tag{4.17}$$

4.3.3.2 Personalized Model Update

Each local model at the FEV f is updated by blending the global model parameters with the local model parameters using the parameter τ, controlling the degree of personalization:

$$\theta_f^{t+1} = \tau \theta_g^t + (1 - \tau)\theta_f^t \tag{4.18}$$

This update mechanism ensures that local models are influenced by global knowledge while preserving local characteristics, which can be crucial for stability and adaptability in diverse network environments.

This framework allows for decentralized yet coordinated learning, enabling each FEV to optimize local objectives while contributing to the global voltage of the DN. The proposed FLE-MA-TD3 algorithm is presented in Algorithm 1.

4.3.4 Simulation Setup

Visual Studio Code IDE was used to code FLE-MA-TD3 algorithm in python. The TD3 algorithm for a single agent was implemented based on the works [84] and [85]. The TD3 agent was converted to an MA-TD3 based on [86]. The FL framework was custom-coded to execute model synchronizations for all the TD3 agents using a central TD3 agent. Federated averaging was selected as the method of model data aggregation in the FL framework. Power flow was carried out leveraging *pandapower*, an open-source tool for power systems modeling[87]. The IEEE 33-bus test case required for the simulation was imported from *pandapower*. The numerical experiments were conducted on a computer with an Apple M2 Pro processor and 32 GB of RAM.

4.4 Results of the FLE-CA-MARL framework

4.4.1 Case Description

The simulation setup was utilized to carry out on a modified IEEE 33 bus, as shown in figure 4.4. FEVCSs are assumed to be located on the buses 14, 21, and 29 on the distribution network. Assuming that these FEVCSs are ready to provide volt-VAR control services to the utility or the distribution system operator, the buses indicated in orange color indicate controllable nodes, which are part of a subnetwork that consists of neighboring nodes. Node 14 is the controllable node in subnetwork SN#0 that consists of visible nodes 6-21. Similarly, controllable nodes 21 and 22 have visibility to the subnetworks SN#1 and SN#2 respectively. From the FEV agent's perspective, the visibility of the subnetwork is in the form of aggregated voltage deviations from the voltage set point of all the nodes in the subnetwork The training environment depends on vehicle data and the load data on the feeder. The voltage

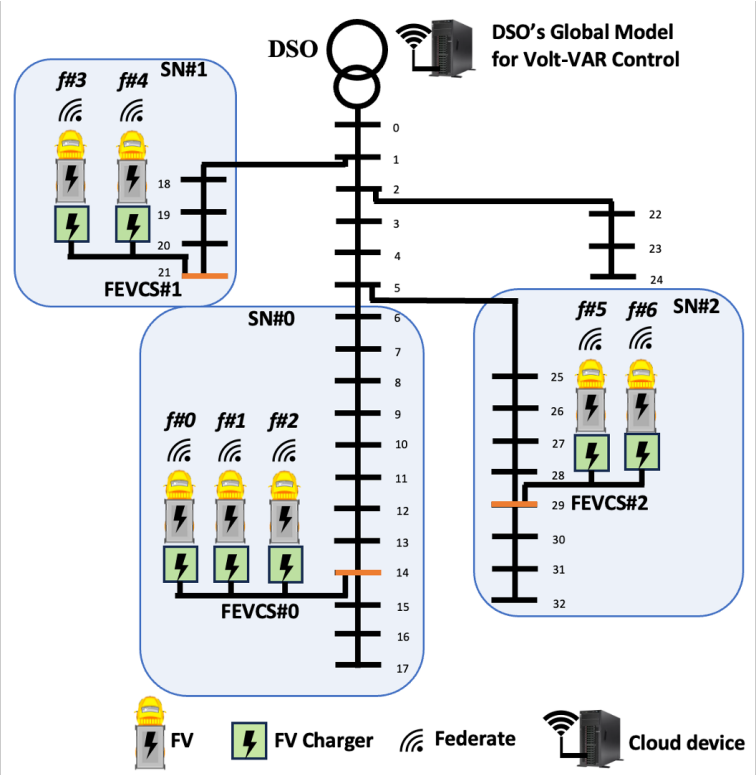

Figure 4.4: Modified IEEE 33 bus test setup : Case TC3

set point considered for this work is 1.p.u. The FEV specific data such as charging status C_t and time to departure TD are assumed to be known for the next time-step. One year data of both C_t and TD were generated with a 15-minute granularity based on the assumptions presented in the Table 4.1. A normal distribution with a mean and standard deviation was used to generate the time of arrivals of the FEVs.

Three different test cases were crafted to test different configurations of multi-agent interactions within in the FLE-CA-MARL framework. The first test case $TC1$ consists of a scenario where three FEV agents are connected to the charging station $FEVCS\#0$ on node 14. This setup evaluates the performance of the multi-agent environment of the FLE-CA-MARL framework for a single FEVCS. Table 4.2 shows the data related to the $TC1$. These agents in the presence of a conflict-aware reward function have to coordinate to improve voltage at the POI of the $FEVCS\#0$. Similarly, the second test case $TC2$ explores a scenario where the seven FEV agents

Table 4.1: FEV data for arrival and departure of vehicles

FEV	**Arrival time**		**Departure time (time)**
	Mean (time)	**Std (hours)**	
0	17:00	0.5	8:00
1	17:00	0.5	8:00
2	17:00	0.5	8:00
3	16:00	0.75	7:00
4	16:00	0.75	7:00
5	18:00	0.5	9:00
6	18:00	0.5	9:00

Table 4.2: Test case TC1

FEV	**FEVCS**	**Bus**	**Charger Capacity (kVA)**	**Battery Storage (kWh)**
0	0	14	100	400
1	0	14	100	400
2	0	14	100	400

Table 4.3: Test case TC2

FEV	**FEVCS**	**Bus**	**Charger Capacity (kVA)**	**Battery Storage (kWh)**
0	0	14	100	400
1	0	14	100	400
2	0	14	100	400
3	0	14	100	400
4	0	14	100	400
5	0	14	100	400
6	0	14	100	400

Table 4.4: Test case TC3

FEV	FEVCS	Bus	Charger Capacity (kVA)	Battery Storage (kWh)
0	0	14	100	400
1	0	14	100	400
2	0	14	100	400
3	1	21	50	200
4	1	21	50	200
5	2	29	150	400
6	2	29	150	400

presented in Table 4.1 are connected to the $FEVCS\#0$. The charging capacities and the battery storage capacities of the agents for the test case $TC2$ are shown in Table 4.3. This scenario evaluates the scalability of the framework for a single charging station. Finally, the third test case $TC3$ presented in Table 4.4 is the setup shown in Figure 4.4. This scenario tests the framework in the presence of agents at multiple FEVCSs. All the nodes on the feeder were assumed to have commercial customers of the type of office, warehouse, and hotels. The 15-minute granularity end-user load profiles from NREL from [88] were used for the load profiles. Out of 35,040 data points which represent one-year data of 8760 hours with 15-minute granularity, 32,064 were used for training the model and 2,976 were used for testing the model. .

4.4.2 Training and Tuning

The FLE-CA-MARL framework was implemented using multiple simulation scenarios, where tuning the hyperparameters of the TD3 agents played a critical role in achieving convergence and optimal performance. Two key steps in tuning a TD3 agent are hyperparameter tuning and reward tuning. Both these tunings were carried out manually for the three test cases. Each test case builds upon the previous one by increasing the complexity of the number of agents involved or the scenario being tested.

The initial test case $TC1$ involves one CA-MARL environment with an FL framework synchronizing the actor and critic of the three FEV agents at a set frequency. The agents were trained with the same hyperparameters as the agents in the FL framework can have equal influence on the global model. The tuned hyperparameters for the Case $TC1$ are *learning rate* at $2e-4$, *tau* at 0.006, *gamma* at 0.92, *memory size* at 300000, *batch size* at 256, *policy noise* at 0.1, *noise clip* at 0.5, and *policy delay* at 1. With the *episode length* set at 144 time steps, with each time step representing the environment variables with a 15-minute granularity, the training was carried out for, 300000 time steps. The final agent models with the converged rewards and policy losses were tested in a testing environment that simulates a similar environment to validate the performance of the agents. For the next test case $TC2$, the same hyperparameters were used to evaluate the performance of the agents in the CA-MARL environment with 7 FEV agents. The training was initiated using transfer learning of a trained agent's policy from $TC1$, and then the training was carried out using the proposed algorithm. The variation of hyperparameters yielded suboptimal rewards, leading to the decision of the same training hyperparameters for the TD3 agents.

For the Case $TC3$ with multiple FEVCS's on the distribution network, we have multiple CA-MARL environments interacting with the grid simulation environment. The same hyperparameters used in the Case $TC1$ and $TC2$ were employed for $TC3$ as well. Similarly, transfer learning was used to initiate the training of agents in the $TC3$.The training was carried for, 350000 time steps until the agent's reward and losses converge.

4.4.3 Results from TC1: Performance at the FEVCS-level

The agents were trained within the framework based on the Case $TC1$ with three FEV agents. In $TC1$, FEV agents 0-2 are connected to bus 14 within the subnetwork $SN\#0$. The schedule for the agents 0,1 and 2 are based on the Table 4.1 and capacities are as shown in Table 4.2. The vehicles connect to the charger in the FEVCS after

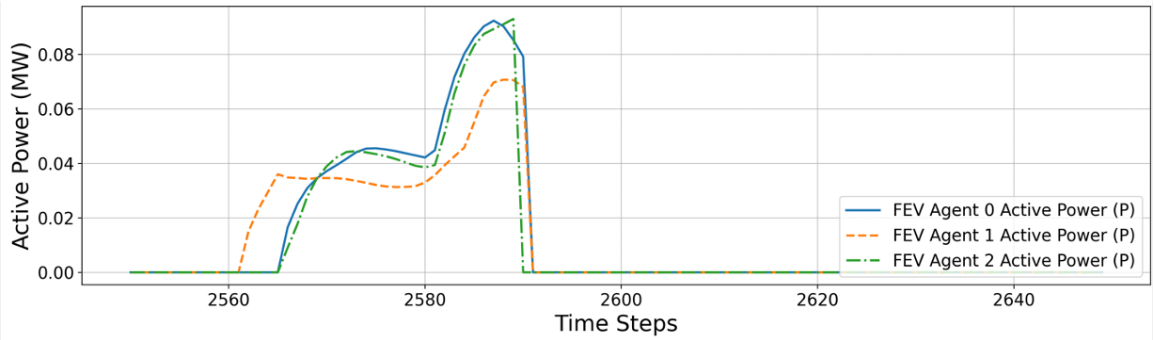

(a) Active power charging action taken by FEV agents

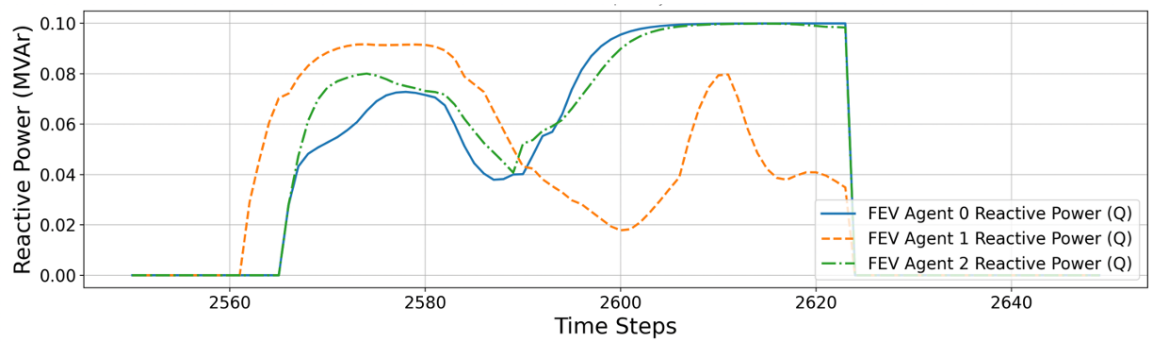

(b) VAr discharging action adopted by the FEV agents

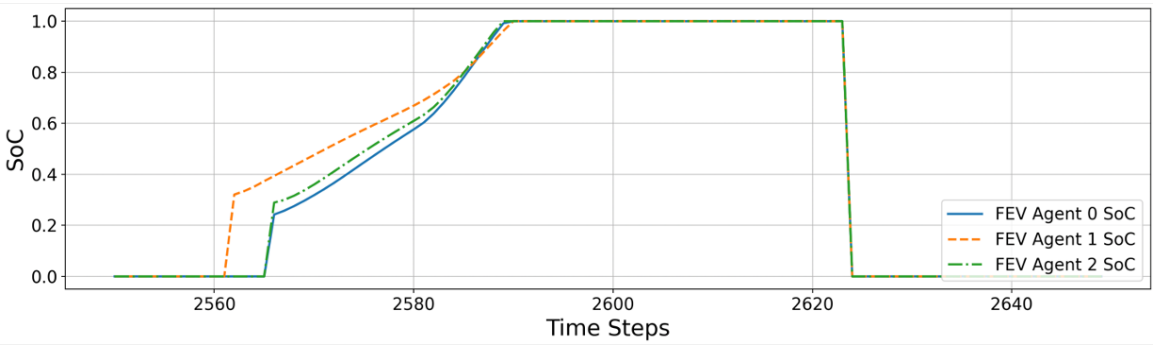

(c) Variation of SOC based on the active power charging

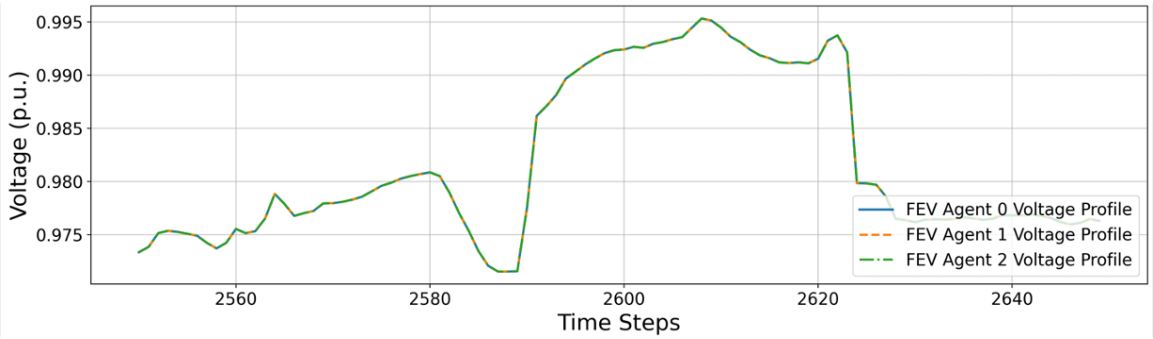

(d) Voltage of the POI of the FEVCS

Figure 4.5: Actions of the FEV agents for Case $TC1$

they arrive, based on their time of arrival. The model was tested by providing the essential observations for each time step to match the testing scenario. The FEV agent chooses the next action based on the previous time step's voltage and grid condition and the policy of how the next time step could change. The results from the Case $TC1$ are after training for $300,000$ time steps, are presented in the figure 4.5. The time step on the x-axis refers to time with 15 minute granularity. $FEV\#1$ arrives early at the charging station, followed by $FEV\#0$ and, $FEV\#2$. $FEV\#1$ starts charging, while injecting reactive power onto the grid to mitigate the voltage drop and enhance the voltage on the POI. When $FEV\#0$ and $FEV\#2$ arrives, they start charging, while providing VAR injections to the grid. The charging pattern of all the agents are similar, with the magnitudes being different based on the required charge and the time of departure. The rate of charging is dependent on the required energy to fill the SOC and the coefficient R_{SC} of the charging and the function controlling the value of the penalty for not charging while the time to departure is approaching. The rate of charging is also dependent on the recommended charging rate at 30% of the rated capacity. While $FEV\#1$ charges close to the recommended charging rate for the majority of the time, it accelerates charging as the time of departure closes by. The agent's reward function is risk-averse, considering the high priority to fulfil the energy required before time of departure goes to zero. The higher penalty and the inability to see the future states makes the charging pattern more conservative, with the FEV agents choosing to fulfil their SOC requirement with half of the time to departure left. This is also because the agent can fulfill the SOC requirement, limiting the voltage deviations within +/-0.03 p.u. The voltage of the POI reduces marginally since the vehicles are injecting reactive power while charging the battery. After meeting their energy requirements, the FEVs focus on boosting the system voltage to 1 p.u. The zero values for SOC indicate the time during which the vehicles are not connected to the charging station.

It is valuable to note that the performance of the agents, as seen in the figure 4.5 is suboptimal since the agents display an accelerated charging behavior with more time to the time to departure, and agent $FEV\#1$ injecting less than maximum capacity of reactive power. This is because of the designed risk-averse reward function and the lack of experience of the agents. This can be clearly identified from the analysis of the results from the Case $TC2$ presented in the following subsection. The fact that further training of the Case $TC1$ to $400,000$ time steps gets rid of the suboptimal levels of reactive power injection from $FEV\#1$ also establishes the value of experience acquired during the agent's interaction with the grid environment.

4.4.4 Results from the Case TC2 : Scaling up at the FEVCS-level

More agents were added to the FEVCS using the Case $TC2$. In $TC2$, FEV agents 0-6 are connected to bus 14 within the subnetwork $SN\#0$. The actions and SOCs and grid voltage at the POI of the FEVCS is shown in the figure 4.6. The vehicles arrive at different point of time. The FEV agents start charging as soon as it reaches the FEVCS. The charging pattern still follows the risk-averse approach of prioritizing fulfillment of SOC requirements. For instance, $FEV\#3$ and $FEV\#4$ charges mostly at the recommended charging rate, since they arrive early at the FEVCS. Similarly, $FEV\#2$ also avoids charging rate exceeding 60% of the rated capacity. Other agents charge slow in the beginning before accelerating, the charging towards the end. Hence, different FEV agents exhibit different charging behavior based on their time of arrival, energy demand and the time to departure. Due to the agent's ability to adapt to the local environment, different agents connected to the same node of the DN, learns different charging behavior that suits their individual requirements while satisfying the FEVCS's goal of regulating the voltage while charging the vehicles at the charging station. Additionally, more agents are behaving optimally with the scale-up at the FEVCS-level and the experience transferred from the trained agent in the Case $TC1$. Hence, collaborative learning combined with the adaptive nature of the agents give

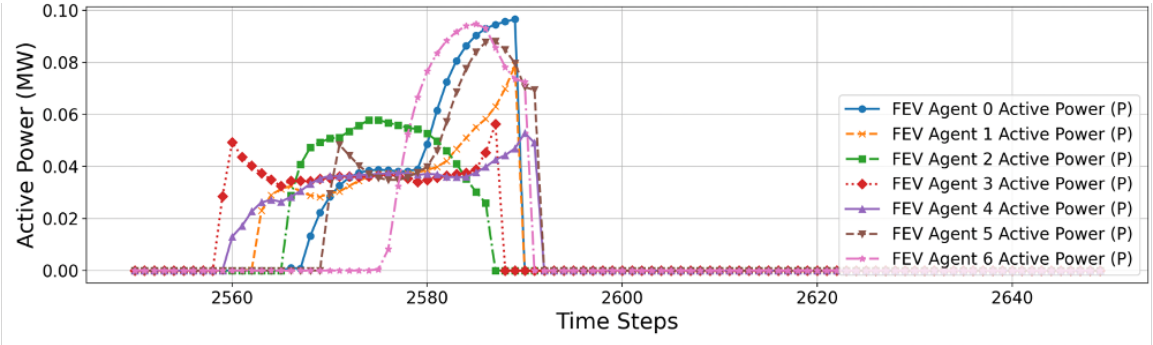

(a) Active power charging action taken by FEV agents

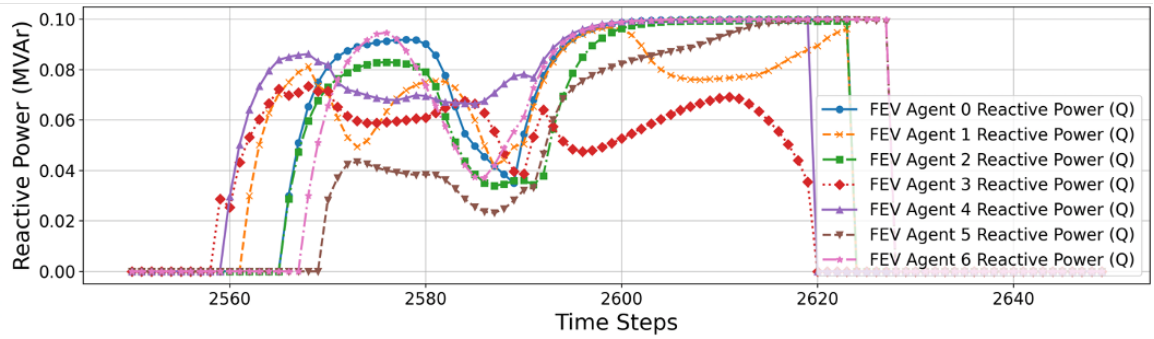

(b) VAr discharging action adopted by the FEV agents

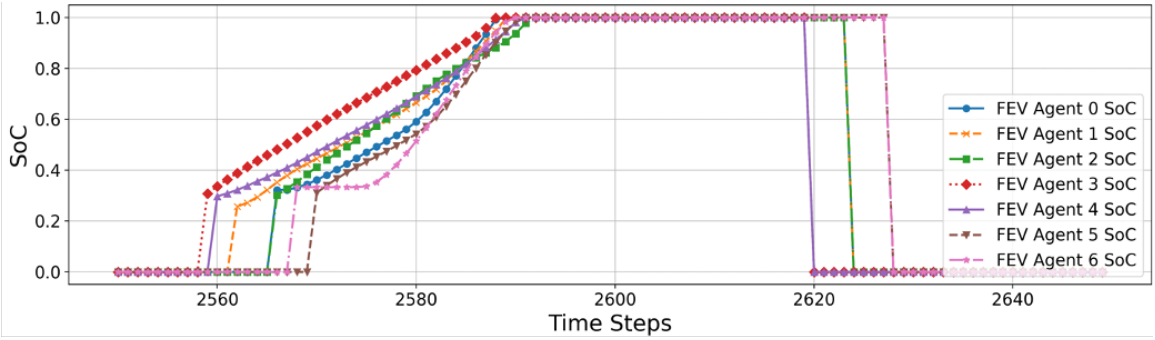

(c) Variation of SOC based on the active power charging

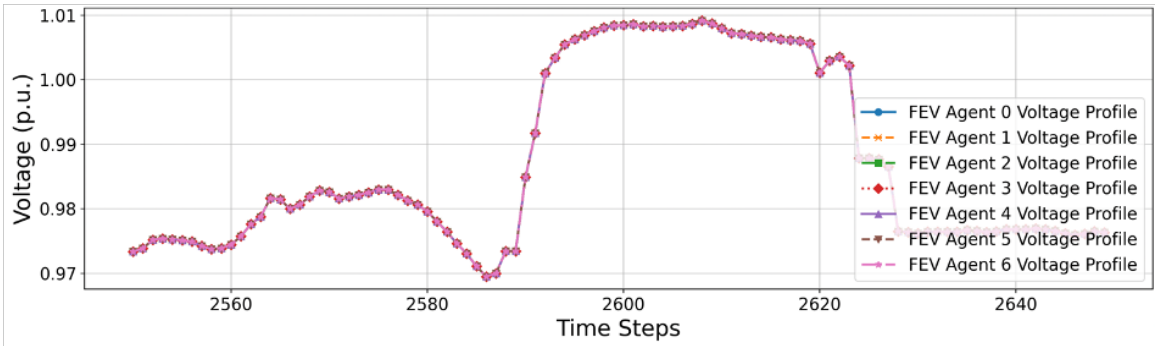

(d) Voltage of the POI of the FEVCS

Figure 4.6: Actions of the FEV agents for Case $TC2$

us the current performance of the framework. Moreover, further training and tuning could lead to more optimal behaviors from the agents.

4.4.5 Results from the Case TC3: Performance at the Distribution Network-level

To test the performance of the framework when integrating multiple charging stations, the Case $TC3$ shown in figure 4.4 is implemented. Agents $FEV\#0$, $FEV\#1$, and $FEV\#3$ are connected to the $FEVCS\#0$ in the subnetwork $SN\#0$. Agents $FEV\#3$ and $FEV\#4$ are connected to $FEVCS\#1$, and agents $FEV\#5$ and $FEV\#6$ are connected to $FEVCS\#2$. The actions of the FEV agents and the response of the environment variables are displayed in Figure 4.7. $FEV\#0$, $FEV\#1$, and $FEV\#3$ acts similar to the response observed in the Case $TC1$. Hence, $FEVCS\#0$ charges all the vehicles with a maximum deviation of +/-0.02 p.u. The deviation at $FEVCS\#0$ is also since it is located on Bus 14 with pre-existing voltage sag conditions. Moreover, the deviation in bus voltage has reduced from the +/- 0.03 p.u deviation in the Case $TC1$. Agents $FEV\#3$ and $FEV\#4$ are connected to, $FEVCS\#1$ which is very close to the DSO's substation. The challenge for the agents located on Bus 21 is to regulate the voltage finely enough to cause the least disturbance on the bus. The agents in $FEVCS\#1$ successfully charged the vehicles with a voltage of 1 p.u at the POI. Moreover, both agents $FEV\#3$ and $FEV\#4$ charged at the recommended charging rate 80% of the charging period. Agents $FEV\#5$ and $FEV\#6$ connected to $FEVCS\#2$ at Bus 29 of the test case. Both the agents of $FEVCS\#2$ charges at the recommended charging rate throughout the charging period. Through reactive power injections and controlled active power charging, agents of $FEVCS\#2$ cooperatively regulate the voltage at bus 29 by +/-0.01 p.u.

4.4.6 Scalability of the FLE-CA-MARL Framework

The case $TC2$ presented in subsection 4.4.4 presents the impact of scaling up at the FEVCS level. It is essential to note that the performance of the agents improves

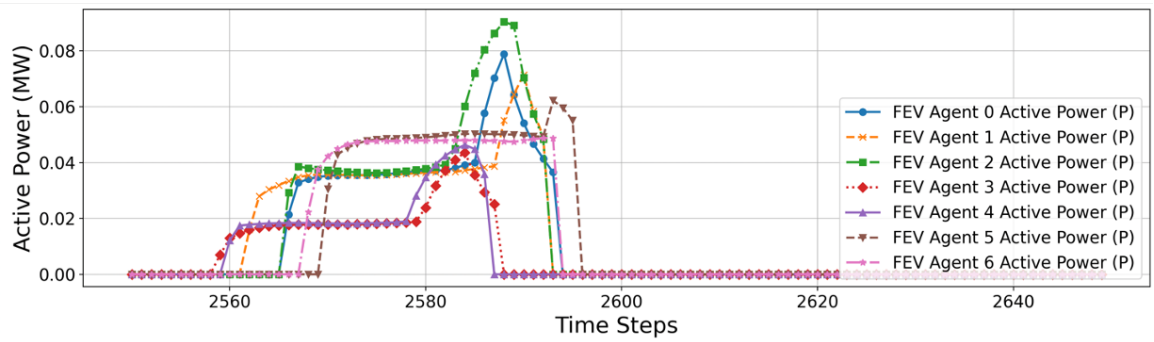

(a) Active power charging action taken by FEV agents

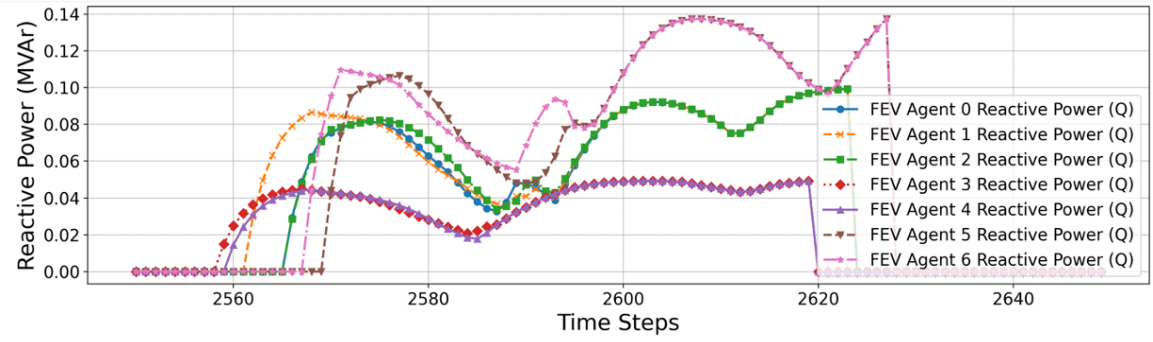

(b) VAr discharging action adopted by the FEV agents

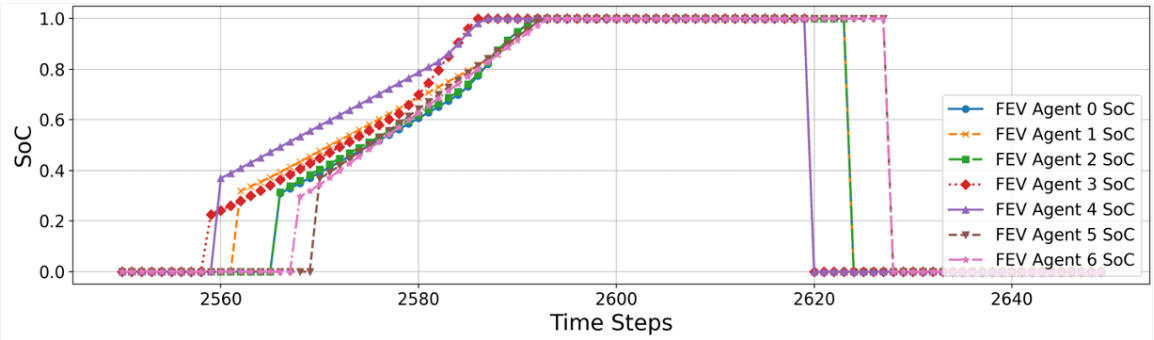

(c) Variation of SOC based on the active power charging

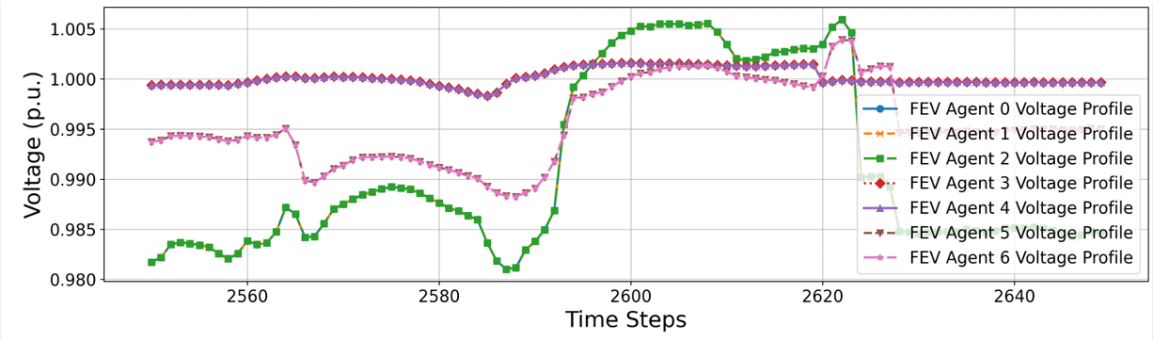

(d) Voltage of the POI of the FEVCS

Figure 4.7: Actions of the FEV agents for Case $TC3$

as the number of agents within the framework increases. Another instance of this can be noted from the Case $TC3$, since the increased number of agents within the framework is distributed among different nodes in the DN. This is due to the key feature of horizontal FRL (HFRL) where the agents interacting within the framework have identical features, contributing to accelerated learning of models within the framework. The advantage that these agents do not need real-time coordination is also a key advantage over other distributed optimization methods. As a result, the proposed framework is highly scalable and can be deployed in larger networks. Additionally, further analysis with a more heterogeneous agent distribution in the framework needs to be investigated to explore the requirement for other enhancements within the framework.

4.4.7 Synchronization Frequency Analysis for the FDRL Framework

The FDRL framework implemented in this study utilizes multiple agents interacting through a federated learning process to achieve a coordinated policy across various nodes. Each agent operates based on localized observations, such as the SOC and bus voltage at the POI, while the global model is periodically synchronized across all agents. A key element in determining the effectiveness of this approach is the number of time steps between global updates, referred to as *synchronization frequency* (SF). SF significantly affects the stability, learning performance, and convergence of the agents. For the presented framework, the actor loss, critic loss, and the episode reward were analyzed by varying the synchronization frequency was varied from 500 - $50,000$ steps.

Figure 4.8 presents the variation of rewards, actor losses, and critic losses of the agent FEV0 with training time steps in the test setup $TC1$. The data of SFs 500, 1000, 3000, 5000, 10,000, 25,000, and 50,000 steps are shown in the figure. *SF_ 500* in the legend represents an SF of 500 steps. For a high SF of 500 steps, the actor loss remains elevated and oscillates throughout the training period. The rapid synchronization

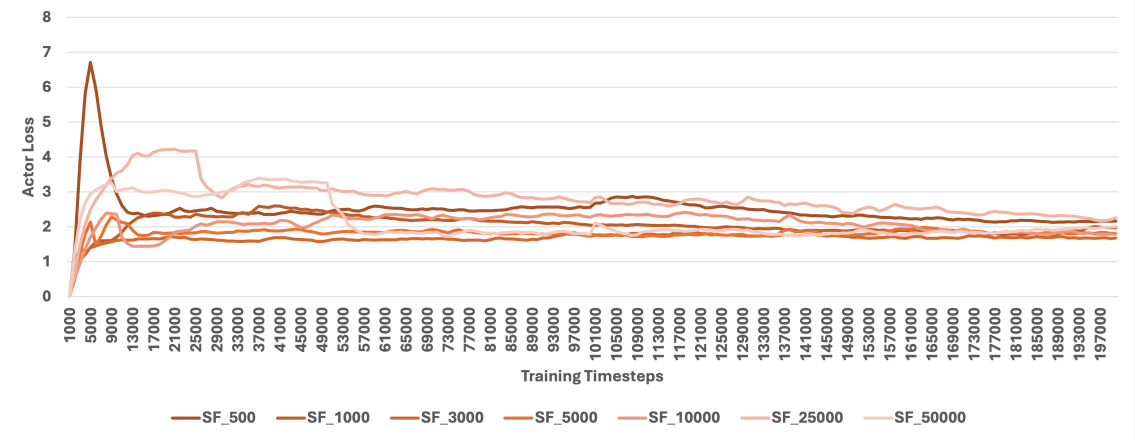

(a) Comparison of actor losses

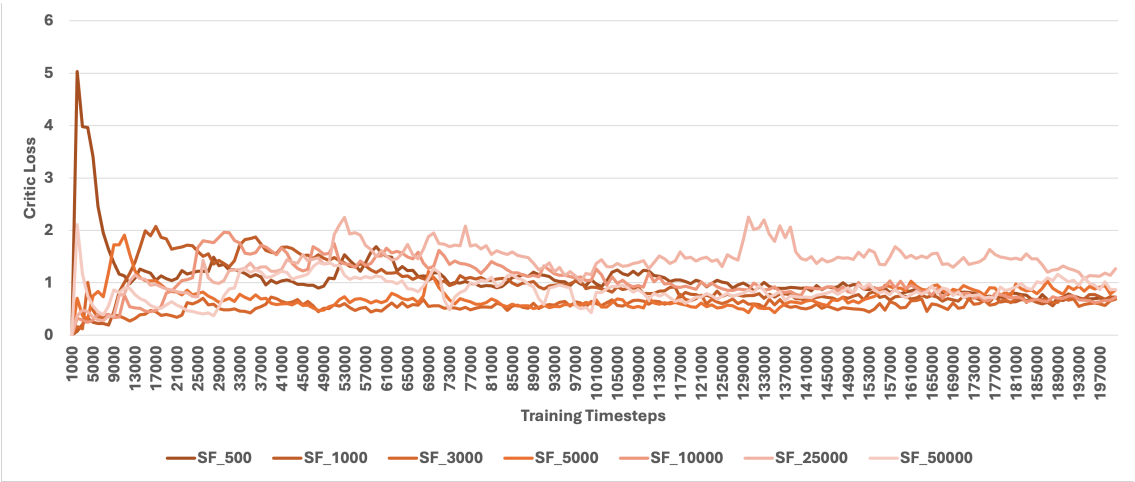

(b) Comparison of critic losses

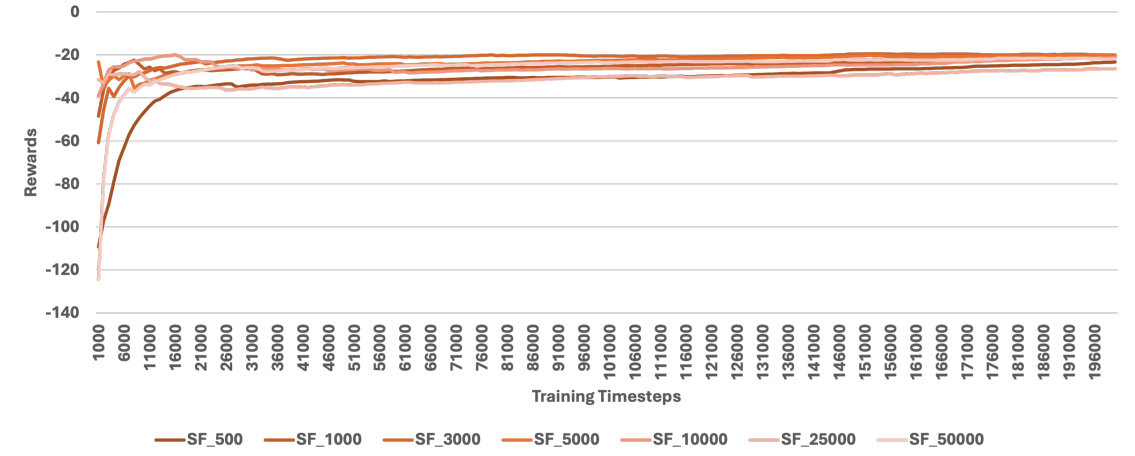

(c) Comparison of rewards

Figure 4.8: Tuning synchronization frequency for Case $TC1$

disrupts both actor and critic learning, causing high fluctuations by not allowing the agent enough time to adjust to the environment, leading to the learning of suboptimal policies that result in low rewards. In contrast, synchronizing too infrequently, like in the case of *SF_ 50000* leads to the divergence of the policies of the individual agents involved in the federated learning process. From the presented options, the optimal SF is 3000 steps, which achieves the lowest and the most stable actor and critic losses. This is a result of both networks being given enough time to refine their policies and value estimations between global updates, leading to smooth and effective learning. Consequently, the episodic reward is also higher for the SF of 3000 steps. Hence, 3000 steps strike a good balance between global coordination and local learning, enabling the agents to converge quickly and effectively. It allows sufficient time for individual learning while maintaining regular global updates to harmonize the agent's policy, resulting in the best overall performance.

4.4.8 Soft-Synchronization in the FLE-CA-MARL framework

Soft synchronization in FL is an approach where local models are updated periodically with a combination of local updates and a global model. The degree of the synchronization is controlled by a synchronization coefficient, which determines how much influence the global model exerts on each local agent. Soft synchronization allows local agents to maintain autonomy and explore the local environment while benefiting from periodic guidance from the global model, reducing overfitting to the local environments and improving the overall performance of the distributed agents.

For the presented analysis, the coefficient of soft synchronization (CoSS) was varied from 0.0001 to 1, and the performance of the training was evaluated based on the metrics actor loss, critic loss and episodic rewards. The purpose of the evaluation is to determine how different values of synchronization affect the stability and convergence of the learning process in the context of VVO using FEVCS. As observed in Figure 4.9, the actor loss and the critic loss of varies significantly throughout the

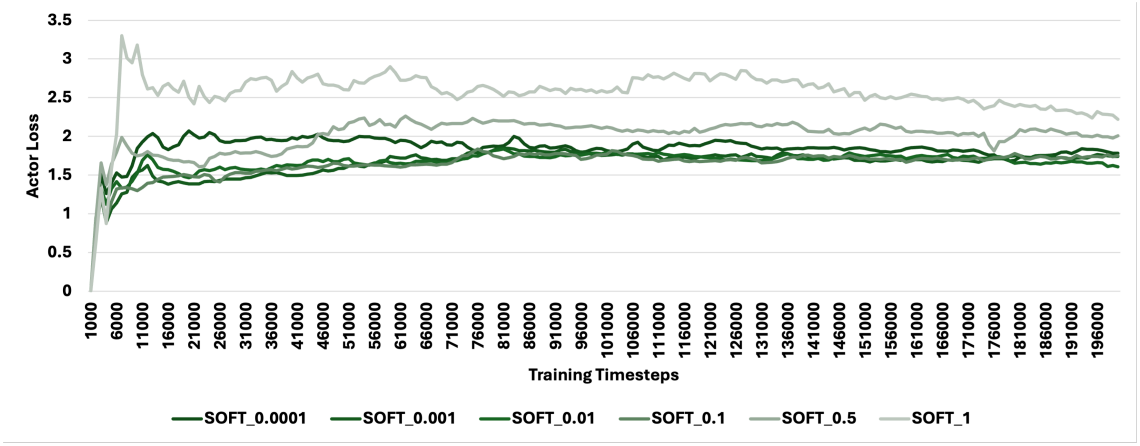

(a) Comparison of actor losses

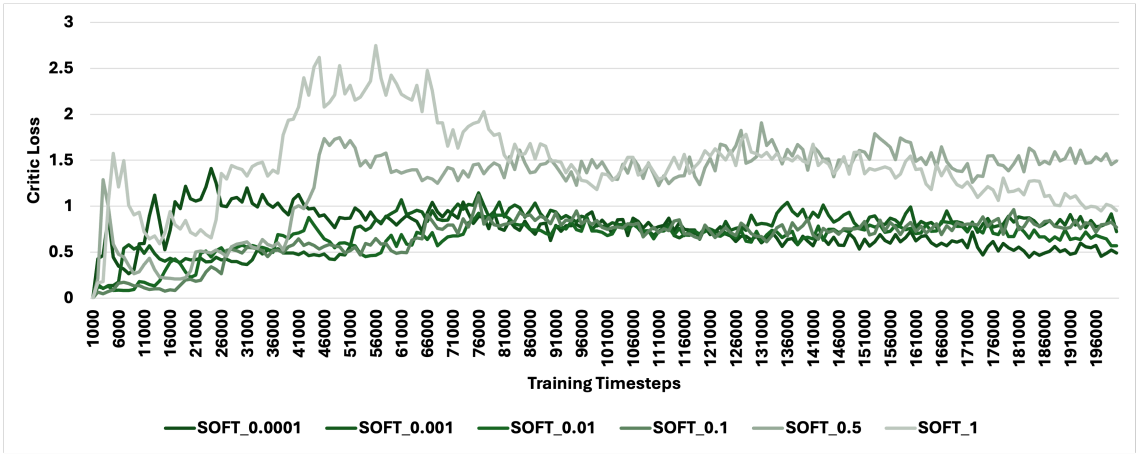

(b) Comparison of critic Losses

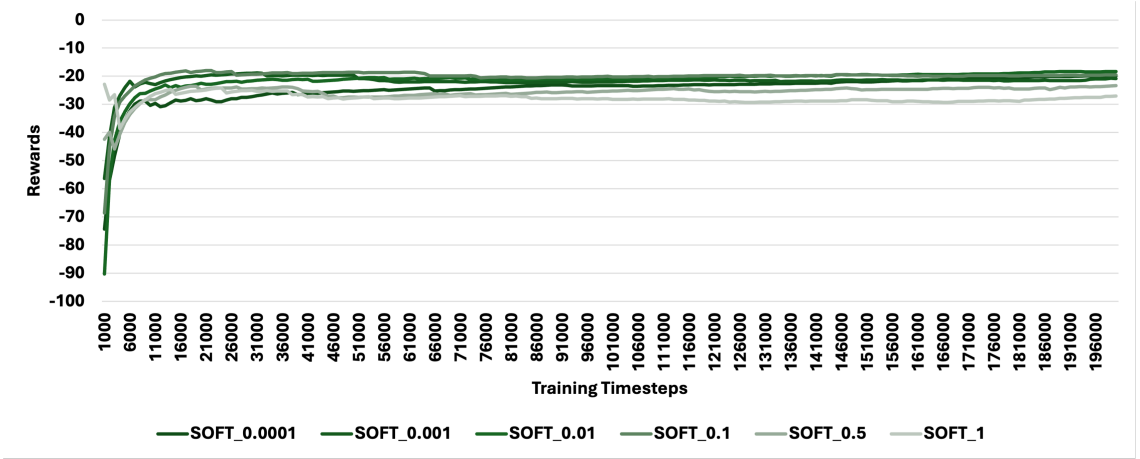

(c) Comparison of rewards

Figure 4.9: Impact of soft-synchronization on actor loss, critic loss and reward for the Case $TC1$

training for full synchronization, shown in the trend *SOFT_1* and *SOFT_0.5*. This indicates instability in learning of the actor and the critic. This is as a result of hard synchronization or complete replacement of model data in the local models, forcing them to continuously adapt to the global model, hindering their ability to fine tune policies effectively. On the other hand, the trainings *SOFT_0.1* and *SOFT_0.01* configurations show much lower and more stable actor losses. These coefficients of synchronization strike a balance, allowing the local agents to learn and adapt to their environments while still benefiting from periodic synchronization. This stability to leads to better convergence and rewards, with fewer oscillations in the actor and critic losses over time. At the lower end, the coefficient values 0.001 and 0.0001, providing better stability but slower convergence to the global policy. This is clear from the relatively slower convergence of the actor loss when the CoSS becomes too small.

The results of the impact of the value of soft-synchronization in FEV#5 in the case $TC3$ is presented in Figure 4.10. This case shows the impact of the value of soft synchronization for the selected SF of 3000 timesteps in a case with agents from different fleet charging stations. For the presented case, the training was initiated without the initial transfer learning process, which was included for the TC3 case's results presented in the above sections. Some key observations from the figure are that with the selected SF, we still see fluctuations in the actor loss and critic loss agents FEV#5 and FEV#6 operating at the node 29. Both agents deviate out of the training process for a value of 1 for the CoSS. This is clearly seen from the trend $SOFT\_1$ diverging or increasing heavily, while it stays at the same value for smaller values of the coefficient. This is due to the diverse experiences of the agents from the global model. Hence, heterogeneity in experience has can be addressed by setting the appropriate value of the CoSS.

The stability achieved during the training of the models in the subsection 4.4.5 was through the power of transfer learning combined with a lower CoSS value. The

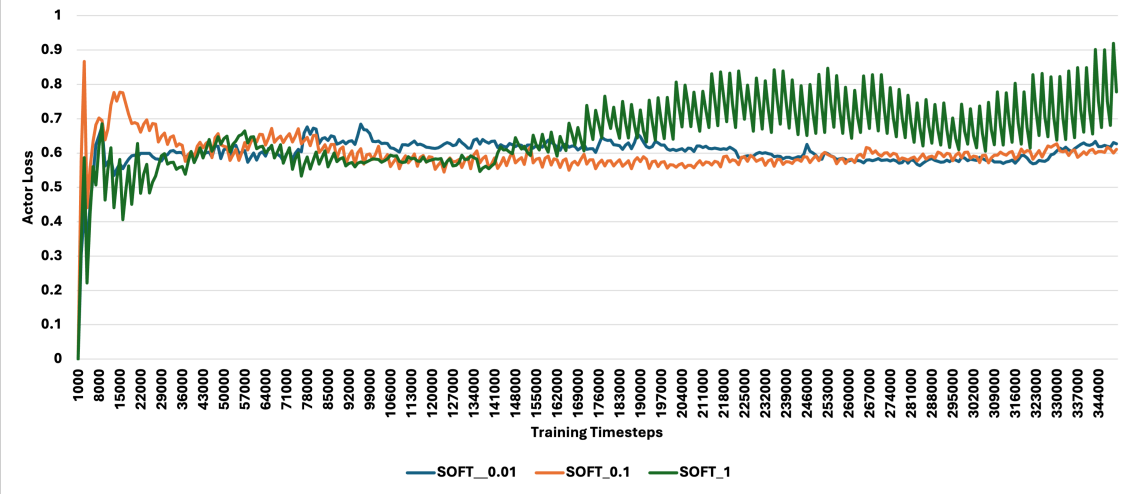

(a) Comparison of actor losses

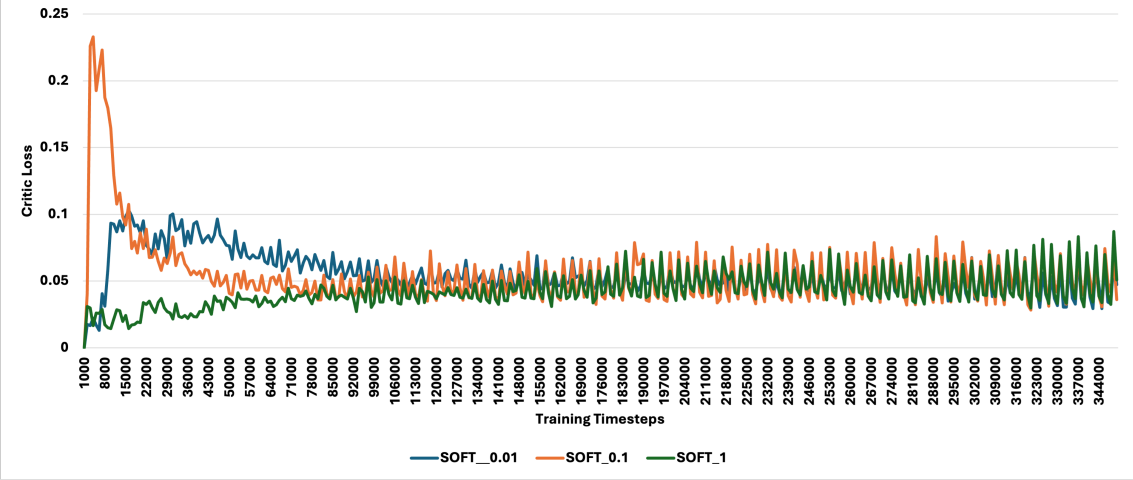

(b) Comparison of critic losses

Figure 4.10: Impact of the value of CoSS on actor loss and critic loss of agent 5 in the Case $TC3$

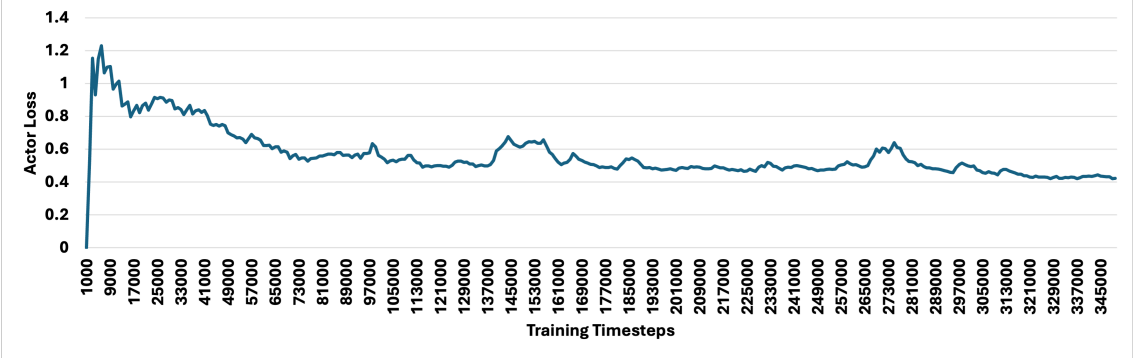

(a) Actor loss

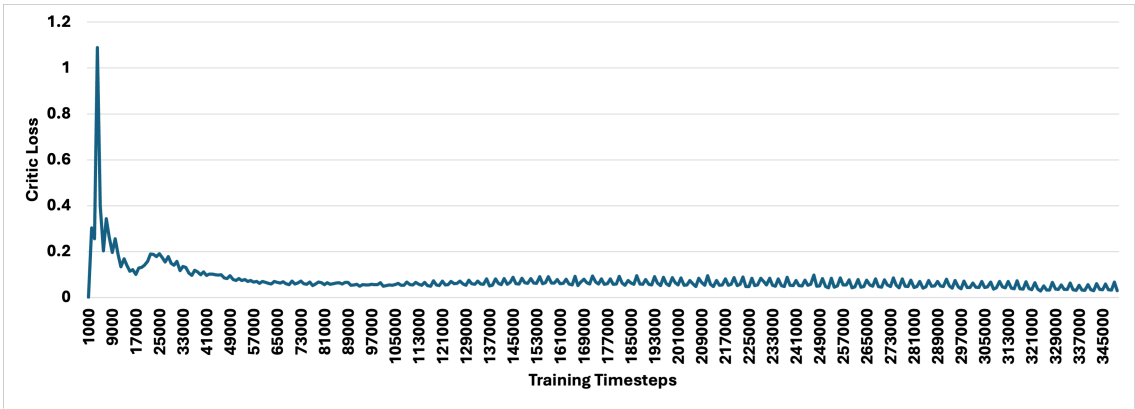

(b) Critic loss

Figure 4.11: Training metrics of transfer learning initiated training of agent 5 in FLE-CA-MARL framework for Case $TC3$

training of agent FEV#5 using transfer learning with the value of CoSS at 0.005 is shown in the figure. The critic loss converges after 150,000 time steps, leading to consistent reduction in actor loss. This is due to a much generalized global model to initiate the training and fine-tuning of the agent models. This further established the requirement for a central or global TD3 model to achieve optimal VVO on the distribution grid.

In a static training process, dependent on historical training data, the relevance of soft synchronization is about learning the best policy in the local environment. On the other hand, the role of soft synchronization in a dynamic environment will be interesting due to the influence of soft synchronization on the stability and the required rate of adaptation required in the control policy. This is one of the key aspects that is to be studied for this policy to be implemented in real-life.

4.5 Conclusion and Future Works

This work presents a novel FLE-CA-MARL framework designed for decentralized Volt/VAR control in the DNs with FEVCs. The proposed model does so by modeling FEV agents employing a POMDP framework with a conflict-aware design to consider FEVCS-level coordination. Furthermore, it utilizes an FLE-MA-TD3 algorithm to train the FEV agents to enable privacy-preserving collaborative-learning among all the agents throughout the DN, promoting a coordinated, generalized, and personalized VAR response from the agents. The proposed framework was validated through simulations on an IEEE 33-bus test system under various scenarios, demonstrating its robustness in both single and multi-charging station configurations. The results indicate that the FLE-CA-MARL framework can effectively manage voltage regulation while accommodating diverse load profiles and FEV characteristics, contributing to the overall voltage stability of the distribution system.

The proposed framework for VVO is part of the vision to have a coordinated and unified response from the distributed FEVCS. The impact of scalability on a DN-

level and the personalization level required at the FEVCS-level are challenges to be explored as we carry further analysis. Although, soft-synchronization has been integrated within the FL update mechanism to accommodate the possibility of rapid changes in policy. The operational and update mechanism, the entry and exit of agents/clients to the FL-frameworks are the underexplored research gaps this work expects to fill in the future. Moreover, we plan to extend this framework to enable DERs to provide other grid services such as frequency regulation and demand response by introducing role-specific agents within a game-theoretic framework.

CHAPTER 5: CONCLUSIONS AND FUTURE WORKS

5.1 Conclusions from the Dissertation

This dissertation addresses various challenges associated with integrating FEVCSs into power grids, with a focus on improving grid resilience, market participation, and adaptive edge control-based grid services such as VVO. The research contributions are structured into three key areas across the chapters:

5.1.1 Resilience-Oriented Strategic Deployment of FEVCS

The research in Chapter 2 developed a two-stage stochastic optimization model to identify the optimal placement of FEVCS within a power distribution network. The proposed model considers EVCS installation or line hardening in the first stage and grid service restoration based on fault scenarios in the second stage. Moreover, the model incorporated transportation network constraints and renewable-supported BESS to enhance realistic service restoration utilizing FEV's mobility. The uncertainty associated with line damage due to the HILP event was integrated through scenarios. The conclusions from the model indicate that optimally locating FEVCS can enhance the post-disaster resilience of the power grid. The reactive power support capability of FEVs can contribute to the improvement of the overall stability of the islanded microgrids. The results of this study were published in the special issue *"Towards a Sustainable Future: The Role of Electric Vehicles and Smart Grids in the Energy Transition"* of the journal *Applied Sciences* under the title *Optimal Siting of EV Fleet Charging Station Considering EV Mobility and Microgrid Formation for Enhanced Grid Resilience* [15].

5.1.2 FEVCS as a Strategic Reserve Provider in the ISO Market

The research in Chapter 3 focused on modeling an optimal dispatch model for FEVCS and other DERs within a DERA. By proposing a bilevel optimization framework, the study modeled an aggregated FEVS and other DERs within an ADN that interacts with the wholesale electricity markets. The research found that DERs could significantly participate in wholesale electricity markets, reducing LMPs by avoiding congestion in the transmission network. Moreover, optimally controlled DERs can increase profits from the ISO reserve markets. This research also shows the potential of the strategic DERA to be a price-maker in the ISO energy market. In the current scenario, considering the cost of battery degradation, FEVCS can optimally be a strategic reserve provider to the ISO. FEVCS could bid on the market as part of the DERA's resources or individually. The findings of this chapter were initially published in the conference *2021 IEEE Power & Energy Society General Meeting (PESGM)* with the title *Modeling the Strategic Behavior of an Active Distribution Network in ISO Markets*, and then extended to a journal published in *IEEE Transactions on Smart Grid* with the title *Stochastic Strategic Participation of Active Distribution Networks With High-Penetration DERs in Wholesale Electricity Markets*

5.1.3 Distributed, Adaptive, and Real-time Control of FEVCS using HFRL

The research in Chapter 4 introduced the FLE-CA-MARL framework, designed to tackle decentralized VVO problems in distribution networks equipped with FEVCS. By leveraging FL and conflict-aware reinforcement learning, the framework enabled decentralized decision-making while ensuring that FEV agents collaboratively contributed to grid stability. The results demonstrated the framework's scalability, adaptability, and effectiveness in local voltage regulation and harmonizing actions across FEV agents to optimize the VAR injections, enhancing both local and global voltage regulation. Results specific to FEVCS decentralized control have been sub-

mitted to *IEEE Transactions on Smart Grid*, with the paper titled *A Federated Learning-Enhanced Conflict-Aware Multi-Agent Reinforcement Learning Framework for Decentralized Volt-VAR Control in Distribution Networks with Fleet EV Charging Stations*.

5.2 Future Works

Building on the foundations laid in this dissertation, future research could expand the functionalities of the proposed frameworks in several directions. One promising area is the integration of energy market participation into the FLE-CA-MARL framework. Extending the existing framework to enable FEVCS to participate in the real-time energy markets and in ancillary services markets, which will enhance the practical application of FEVCS as both grid stabilizers and active market participants.

Post-disaster restoration offers another significant extension, especially considering the resilience-focused deployment strategies presented in this work. Further research can explore how decentralized FEVCS control strategies could support real-time grid restoration following HILP events. Future efforts may include optimizing coordination between FEVCS and renewable-supported BESS to restore critical services and leverage FEV mobility for dynamic service provision during recovery.

Finally, the real-time operational challenges of a decentralized framework like FDRL require continued attention. Ensuring dynamic adaptation of policies, managing the frequent entry and exit of FEV agents, and overcoming communication delays between agents and the central aggregator are crucial areas of exploration. As FEVCS penetration increases, scalability and the efficient operation of the FRL framework under larger, more complex network conditions will need to be rigorously tested to ensure robust performance across diverse real-world scenarios.

REFERENCES

[1] M. L. Di Silvestre, S. Favuzza, E. R. Sanseverino, and G. Zizzo, "How decarbonization, digitalization and decentralization are changing key power infrastructures," *Renewable and Sustainable Energy Reviews*, vol. 93, pp. 483–498, 2018.

[2] H. S. Das, M. M. Rahman, S. Li, and C. W. Tan, "Electric vehicles standards, charging infrastructure, and impact on grid integration: A technological review," *Renewable and Sustainable Energy Reviews*, vol. 120, p. 109618, 2020.

[3] Duke Energy, "Carolinas resource plan," 2024. Accessed: 2024-07-31.

[4] S. S. Acharige, M. E. Haque, M. T. Arif, and N. Hosseinzadeh, "Review of electric vehicle charging technologies, configurations, and architectures," *arXiv preprint arXiv:2209.15242*, 2022.

[5] O. Veneri, L. Ferraro, C. Capasso, and D. Iannuzzi, "Charging infrastructures for ev: Overview of technologies and issues," *2012 Electrical Systems for Aircraft, Railway and Ship Propulsion*, pp. 1–6, 2012.

[6] S. Rahman, I. A. Khan, and M. H. Amini, "A review on impact analysis of electric vehicle charging on power distribution systems," in *2020 2nd International Conference on Smart Power & Internet Energy Systems (SPIES)*, pp. 420–425, IEEE, 2020.

[7] M. Mohanpurkar, R. Krishan, M. Panwar, S. Vyas, L. Slezak, N. Rodrigues, A. Datta, A. Meintz, and R. Hovsapian, "Enabling seamless integration of ev charging infrastructure with weak electric grids," in *2019 IEEE Transportation Electrification Conference (ITEC-India)*, pp. 1–6, IEEE, 2019.

[8] ChatGPT, "Image created using chatgpt." Generated image using OpenAI's ChatGPT, 2024. Image creation assistance by ChatGPT, OpenAI, https://chat.openai.com.

[9] International Energy Agency (IEA), "Global ev outlook 2023," 2023. Accessed: 2024-07-31.

[10] A. Ravi, "Integrating electric vehicles into integrated resource planning," Master's thesis, The University of North Carolina at Charlotte, 2023.

[11] A. Ravi, L. Bai, G. Wollam, and J. Enslin, "Ev adoption impacts on residential, commercial and urban-commercial feeders," in *2023 IEEE Energy Conversion Congress and Exposition (ECCE)*, pp. 1212–1217, IEEE, 2023.

[12] N. R. E. Laboratory, "Fleet DNA Project Data Summary Report." https://www.nrel.gov/transportation/assets/pdfs/fleet_dna_delivery_trucks_report.pdf. Accessed: 2023-01-16.

[13] N. K. Kandasamy, K. Kandasamy, and K. J. Tseng, "Loss-of-life investigation of ev batteries used as smart energy storage for commercial building-based solar photovoltaic systems," *IET Electrical Systems in Transportation*, vol. 7, no. 3, pp. 223–229, 2017.

[14] A. A. Nikitina, F. V. Lavrentev, V. Y. Yurova, D. Y. Piarnits, O. O. Volkova, E. V. Skorb, and D. G. Shchukin, "Layered nanomaterials for renewable energy generation and storage," *Materials Advances*, vol. 5, no. 2, pp. 394–408, 2024.

[15] A. Ravi, L. Bai, and H. Wang, "Optimal siting of ev fleet charging station considering ev mobility and microgrid formation for enhanced grid resilience," *Applied Sciences*, vol. 13, no. 22, p. 12181, 2023.

[16] A. Ravi, L. Bai, V. Cecchi, and F. Ding, "Stochastic strategic participation of active distribution networks with high-penetration ders in wholesale electricity markets," *IEEE Transactions on Smart Grid*, vol. 14, no. 2, pp. 1515–1527, 2022.

[17] S. E. Ahmadi, M. Marzband, A. Ikpehai, and A. Abusorrah, "Optimal stochastic scheduling of plug-in electric vehicles as mobile energy storage systems for resilience enhancement of multi-agent multi-energy networked microgrids," *Journal of Energy Storage*, vol. 55, p. 105566, 2022.

[18] F. Yao, J. Wang, F. Wen, J. Zhao, X. Zhao, and W. Liu, "Resilience enhancement for a power system with electric vehicles under extreme weather conditions," in *2019 IEEE Innovative Smart Grid Technologies-Asia (ISGT Asia)*, pp. 3674–3679, IEEE, 2019.

[19] S. Yao, P. Wang, and T. Zhao, "Transportable energy storage for more resilient distribution systems with multiple microgrids," *IEEE Transactions on Smart Grid*, vol. 10, no. 3, pp. 3331–3341, 2018.

[20] A. K. Erenoğlu, S. Sancar, İ. S. Terzi, O. Erdinç, M. Shafie-khah, and J. P. Catalão, "Resiliency-driven multi-step critical load restoration strategy integrating on-call electric vehicle fleet management services," *IEEE Transactions on Smart Grid*, 2022.

[21] S. Ma, B. Chen, and Z. Wang, "Resilience enhancement strategy for distribution systems under extreme weather events," *IEEE Transactions on Smart Grid*, vol. 9, no. 2, pp. 1442–1451, 2016.

[22] M. Nazemi, M. Moeini-Aghtaie, M. Fotuhi-Firuzabad, and P. Dehghanian, "Energy storage planning for enhanced resilience of power distribution networks against earthquakes," *IEEE Transactions on Sustainable Energy*, vol. 11, no. 2, pp. 795–806, 2019.

[23] N. L. Dehghani, A. B. Jeddi, and A. Shafieezadeh, "Intelligent hurricane resilience enhancement of power distribution systems via deep reinforcement learning," *Applied energy*, vol. 285, p. 116355, 2021.

[24] M. Ghasemi, A. Kazemi, M. A. Gilani, and M. Shafie-Khah, "A stochastic planning model for improving resilience of distribution system considering master-slave distributed generators and network reconfiguration," *IEEE Access*, vol. 9, pp. 78859–78872, 2021.

[25] D. Faramarzi, H. Rastegar, G. Riahy, and H. Doagou-Mojarrad, "A three-stage hybrid stochastic/igdt framework for resilience-oriented distribution network planning," *International Journal of Electrical Power & Energy Systems*, vol. 146, p. 108738, 2023.

[26] A. Poudyal, S. Poudel, and A. Dubey, "Risk-based active distribution system planning for resilience against extreme weather events," *IEEE Transactions on Sustainable Energy*, 2022.

[27] M. Panteli, D. N. Trakas, P. Mancarella, and N. D. Hatziargyriou, "Power systems resilience assessment: Hardening and smart operational enhancement strategies," *Proceedings of the IEEE*, vol. 105, no. 7, pp. 1202–1213, 2017.

[28] A. Hussain and P. Musilek, "Resilience enhancement strategies for and through electric vehicles," *Sustainable Cities and Society*, p. 103788, 2022.

[29] M. A. Brown and A. Soni, "Expert perceptions of enhancing grid resilience with electric vehicles in the united states," *Energy Research & Social Science*, vol. 57, p. 101241, 2019.

[30] T. Ding, Y. Lin, Z. Bie, and C. Chen, "A resilient microgrid formation strategy for load restoration considering master-slave distributed generators and topology reconfiguration," *Applied energy*, vol. 199, pp. 205–216, 2017.

[31] A. Ravi, L. Bai, V. Cecchi, and F. Ding, "Stochastic strategic participation of active distribution networks with high-penetration ders in wholesale electricity markets," *IEEE Transactions on Smart Grid*, vol. 14, no. 2, pp. 1515–1527, 2023.

[32] A. Oceanographic and M. L. (AOML), "Hurricane Database." https://www.aoml.noaa.gov/hrd/hurdat/hurdat2.html. Accessed: 2021-07-16.

[33] P. Sopasakis, "PDFsampler: Probability Density Function Sampler." https://www.mathworks.com/matlabcentral/fileexchange/41689-pdfsampler, 2023. Retrieved January 20, 2023.

[34] L. (2023), "scenred." https://github.com/supsi-dacd-isaac/scenred. Accessed: January 20, 2023.

[35] G. E. Asimakopoulou and N. D. Hatziargyriou, "Evaluation of economic benefits of der aggregation," *IEEE Transactions on Sustainable Energy*, vol. 9, no. 2, pp. 499–510, 2018.

[36] A. A. Algarni, K. Bhattacharya, and R. A. El-Shatshat, "Optimal operation of a disco in competitive electricity markets with elasticity effects," in *2007 IEEE Power Engineering Society General Meeting*, pp. 1–7, IEEE, 2007.

[37] S. Sarkhani, S. Soleymani, B. Mozafari, and H. Afaghzadeh, "Impact of distributed generation and interruptible load on energy supply strategies of distribution companies in day-ahead market," in *16th Electrical Power Distribution Conference*, pp. 1–6, IEEE, 2011.

[38] M. Di Somma, G. Graditi, and P. Siano, "Optimal bidding strategy for a der aggregator in the day-ahead market in the presence of demand flexibility," *IEEE Transactions on Industrial Electronics*, vol. 66, no. 2, pp. 1509–1519, 2018.

[39] J. Wang, H. Zhong, Q. Xia, Z. Ma, Z. Wang, and X. Wu, "Robust bidding strategy for microgrids in joint energy, reserve and regulation markets," in *2017 IEEE Power & Energy Society General Meeting*, pp. 1–5, IEEE, 2017.

[40] A. Safdarian, M. Fotuhi-Firuzabad, and M. Lehtonen, "A stochastic framework for short-term operation of a distribution company," *IEEE Transactions on Power Systems*, vol. 28, no. 4, pp. 4712–4721, 2013.

[41] D. Pudjianto, C. Ramsay, and G. Strbac, "Microgrids and virtual power plants: concepts to support the integration of distributed energy resources," *Proceedings of the Institution of Mechanical Engineers, Part A: Journal of Power and Energy*, vol. 222, no. 7, pp. 731–741, 2008.

[42] M. Rahimiyan and L. Baringo, "Strategic bidding for a virtual power plant in the day-ahead and real-time markets: A price-taker robust optimization approach," *IEEE Transactions on Power Systems*, vol. 31, no. 4, pp. 2676–2687, 2015.

[43] D. Koraki and K. Strunz, "Wind and solar power integration in electricity markets and distribution networks through service-centric virtual power plants," *IEEE Transactions on Power Systems*, vol. 33, no. 1, pp. 473–485, 2017.

[44] W. Xu, P. Zhang, and D. Wen, "Decision-making model of electricity purchasing for electricity retailers based on conditional value-atrisk in day-ahead market," in *2020 12th IEEE PES Asia-Pacific Power and Energy Engineering Conference (APPEEC)*, pp. 1–5, IEEE, 2020.

[45] M. Wang, Y. Mu, Q. Shi, H. Jia, and F. Li, "Electric vehicle aggregator modeling and control for frequency regulation considering progressive state recovery," *IEEE Transactions on Smart Grid*, vol. 11, no. 5, pp. 4176–4189, 2020.

[46] A. Oshnoei, M. Kheradmandi, and S. M. Muyeen, "Robust control scheme for distributed battery energy storage systems in load frequency control," *IEEE Transactions on Power Systems*, vol. 35, no. 6, pp. 4781–4791, 2020.

[47] Y. Wang, T. Zhao, C. Ju, Y. Xu, and P. Wang, "Two-level distributed volt/var control using aggregated pv inverters in distribution networks," *IEEE Transactions on Power Delivery*, vol. 35, no. 4, pp. 1844–1855, 2020.

[48] H. Chen, H. Li, C. Lin, X. Jin, R. Zhang, and X. Li, "An integrated market solution to enable active distribution network to provide reactive power ancillary service using transmission–distribution coordination," *IET Energy Systems Integration*, 2021.

[49] Z. Zhao, Y. Liu, L. Guo, L. Bai, and C. Wang, "Locational marginal pricing mechanism for uncertainty management based on improved multi-ellipsoidal uncertainty set," *Journal of Modern Power Systems and Clean Energy*, vol. 9, no. 4, pp. 734–750, 2021.

[50] M. Fan, "A novel optimal generation dispatch algorithm to reduce the uncertainty impact of renewable energy," in *2016 IEEE Power and Energy Society General Meeting (PESGM)*, pp. 1–5, IEEE, 2016.

[51] H. Nosair and F. Bouffard, "Economic dispatch under uncertainty: The probabilistic envelopes approach," *IEEE Transactions on Power Systems*, vol. 32, no. 3, pp. 1701–1710, 2016.

[52] Y. Chen, S. M. Mazhari, C. Chung, and S. O. Faried, "A preventive dispatching method for high wind power-integrated electrical systems considering probabilistic transient stability constraints," *IEEE Open Access Journal of Power and Energy*, vol. 8, pp. 472–483, 2021.

[53] A. M. Palani, H. Wu, and M. M. Morcos, "A fast penalty-based gauss-seidel method for stochastic unit commitment with uncertain load and wind generation," *IEEE Open Access Journal of Power and Energy*, vol. 8, pp. 211–222, 2021.

[54] H. Li, Y. Li, and Z. Li, "A multiperiod energy acquisition model for a distribution company with distributed generation and interruptible load," *IEEE Transactions on Power Systems*, vol. 22, no. 2, pp. 588–596, 2007.

[55] C. Zhang, Q. Wang, J. Wang, M. Korpås, P. Pinson, J. Østergaard, and M. E. Khodayar, "Trading strategies for distribution company with stochastic distributed energy resources," *Applied energy*, vol. 177, pp. 625–635, 2016.

[56] S. Bahramara, M. Yazdani-Damavandi, J. Contreras, M. Shafie-Khah, and J. P. Catalão, "Modeling the strategic behavior of a distribution company in wholesale energy and reserve markets," *IEEE Transactions on Smart Grid*, vol. 9, no. 4, pp. 3857–3870, 2017.

[57] A. Ravi, L. Bai, V. Cecch, Y. Xue, and F. Ding, "Modeling the strategic behavior of an active distribution network in the iso markets," in *2021 IEEE Power & Energy Society General Meeting (PESGM)*, pp. 01–05, IEEE, 2021.

[58] M. E. Baran and F. F. Wu, "Network reconfiguration in distribution systems for loss reduction and load balancing," *IEEE Power Engineering Review*, vol. 9, no. 4, pp. 101–102, 1989.

[59] L. Bai, J. Wang, C. Wang, C. Chen, and F. Li, "Distribution locational marginal pricing (dlmp) for congestion management and voltage support," *IEEE Transactions on Power Systems*, vol. 33, no. 4, pp. 4061–4073, 2017.

[60] S. Bahramara, M. P. Moghaddam, and M. R. Haghifam, "Modelling hierarchical decision making framework for operation of active distribution grids," *IET Generation, Transmission & Distribution*, vol. 9, no. 16, pp. 2555–2564, 2015.

[61] S. J. Kazempour, A. J. Conejo, and C. Ruiz, "Strategic generation investment using a complementarity approach," *IEEE transactions on power systems*, vol. 26, no. 2, pp. 940–948, 2010.

[62] M. Shafiekhani, A. Badri, and F. Khavari, "A bi-level model for strategic bidding of virtual power plant in day-ahead and balancing market," in *2017 smart grid conference (SGC)*, pp. 1–6, IEEE, 2017.

[63] A. Ravi, "Test Case Data for I5-A9 Network."

[64] NREL, "The Wind Prospector-Eastern Wind Dataset ."

[65] J. Zhu, Y. Zhuo, J. Chen, Y. Guo, X. Mo, and M. Liu, "An expected-cost realization-probability optimization approach for the dynamic energy management of microgrid," *International Journal of Electrical Power & Energy Systems*, vol. 136, p. 107620, 2022.

[66] S. Lu, B. Han, F. Xue, L. Jiang, and X. Feng, "Stochastic bidding strategy of electric vehicles and energy storage systems in uncertain reserve market," *IET Renewable Power Generation*, vol. 14, no. 18, pp. 3653–3661, 2020.

[67] X. Duan, Z. Hu, and Y. Song, "Bidding strategies in energy and reserve markets for an aggregator of multiple ev fast charging stations with battery storage," *IEEE Transactions on Intelligent Transportation Systems*, vol. 22, no. 1, pp. 471–482, 2020.

[68] N. Growe-Kuska, H. Heitsch, and W. Romisch, "Scenario reduction and scenario tree construction for power management problems," in *2003 IEEE Bologna Power Tech Conference Proceedings,*, vol. 3, pp. 7–pp, IEEE, 2003.

[69] Z. Zhang, D. Zhang, and R. C. Qiu, "Deep reinforcement learning for power system applications: An overview," *CSEE Journal of Power and Energy Systems*, vol. 6, no. 1, pp. 213–225, 2019.

[70] M. G. Dastgir, X. Huo, and M. Liu, "Multi-agent reinforcement learning based electric vehicle charging control for grid-level services," in *IECON 2022–48th Annual Conference of the IEEE Industrial Electronics Society*, pp. 1–6, IEEE, 2022.

[71] Y. Chu, Z. Wei, X. Fang, S. Chen, and Y. Zhou, "A multiagent federated reinforcement learning approach for plug-in electric vehicle fleet charging coordination in a residential community," *IEEE Access*, vol. 10, pp. 98535–98548, 2022.

[72] Y. Wang, D. Qiu, G. Strbac, and Z. Gao, "Coordinated electric vehicle active and reactive power control for active distribution networks," *IEEE Transactions on Industrial Informatics*, vol. 19, no. 2, pp. 1611–1622, 2022.

[73] E. Cording and J. Thakur, "Fleetrl: Realistic reinforcement learning environments for commercial vehicle fleets," *SoftwareX*, vol. 26, p. 101671, 2024.

[74] L. Yan, X. Chen, Y. Chen, and J. Wen, "A cooperative charging control strategy for electric vehicles based on multiagent deep reinforcement learning," *IEEE Transactions on Industrial Informatics*, vol. 18, no. 12, pp. 8765–8775, 2022.

[75] H. Cheng, H. Luo, Z. Liu, W. Sun, W. Li, and Q. Li, "Reinforcement learning based robust volt/var control in active distribution networks with imprecisely known delay," *arXiv preprint arXiv:2402.17268*, 2024.

[76] B. McMahan, E. Moore, D. Ramage, S. Hampson, and B. A. y Arcas, "Communication-efficient learning of deep networks from decentralized data," in *Artificial intelligence and statistics*, pp. 1273–1282, PMLR, 2017.

[77] Y. Shang, Z. Li, S. Li, Z. Shao, and L. Jian, "An information security solution for vehicle-to-grid scheduling by distributed edge computing and federated deep learning," *IEEE Transactions on Industry Applications*, 2024.

[78] L. Yang, S. Guo, C.-K. Tham, M. Li, G. Liu, and P. Zhou, "Prem-fediov: A novel federated reinforcement learning framework for predictive maintenance in iov," *IEEE Transactions on Mobile Computing*, 2024.

[79] J. Qian, Y. Jiang, X. Liu, Q. Wang, T. Wang, Y. Shi, and W. Chen, "Federated reinforcement learning for electric vehicles charging control on distribution networks," *IEEE Internet of Things Journal*, 2023.

[80] S. M. Danish, A. Hameed, A. Ranjha, G. Srivastava, and K. Zhang, "Blockfedl: Electric vehicle charging load forecasting using federated learning and blockchain," *IEEE Transactions on Vehicular Technology*, 2024.

[81] Y. Shang and S. Li, "Fedpt-v2g: Security enhanced federated transformer learning for real-time v2g dispatch with non-iid data," *Applied Energy*, vol. 358, p. 122626, 2024.

[82] X. Sun and J. Qiu, "A customized voltage control strategy for electric vehicles in distribution networks with reinforcement learning method," *IEEE Transactions on Industrial Informatics*, vol. 17, no. 10, pp. 6852–6863, 2021.

[83] T. Ding, Z. Zeng, J. Bai, B. Qin, Y. Yang, and M. Shahidehpour, "Optimal electric vehicle charging strategy with markov decision process and reinforcement learning technique," *IEEE Transactions on Industry Applications*, vol. 56, no. 5, pp. 5811–5823, 2020.

[84] S. Fujimoto, H. Hoof, and D. Meger, "Addressing function approximation error in actor-critic methods," in *International conference on machine learning*, pp. 1587–1596, PMLR, 2018.

[85] T. Haarnoja, A. Zhou, K. Hartikainen, G. Tucker, S. Ha, J. Tan, V. Kumar, H. Zhu, A. Gupta, P. Abbeel, *et al.*, "Soft actor-critic algorithms and applications," *arXiv preprint arXiv:1812.05905*, 2018.

[86] J. Ackermann, V. Gabler, T. Osa, and M. Sugiyama, "Reducing overestimation bias in multi-agent domains using double centralized critics," *arXiv preprint arXiv:1910.01465*, 2019.

[87] L. Thurner, A. Scheidler, F. Schäfer, J. Menke, J. Dollichon, F. Meier, S. Meinecke, and M. Braun, "pandapower â an open-source python tool for convenient modeling, analysis, and optimization of electric power systems," *IEEE Transactions on Power Systems*, vol. 33, pp. 6510–6521, Nov 2018.

[88] National Renewable Energy Laboratory (NREL), "End-use load profiles for u.s. building stock - comstock amy2018 release 1: Timeseries aggregates by county for north carolina." https://data.openei.org/, 2021. Accessed: 2024-07-13.